Quorum Sensing as Potential Biomarker Targets to Diagnose Bacterial Infections

Juan Raya Beltrán

UNIVERSITAT DE BARCELONA

CSIC
CONSEJO SUPERIOR DE INVESTIGACIONES CIENTÍFICAS

Quorum Sensing as Potential Biomarker Targets to Diagnose Bacterial Infections

Juan Raya Beltrán

2024



Faculty of Chemistry

Doctoral program in Organic Chemistry

Quorum Sensing as Potential Biomarker Targets to Diagnose Bacterial Infections

Dissertation presented by Juan Raya Beltrán in fulfillment of the requirements for the degree of doctor by Universitat de Barcelona

Director:

Prof. Mª Pilar Marco Colás
Research Professor
Heat of Nanobiotechnology for Diagnostics group,
IQAC-CSIC

Tutor:

Prof. Francesc Rabanal Anglada
Professor of Organic Chemistry
Dep. of Inorganic and Organic Chemistry
Faculty of Chemistry
Universitat de Barcelona

AGRADECIMIENTOS

El momento que parecía tan lejano, finalmente ha llegado. Esta tesis es el fruto de años de trabajo, esfuerzo y dedicación. Sin embargo, lo que no se puede capturar en estas páginas son las experiencias, emociones, temores, frustraciones y alegrías que han acompañado este proceso. Han sido casi cuatro años de aprendizajes y crecimiento, y en este camino, he tenido la suerte de encontrarme con personas que han dejado una huella imborrable en mi vida.

Quiero comenzar expresando mi más sincero agradecimiento a todos los que formaron parte del grupo de investigación Nb4D. Después de tantas horas de trabajo compartido, viajes, celebraciones y momentos inolvidables, hemos formado una familia unida, con todos los desafíos y alegrías que ello conlleva. Por eso, una parte esencial de esta tesis está dedicada a todos vosotros.

En primer lugar, quiero expresar mi más profundo agradecimiento a Pilar, mi directora de tesis. Su confianza en mí me brindó la oportunidad de realizar esta tesis en este maravilloso grupo. No solo he aprendido mucho a nivel científico, sino que también he crecido enormemente a nivel personal, gracias a su calidad humana excepcional y su constante apoyo.

También quiero agradecer a Lluïsa, Nuria, Roger y Pablo. Son grandes científicos de los que he aprendido muchísimo, y les agradezco de corazón todo lo que me han ayudado a lo largo de estos años.

A todos los miembros del Nb4D, la familia que hemos formado en estos años ha sido increíble. Los momentos y experiencias que hemos vivido juntos son inolvidables, y es casi increíble pensar que todo esto ha sido posible con personas con las que comparto el trabajo diario. Solo nosotros entendemos la conexión que hemos creado, y cómo podemos pasar de discutir los temas más profundamente científicos a subir montañas en Mallorca, coger un vuelo a Marrakech o irnos de Ravalada. Es increíble poder compartir experiencias tan diversas con la misma gente.

A Montse, por haberme enseñado tanto. Siempre serás un referente científico para mí en todos los ámbitos, pero sobre todo, una gran persona. Siempre has estado ahí cuando he necesitado ayuda, siempre con la respuesta correcta y el tiempo para apoyarme. De verdad, muchísimas gracias, te aprecio mucho.

A David, por ser esa persona que cada día traía alegría al laboratorio con sus bromas y risas, y por transmitirnos esas ganas de viajar. Sin duda, esta tesis habría sido muy diferente sin ti.

Quiero también agradecer a Andrea, Lidia e Idoia. Desde que llegaron, todo cambió. Son personas con las que fue muy fácil conectar desde el primer momento, y con quienes he compartido tantos momentos. Siempre habéis estado ahí cuando os he necesitado, en risas, momentos duros, consejos y charlas existenciales que me han hecho aprender mucho y disfrutar cada día en el Nb4D.

A mis compañeros de ELISA, primero quiero agradecer a Carla, mi compañera de tesis, con quien he compartido frustraciones, alegrías y discusiones científicas que nos han hecho aprender mucho a ambos. Los momentos vividos desde nuestro primer viaje a Madrid, pasando por Austria y hasta Filipinas, han sido inolvidables. No podría haber tenido mejor compañera de tesis, siempre dispuesta a cualquier aventura. A Julián, por todas esas charlas interminables que empezaban en temas científicos y acababan en cualquier tema de la vida, y por todas las risas. Has sido alguien con quien me he entendido a la perfección. Nerea, una persona cercana en la que siempre se puede confiar. Gracias por aportar esa alegría diaria que en algunos momentos

ha sido tan necesaria. Gemma, siempre con una sonrisa y dispuesta a todo. No podría haber tenido mejor compañera, te deseo lo mejor. A Marc, por todos los momentos vividos, por apuntarse siempre a todo y por esos increíbles viajes a Mallorca. Sin tu ayuda, esto no habría sido posible. Francesc, gracias por tu constante disposición para ayudar y por estar siempre presente cuando te he necesitado. Tu ayuda ha sido fundamental en muchos momentos. Irene, me encanta tu sentido del humor y ojalá escucharte cantar en muchas más fiestas, estoy seguro que se vienen grandes momentos. A Eva, por estar siempre dispuesta a ayudarme cuando lo he necesitado, siempre me has aportado grandes consejos científicos.

También quiero expresar mi agradecimiento a los colaboradores de los diversos hospitales: Maite Martín, Antonio Oliver, Carla López y Juan Pablo Horcajada. Agradezco sinceramente el tiempo que habéis dedicado para ayudarme a sacar adelante esta tesis. Asimismo, me gustaría agradecer al grupo del IBEC liderado por Santiago Marco y a Agustín Gutiérrez por su valiosa colaboración en el análisis bioinformático de este trabajo.

Finalmente, quiero agradecer a todas las personas que han pasado por el Nb4D y con quienes he coincidido, que han hecho que ir a trabajar cada día sea un placer, y que siempre han estado dispuestas a ayudar con todo: Luciano, Bárbara, Enrique, Ana, Ástrid, Gemma, Tamas, Melek, Fabiola, Joel, Min.

A mi familia, por apoyarme siempre y hacerme creer que puedo lograr cualquier cosa que me proponga. Esto nunca habría sido posible sin vosotros.

A mis amigos y compañeros de piso, por escucharme cuando lo he necesitado, por aguantar mis quejas y frustraciones, y por estar siempre ahí apoyándome y dándome la confianza para seguir adelante.

A todos mis amigos, que habéis hecho que estos cuatro años hayan sido increíbles, que me habéis escuchado y apoyado siempre, y que, sin duda, esta tesis también lleva un poco de vosotros.

THESIS ABSTRACT

Pseudomonas aeruginosa is a Gram-negative bacterium known for its ability to cause a wide range of infections, particularly in individuals with compromised immune systems or underlying health conditions such as cystic fibrosis. This opportunistic pathogen exploits breaches in tissue barriers and evades the host immune response through diverse biological mechanisms. Additionally, *P. aeruginosa* is frequently isolated in healthcare-associated and community-acquired infections, and its multidrug-resistant strains contribute to severe and persistent infections. The prevalence and adaptability of *P. aeruginosa* have resulted in a significant global health and economic burden, exacerbated by the limited efficacy of conventional therapeutic options.

Bacterial diagnosis remains challenging, with traditional culture methods still considered the gold standard. However, these methods are time-consuming, often delaying diagnosis and leading to the administration of broad-spectrum antibiotics, which in turn drives the increasing prevalence of antimicrobial resistance. This issue is particularly critical in infections caused by *P. aeruginosa*, where delayed or inappropriate treatment can worsen patient outcomes and contribute to the spread of resistant strains.

One of the key factors underlying the pathogenicity of *P. aeruginosa* is its sophisticated bacterial communication system, *Quorum Sensing* (QS). QS enables bacteria to coordinate gene expression and behavior in response to changes in population density. In *P. aeruginosa*, QS regulates various pathogenic processes, including biofilm formation, virulence factor production, and antibiotic resistance. The ability of *P. aeruginosa* to adapt to hostile environments and its reliance on QS make this system a promising target for developing diagnostic and therapeutic strategies.

This PhD thesis focuses on developing new diagnostic tools to improve the detection and management of *P. aeruginosa* infections. The central hypothesis is that the QS molecular signature of *P. aeruginosa* at different stages of infection can provide valuable insights into the infection's progression, underlying pathogenic mechanisms, and potential treatment strategies. Additionally, QS signaling molecules (QSsm) could serve as biomarkers for early-stage infection diagnosis, offering a more efficient approach to managing these infections.

To achieve these objectives, this project employed an immunological approach to detect the key QSsm and virulence factors (VF) of *P. aeruginosa*. The study involved the development of high-affinity antibodies against these molecules, the establishment of robust ELISAs for their detection in both buffer and complex clinical samples, and the application of these tools to analyze biological samples and clinical isolates from patients with lower respiratory tract and urinary tract infections with the aim to probe our hypotheses .

Key findings of the thesis include the successful production of monoclonal antibodies against PQS, the principal molecule of the Pqs QS system of *P. aeruginosa*. Using these antibodies, an ELISA for PQS was developed with a limit of detection (LOD) below 1 nM in buffer and in Müller-Hinton culture media, demonstrating high specificity and robustness across various physicochemical conditions. Additionally, polyclonal antibodies were produced against the autoinducers of the Las and Rhl QS systems of *P. aeruginosa*, 3-oxo-C12-HSL and C4-HSL. ELISAs were developed using these antibodies, achieving LODs of 3.75 nM and 16.29 nM, respectively. Moreover, the ELISA for 3-oxo-C12-HSL was optimized for its use analyzing Müller-Hinton media, with a LOD of 10 nM.

Implementing the QS immunochemical assays to the analysis of sputum samples has been the bottleneck of this research project due to its complexity and wide variability between distinct samples. Various sputum sample treatment procedures for detecting QSsm have been devised and evaluated, based on reported literature and knowledge of the sputum composition. The efforts invested allowed to successfully accomplish immunochemical detection of PQS and HHQ, two signaling molecules of the Pqs QS system, in sputum samples from patients with lower respiratory tract infections (LRTI) caused by *P. aeruginosa*. This achievement opens the door to the development of point-of-care devices for rapid diagnosis of *P. aeruginosa* LRT infections.

Furthermore, a study was conducted with different bacterial isolates of *P. aeruginosa* from LRTI and urinary tract infection (UTI) cases. The QS molecular footprint and VF levels of these isolates were analyzed, revealing clear differences between isolates from acute and chronic infections. A threshold was established that could potentially distinguish between these two infection types, with significant implications for infection classification and treatment strategies. Evolution of the QS molecular footprint was also observed in bacteria isolates from patients with chronic infection through the time, although it has not been possible to stablish a correlation with the clinical status of the patient due to the lack of access to the clinical records at this stage.

The analysis of clinical isolates also revealed a correlation between QSsm and VF production and antibiotic resistance patterns, suggesting that QS profiles could be used to predict antibiotic resistance and guide more targeted therapies. Additionally, the research identified HQNO as a significant biomarker for bacteremia detection in UTI, achieving high classification accuracy, sensitivity, and specificity. However, further validation is necessary to confirm HQNO's clinical utility in predicting bacteremia onset.

Overall, this thesis underscores the potential of QS-associated biomarkers in *P. aeruginosa* for rapid diagnosing *P. aeruginosa* infections, patient stratification and monitoring of the disease as well as the development of personalized treatment approaches. The findings suggest that by leveraging these biomarkers, clinicians can improve patient outcomes through more precise diagnosis and targeted therapies. Future research should focus on further elucidating the mechanisms driving these biomarker dynamics and exploring their broader clinical applications.

RESUMEN DE LA TESIS

Pseudomonas aeruginosa es una bacteria gramnegativa conocida por su capacidad de causar una amplia gama de infecciones, especialmente en individuos con sistemas inmunológicos comprometidos o condiciones de salud subyacentes como la fibrosis quística. Este patógeno oportunista aprovecha las brechas en tejidos y evade la respuesta inmune del huésped a través de diversos mecanismos biológicos. Además, *P. aeruginosa* se aísla con frecuencia en infecciones asociadas a la atención médica y adquiridas en la comunidad, y sus cepas multirresistentes contribuyen a infecciones graves y persistentes. La prevalencia y adaptabilidad de *P. aeruginosa* han resultado en una carga global significativa en términos de salud y economía, agravada por la eficacia limitada de las opciones terapéuticas convencionales.

El diagnóstico bacteriano sigue siendo un desafío, con los métodos tradicionales de cultivo considerados el estándar de oro. Sin embargo, estos métodos son lentos, lo que a menudo retrasa el diagnóstico y conduce a la administración de antibióticos de amplio espectro, lo que a su vez impulsa el aumento de la resistencia antimicrobiana. Este problema es especialmente crítico en las infecciones causadas por *P. aeruginosa*, donde el tratamiento retrasado o inapropiado puede empeorar los resultados de los pacientes y contribuir a la propagación de cepas resistentes.

Uno de los factores clave que subyacen a la patogenicidad de *P. aeruginosa* es su sofisticado sistema de comunicación bacteriana, el Quorum Sensing (QS). El QS permite a las bacterias coordinar la expresión génica y el comportamiento en respuesta a cambios en la densidad poblacional. En *P. aeruginosa*, el QS regula varios procesos patogénicos, incluyendo la formación de biopelículas, la producción de factores de virulencia y la resistencia a los antibióticos. La capacidad de *P. aeruginosa* para adaptarse a entornos hostiles y su dependencia del QS hacen de este sistema un objetivo prometedor para el desarrollo de estrategias diagnósticas y terapéuticas.

Esta tesis doctoral se centra en el desarrollo de nuevas herramientas diagnósticas para mejorar la detección y el manejo de las infecciones por *P. aeruginosa*. La hipótesis central es que la firma molecular del QS de *P. aeruginosa* en diferentes etapas de la infección puede proporcionar información valiosa sobre la progresión de la infección, los mecanismos patogénicos subyacentes y posibles estrategias de tratamiento. Además, las moléculas de señalización del QS (QSsm) podrían servir como biomarcadores para el diagnóstico temprano de la infección, ofreciendo un enfoque más eficiente para gestionar estas infecciones.

Para lograr estos objetivos, este proyecto empleó un enfoque inmunológico para detectar los QSsm clave y los factores de virulencia (VF) de *P. aeruginosa*. El estudio implicó el desarrollo de anticuerpos de alta afinidad contra estas moléculas, el establecimiento de ELISAs robustos para su detección tanto en tampones como en muestras clínicas complejas, y la aplicación de estas herramientas para analizar muestras biológicas e aislados clínicos de pacientes con infecciones del tracto respiratorio inferior y del tracto urinario con el objetivo de probar nuestras hipótesis.

Los hallazgos clave de la tesis incluyen la producción exitosa de anticuerpos monoclonales contra PQS, la principal molécula del sistema Pqs QS de *P. aeruginosa*. Usando estos anticuerpos, se desarrolló un ELISA para PQS con un límite de detección (LOD) inferior a 1 nM en tampones y en medio de cultivo Müller-Hinton, demostrando alta especificidad y robustez en diversas condiciones fisicoquímicas. Además, se produjeron anticuerpos policlonales contra los autoinductores de los sistemas Las y Rhl QS de P. aeruginosa, 3-oxo-C12-HSL y C4-HSL. Se

desarrollaron ELISAs utilizando estos anticuerpos, logrando LODs de 3.75 nM y 16.29 nM, respectivamente. Además, el ELISA para 3-oxo-C12-HSL fue optimizado para su uso en el análisis de medio Müller-Hinton, con un LOD de 10 nM.

La implementación de los ensayos inmunoquímicos del QS para el análisis de muestras de esputo ha sido la parte más compleja de este proyecto de investigación debido a su complejidad y amplia variabilidad entre distintas muestras. Se han ideado y evaluado varios procedimientos de tratamiento de muestras de esputo para detectar QSsm, basados en la literatura reportada y en el conocimiento de la composición del esputo. Los esfuerzos invertidos permitieron lograr la detección inmunoquímica de PQS y HHQ, dos moléculas de señalización del sistema Pqs QS, en muestras de esputo de pacientes con infecciones del tracto respiratorio inferior (LRTI) causadas por *P. aeruginosa*. Este logro abre la puerta al desarrollo de dispositivos de diagnóstico rápido en el punto de atención para infecciones respiratorias por *P. aeruginosa*.

Además, se realizó un estudio con diferentes aislados bacterianos de *P. aeruginosa* de casos de LRTI e infecciones del tracto urinario (UTI). Se analizaron la huella molecular del QS y los niveles de VF de estos aislados, revelando claras diferencias entre los aislados de infecciones agudas y crónicas. Se estableció un umbral que podría distinguir potencialmente entre estos dos tipos de infecciones, con implicaciones significativas para la clasificación de infecciones y estrategias de tratamiento. También se observó la evolución de la huella molecular del QS en los aislados bacterianos de pacientes con infecciones crónicas a lo largo del tiempo, aunque no ha sido posible establecer una correlación con el estado clínico del paciente debido a la falta de acceso a los registros clínicos en esta etapa.

El análisis de los aislados clínicos también reveló una correlación entre la producción de QSsm y VF y los patrones de resistencia a los antibióticos, lo que sugiere que los perfiles de QS podrían usarse para predecir la resistencia a los antibióticos y guiar terapias más dirigidas. Además, la investigación identificó HQNO como un biomarcador significativo para la detección de bacteriemia en infecciones urinarias, logrando alta precisión, sensibilidad y especificidad de clasificación. Sin embargo, es necesario realizar más validaciones para confirmar la utilidad clínica de HQNO en la predicción del inicio de la bacteriemia.

En general, esta tesis destaca el potencial de los biomarcadores asociados al QS en *P. aeruginosa* para el diagnóstico rápido de infecciones por *P. aeruginosa*, la estratificación de pacientes y el monitoreo de la enfermedad, así como el desarrollo de enfoques de tratamiento personalizado. Los hallazgos sugieren que al aprovechar estos biomarcadores, los médicos pueden mejorar los resultados de los pacientes mediante un diagnóstico más preciso y terapias dirigidas. Las investigaciones futuras deben centrarse en seguir elucidando los mecanismos que impulsan la dinámica de estos biomarcadores y explorar sus aplicaciones clínicas más amplias.

RESUM DE LA TESI

Pseudomonas aeruginosa és una bacteri gramnegativa coneguda per la seva capacitat de causar un ampli ventall d'infeccions, especialment en individus amb sistemes immunològics compromesos o condicions de salut subjacents com la fibrosi quística. Aquest patogen oportunista aprofita les bretxes en les barreres tissulars i evadeix la resposta immune de l'hoste a través de diversos mecanismes biològics. A més, *P. aeruginosa* s'aïlla amb freqüència en infeccions associades a l'atenció mèdica i adquirides en la comunitat, i les seves soques multiresistents contribueixen a infeccions greus i persistents. La prevalença i l'adaptabilitat de *P. aeruginosa* han resultat en una càrrega global significativa en termes de salut i economia, agreujada per l'eficàcia limitada de les opcions terapèutiques convencionals.

El diagnòstic bacterià continua sent un desafiament, amb els mètodes tradicionals de cultiu considerats l'estàndard d'or. No obstant això, aquests mètodes són lents, cosa que sovint retarda el diagnòstic i condueix a l'administració d'antibiòtics d'ampli espectre, cosa que, al seu torn, impulsa l'augment de la resistència antimicrobiana. Aquest problema és especialment crític en les infeccions causades per *P. aeruginosa*, on el tractament retardat o inadequat pot empitjorar els resultats dels pacients i contribuir a la propagació de soques resistents.

Un dels factors clau que subjeuen a la patogenicitat de *P. aeruginosa* és el seu sofisticat sistema de comunicació bacteriana, el Quorum Sensing (QS). El QS permet a les bacteris coordinar l'expressió gènica i el comportament en resposta a canvis en la densitat poblacional. En *P. aeruginosa*, el QS regula diversos processos patogènics, incloent-hi la formació de biopel·lícules, la producció de factors de virulència i la resistència als antibiòtics. La capacitat de *P. aeruginosa* per adaptar-se a entorns hostils i la seva dependència del QS fan d'aquest sistema un objectiu prometedor per al desenvolupament d'estratègies diagnòstiques i terapèutiques.

Aquesta tesi doctoral se centra en el desenvolupament de noves eines diagnòstiques per millorar la detecció i el maneig de les infeccions per *P. aeruginosa*. La hipòtesi central és que la signatura molecular del QS de *P. aeruginosa* en diferents etapes de la infecció pot proporcionar informació valuosa sobre la progressió de la infecció, els mecanismes patogènics subjacents i possibles estratègies de tractament. A més, les molècules de senyalització del QS (QSsm) podrien servir com a biomarcadors per al diagnòstic precoç de la infecció, oferint un enfocament més eficient per gestionar aquestes infeccions.

Per assolir aquests objectius, aquest projecte va emprar un enfocament immunològic per detectar els QSsm clau i els factors de virulència (VF) de *P. aeruginosa*. L'estudi va implicar el desenvolupament d'anticossos d'alta afinitat contra aquestes molècules, l'establiment d'ELISAs robustos per a la seva detecció tant en tampó com en mostres clíniques complexes, i l'aplicació d'aquestes eines per analitzar mostres biològiques i aïllats clínics de pacients amb infeccions del tracte respiratori inferior i del tracte urinari amb l'objectiu de provar les nostres hipòtesis.

Les troballes clau de la tesi inclouen la producció amb èxit d'anticossos monoclonals contra PQS, la molècula principal del sistema Pqs QS de *P. aeruginosa*. Usant aquests anticossos, es va desenvolupar un ELISA per a PQS amb un límit de detecció (LOD) inferior a 1 nM en tampó i en medi de cultiu Müller-Hinton, demostrant alta especificitat i robustesa en diverses condicions fisicoquímiques. A més, es van produir anticossos policlonals contra els autoinductors dels sistemes Las i Rhl QS de *P. aeruginosa*, 3-oxo-C12-HSL i C4-HSL. Es van desenvolupar ELISAs utilitzant aquests anticossos, assolint LODs de 3.75 nM i 16.29 nM, respectivament. A més,

l'ELISA per a 3-oxo-C12-HSL va ser optimitzat per al seu ús en l'anàlisi del medi Müller-Hinton, amb un LOD de 10 nM.

La implementació dels assaigs immunoquímics del QS per a l'anàlisi de mostres d'esput ha estat ella part més complexa d'aquest projecte de recerca a causa de la seva complexitat i àmplia variabilitat entre les diferents mostres. S'han ideat i avaluat diversos procediments de tractament de mostres d'esput per detectar QSsm, basats en la literatura reportada i en el coneixement de la composició de l'esput. Els esforços invertits van permetre aconseguir la detecció immunoquímica de PQS i HHQ, dues molècules de senyalització del sistema Pqs QS, en mostres d'esput de pacients amb infeccions del tracte respiratori inferior (LRTI) causades per *P. aeruginosa*. Aquest assoliment obre la porta al desenvolupament de dispositius de diagnòstic ràpid en el punt d'atenció per a infeccions respiratòries per *P. aeruginosa*.

A més, es va realitzar un estudi amb diferents aïllats bacterians de *P. aeruginosa* de casos de LRTI i infeccions del tracte urinari (UTI). Es van analitzar la petjada molecular del QS i els nivells de VF d'aquests aïllats, revelant diferències clares entre els aïllats d'infeccions agudes i cròniques. Es va establir un llindar que podria distingir potencialment entre aquests dos tipus d'infeccions, amb implicacions significatives per a la classificació d'infeccions i estratègies de tractament. També es va observar l'evolució de la petjada molecular del QS en els aïllats bacterians de pacients amb infeccions cròniques al llarg del temps, tot i que no ha estat possible establir una correlació amb l'estat clínic del pacient a causa de la manca d'accés als registres clínics en aquesta etapa.

L'anàlisi dels aïllats clínics també va revelar una correlació entre la producció de QSsm i VF i els patrons de resistència als antibiòtics, suggerint que els perfils de QS podrien utilitzar-se per predir la resistència als antibiòtics i guiar teràpies més dirigides. A més, la investigació va identificar HQNO com un biomarcador significatiu per a la detecció de bacterièmia en infeccions urinàries, assolint alta precisió, sensibilitat i especificitat de classificació. No obstant això, és necessari realitzar més validacions per confirmar la utilitat clínica de HQNO en la predicció de l'inici de la bacterièmia.

En general, aquesta tesi subratlla el potencial dels biomarcadors associats al QS en *P. aeruginosa* per al diagnòstic ràpid d'infeccions per *P. aeruginosa*, l'estratificació de pacients i el monitoratge de la malaltia, així com el desenvolupament d'enfocaments de tractament personalitzats. Les troballes suggereixen que, aprofitant aquests biomarcadors, els metges poden millorar els resultats dels pacients mitjançant un diagnòstic més precís i teràpies dirigides. Les investigacions futures haurien de centrar-se en seguir elucidant els mecanismes que impulsen la dinàmica d'aquests biomarcadors i explorar les seves aplicacions clíniques més àmplies.

1.INTRODUCTION TO DIAGNOSTIC OF *PSEUDOMONAS AERUGINOSA INFECTIONS*

1.1 Infectious diseases

The twenty-first century has experienced a series of significant infectious disease outbreaks, with the COVID-19 pandemic standing out as particularly impactful, causing widespread devastation to lives and livelihoods globally. Previous instances, such as the 2003 outbreak of severe acute respiratory syndrome coronavirus, the 2009 swine flu pandemic, the 2012 Middle East respiratory syndrome coronavirus outbreak, the 2013–2016 Ebola virus disease epidemic in West Africa, and the 2015 Zika virus disease epidemic, all led to substantial morbidity and mortality, crossing international borders to affect populations in numerous countries (Figure 1.1).

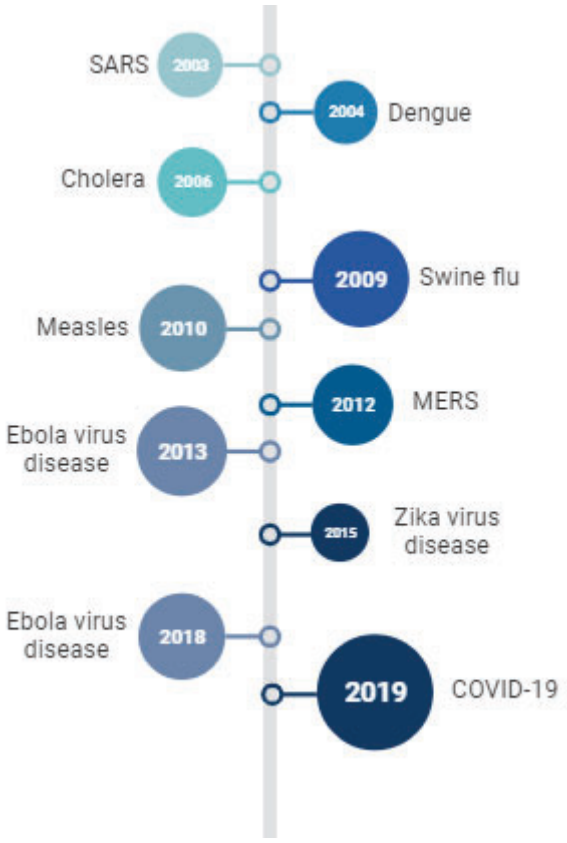

Figure 1.1: Deaths from major epidemics in the 21st century. The size of the circle indicates the number of deaths. Adapted from Baker et al., 2022.

Simultaneously, the recent decades have brought unprecedented changes in technology, demographics, and climate. Airline flights have doubled since 2000, urban areas have surpassed rural areas in population since 2007, global population numbers continue to rise, and the escalating threat of climate change faces challenges to society[1].

1.1.1 Antimicrobial resistance problematic

Antimicrobial resistance (AMR) represents a critical and escalating threat to global public health. According to the World Health Organization (WHO), AMR could cause 10 million deaths annually by 2050, surpassing the current mortality rate of cancer. This stark projection underscores the urgency to address this silent pandemic [2]. In the United States alone, the Centers for Disease Control and Prevention (CDC) estimates that at least 2.8 million people acquire an antibiotic-resistant infection each year, leading to over 35,000 deaths [3]. An analysis published in The Lancet in 2019 highlighted the adverse impact of drug-resistant infections, with 1.27 million deaths directly attributed to and 4.9 million deaths associated with resistant bacteria[4].

The primary drivers of AMR include the overuse and misuse of antibiotics in humans and animals, poor infection prevention and control practices, and the lack of rapid diagnostic tools. However, a significant contributing factor is the alarming slowdown in the discovery of new antibiotic molecules. The last few decades have witnessed a dramatic decline in the introduction of novel antibiotics. Since the 1980s, only a handful of new antibiotics have been approved, with the majority being modifications of existing classes rather than novel entities[5]. This lack of innovation is attributed to several challenges: the scientific difficulty of discovering new antibiotic classes, the high cost and low financial return on investment in antibiotic research, and stringent regulatory hurdles[6].

The consequence of this innovation gap is a growing reliance on a diminishing arsenal of effective antibiotics, leading to the increased prevalence of multidrug-resistant organisms. This scenario suggests a future where common infections and minor injuries, once easily treatable, could become life-threatening. To address this crisis, it is imperative to revitalize the antibiotic pipeline through coordinated global efforts that incentivize research and development, promote prudent antibiotic use, and implement robust surveillance mechanisms[7].

1.1.2 Respiratory infections

Respiratory infections, whether they manifest as acute or chronic conditions, occur frequently in both adults and children, posing a heightened economic burden on healthcare systems and contributing to increased morbidity and mortality. These infections may originate either in the community or within a hospital setting. Both non-immunosuppressed and immunosuppressed individuals can experience such health challenges, although the prevalence is notably higher in the immunosuppressed population[8].

In just 24 months, the COVID-19 pandemic resulted in the loss of over 5.7 million lives[9], primarily due to respiratory causes. But even before the pandemic, three respiratory illnesses were consistently ranked in the top 10 global causes of death[10]. Globally, chronic obstructive pulmonary disease (COPD) is the third most common cause of death, claiming the lives of 3.2 million individuals annually and constituting a staggering 81.7 % of all deaths attributed to chronic respiratory diseases[11]. Pneumonia ranks among the primary causes of death in children under 5 years old beyond the neonatal period and in adults over 65 years old [12]. Without the ongoing COVID-19 pandemic, which has resulted in an estimated 450,000 new cases of rifampicin-resistant or multidrug-resistant tuberculosis in 2019 alone, tuberculosis would be the leading infectious cause of death[13].

Lower respiratory tract infections (LRTIs), that in 2019 caused 2.4 million deaths affect the airways and lungs and can be caused by various bacteria. Common bacterial agents responsible for LRTIs include *Streptococcus pneumoniae*, *Haemophilus influenzae*, *Klebsiella pneumoniae*, and *Pseudomonas aeruginosa*. LRTIs encompass conditions such as pneumonia, bronchitis, and bronchiolitis, with pneumonia being the most common bacterial LRTI. Pneumonia, demonstrates an annual incidence of 24.8 per 10,000 adults, with higher rates observed in individuals aged 65-79 years (63.0/10,000 adults) and over 80 years (164.3/10,000 adults). Pneumococcal pneumonia emerges as the primary cause of mortality from LRTI, contributing to over 1.5 million deaths globally in 2015, particularly affecting children under 5 years old[14].

In outpatient settings, community-acquired pneumonia (CAP) and acute exacerbation of chronic bronchitis (AECB) are commonly encountered acute LRTIs. CAP displays an annual incidence of 5-11 per 1,000 population, with higher rates among the elderly. Notably, it stands as a leading cause of death from infectious diseases in developed countries and poses significant morbidity and mortality challenges in developing nations, with annual medical costs surpassing $10 billion in the US alone. Mortality rates associated with CAP escalate with illness severity, with rates below 5% for outpatients, 10% for hospitalized cases, and exceeding 30% for those requiring intensive care.

1.1.3 Urinary tract infections

Urinary tract infections (UTIs) stand as one of the most widespread bacterial infections globally, affecting approximately 150 million people each year[15]. They rank as the fifth most common healthcare-associated infection, with about 62,700 cases documented in acute care hospitals in 2015 alone[16]. UTIs are linked to over 13,000 deaths annually, emphasizing the significant health impact and the pressing need for effective prevention and management strategies[17]. They constitute more than 9.5% of all infections reported by acute care hospitals[16]. In Spain, UTIs are the second most common reason for antibiotic prescriptions. Nearly 60% of women experience at least one episode during their lifetime[18].

UTIs present considerable health risks, particularly affecting infants, elderly men, and females of all ages, often resulting in recurring episodes, severe kidney infections, sepsis, renal damage in young children, premature birth, and complications arising from frequent antibiotic usage, including antibiotic resistance and *Clostridium difficile* colitis[19].

Clinically, UTIs are classified as either uncomplicated or complicated. Uncomplicated UTIs primarily affect healthy individuals without structural or neurological urinary tract abnormalities, further categorized into lower UTIs (cystitis) and upper UTIs (pyelonephritis). Various risk factors contribute to cystitis, including female gender, previous UTI, sexual activity, vaginal infections, diabetes, obesity, and genetic predisposition. Complicated UTIs are associated with conditions compromising urinary tract function or host defense mechanisms, such as urinary obstruction, neurological disorders leading to urinary retention, immunosuppression, renal dysfunction, pregnancy, and the presence of foreign bodies like stones, catheters, or other drainage devices[20]. Indwelling catheters account for a significant proportion of complicated UTIs in the U.S., resulting in approximately 1 million cases annually and contributing to increased morbidity and mortality, making them the primary cause of secondary bloodstream infections[19]. Risk factors for catheter-associated UTIs include prolonged catheterization, female gender, advanced age, and diabetes[21]. Around 12%-16% of adult hospital inpatients undergo indwelling urinary catheter placement during their hospitalization, with each day of catheterization carrying a 3%-7% increased risk of catheter-associated urinary tract infection acquisition[22].

UTIs are caused by a spectrum of Gram-negative and Gram-positive bacteria, as well as certain fungi. The most prevalent causative agent for both uncomplicated and complicated UTIs is uropathogenic *Escherichia coli* (UPEC), being responsible of 80 % of the infections. Following UPEC, other bacteria play significant roles, such as *Klebsiella pneumoniae*, *Staphylococcus saprophyticus*, *Enterococcus faecalis*, group B Streptococcus, *Proteus mirabilis*, *Pseudomonas aeruginosa* and *Candida spp*. While the prevalence of these agents varies between uncomplicated and complicated UTIs, UPEC consistently maintains its status as the most predominant causative agent in both scenarios[19].

1.2 Diagnostic of bacterial infections

Bacterial diagnosis is a critical process in healthcare for identifying the specific bacteria causing an infection. It plays a vital role in preventing the overuse of broad-spectrum antibiotics, which can lead to the disruption of normal bacterial flora and the development of AMR. To address this, the use of rapid and sensitive diagnostics to identify the bacterial cause of infection is essential to apply a targeted treatment with narrow-spectrum antibiotics[23]. By accurately identifying the pathogens, healthcare providers can prescribe the most effective and specific antibiotics, reducing the reliance on broad-spectrum antibiotics and helping to mitigate the

development of AMR[24]. Therefore, bacterial diagnosis plays a crucial role in guiding appropriate antibiotic therapy, ultimately contributing to the effective management of bacterial infections.

In the diagnosis of LRTI, the selection of appropriate sampling methods is essential for accurate identification and subsequent treatment. Among the primary samples collected for this purpose, several methods stand out, each presenting distinct advantages and challenges.

The foremost nonsterile sample employed in diagnosing LRTIs is sputum, gathered through either spontaneous expectoration or induced collection. For sputum specimens to fulfill their diagnostic purpose in microbiology, they must accurately represent lower respiratory secretions while avoiding contamination by saliva or upper respiratory tract flora. Consequently, the presence of purulence, signaling the existence of inflammatory cells and potential pathogens, is crucial. Such sputum typically presents as thick, opaque, and yellow, green or reddish in color, owing to the abundance of neutrophils, bacteria, and cellular debris. Its consistency should lean towards being mucoid or mucopurulent rather than watery or saliva-like[25].

Assessment of specimen suitability relies on cytological criteria, primarily determined by microscopic examination for the ratio of polymorphonuclear cells to squamous epithelial cells in a low-power field (×10). Specimens falling below acceptable thresholds, containing ≥10 squamous epithelial cells and ≤25 polymorphonuclear cells per field, are deemed invalid and should not undergo further examination. The prevalence of squamous epithelial cells indicates potential contamination with saliva and upper respiratory tract flora, compromising diagnostic accuracy. However, a significant challenge lies in procuring high-quality, purulent sputum, particularly evident in pneumonia cases where sputum production may be limited, especially among older patients[26].

There are other types of samples that can be used for the microbiological analysis of LRTIs, such as bronchoalveolar lavage (BAL). BAL offers a more direct sampling approach, resulting in higher diagnostic accuracy compared to sputum. This technique involves bronchoscopy to access the lower respiratory tract, enabling quantitative culture and precise identification of pathogens. Despite its effectiveness, BAL is an invasive procedure associated with inherent risks like bleeding, infection, or bronchospasm. Additionally, its reliance on specialized equipment and trained personnel contributes to its higher cost compared to sputum collection[26].

Endotracheal aspirate (ETA) is another valuable sampling method, particularly useful in the context of ventilator-associated pneumonia (VAP). ETA can be easily obtained from intubated patients without the need for bronchoscopy, providing a sample from the lower respiratory tract that aids in infection diagnosis. However, its susceptibility to contamination from upper respiratory tract flora or ventilator equipment limits its specificity, especially when compared to BAL[27].

Regarding UTIs, urine is the biological sample used for the diagnosis of this type of infection. One common method for diagnosing UTIs is through the use of urine dipstick tests. These small, disposable sticks contain chemical reagents that react to certain substances in the urine, such as pH, protein, sugar, nitrite, ketones, bilirubin, urobilinogen, red blood cells, and white blood cells. The levels of these biomarkers can indicate urinary infection, such as elevated leukocytes or nitrite levels, or an increase in urine pH. They can also be indicators of other diseases; for instance, high levels of proteins may indicate nephritis (kidney inflammation)[28].

However, while urine dipstick tests provide rapid results, they may not always be conclusive, and further testing, such as urine culture, is often necessary for definitive diagnosis. Urine culture involves growing bacteria from a urine sample in a laboratory, allowing healthcare providers to identify the specific bacteria causing the infection and determine their susceptibility to antibiotics[29].

In addition to laboratory tests, healthcare providers may also consider a patient's symptoms and medical history when diagnosing UTIs. Common symptoms include frequent urination, burning sensation during urination, cloudy or foul-smelling urine, and pelvic pain. Early detection and appropriate treatment are essential for preventing complications and ensuring optimal patient outcomes[29].

1.2.1 Current diagnostic methods: Cell culture

Cell culture stands as the gold standard methodology for detecting and identifying microorganisms in biological fluids. When there's suspicion of a bacterial infection in patients, the typical approach involves isolating colonies of the organism on cultures plates and subsequently identifying the organism's species. Classical methods for bacterial identification rely on morphological and metabolic characteristics[30, 31].

Understanding the microbial composition of the lower respiratory tract is essential in diagnosing and treating respiratory infections, which remain a significant global health concern. The collection and analysis of samples from the lower respiratory tract are crucial steps in elucidating the complex interplay between microbial communities and respiratory health.

The process of isolating and identifying the bacterium is the following (see Figure 1.2): i) Clinical samples are collected and cultured on plates, after an incubation period, colonies are obtained. Parameters like size, texture, colour, along with tests such as the hemolysis reaction (cultured on blood agar) or measuring oxygen requirements, offer valuable insights into the bacterium type at this initial culture stage. ii) Gram stains are applied to isolated colonies, and individual cells are observed under a microscope. iii) Isolated colonies undergo growth on selective culture media, facilitating species identification. This stage typically requires an additional 24-hour growth period, enriching the culture in terms of bacterial quantity[32].

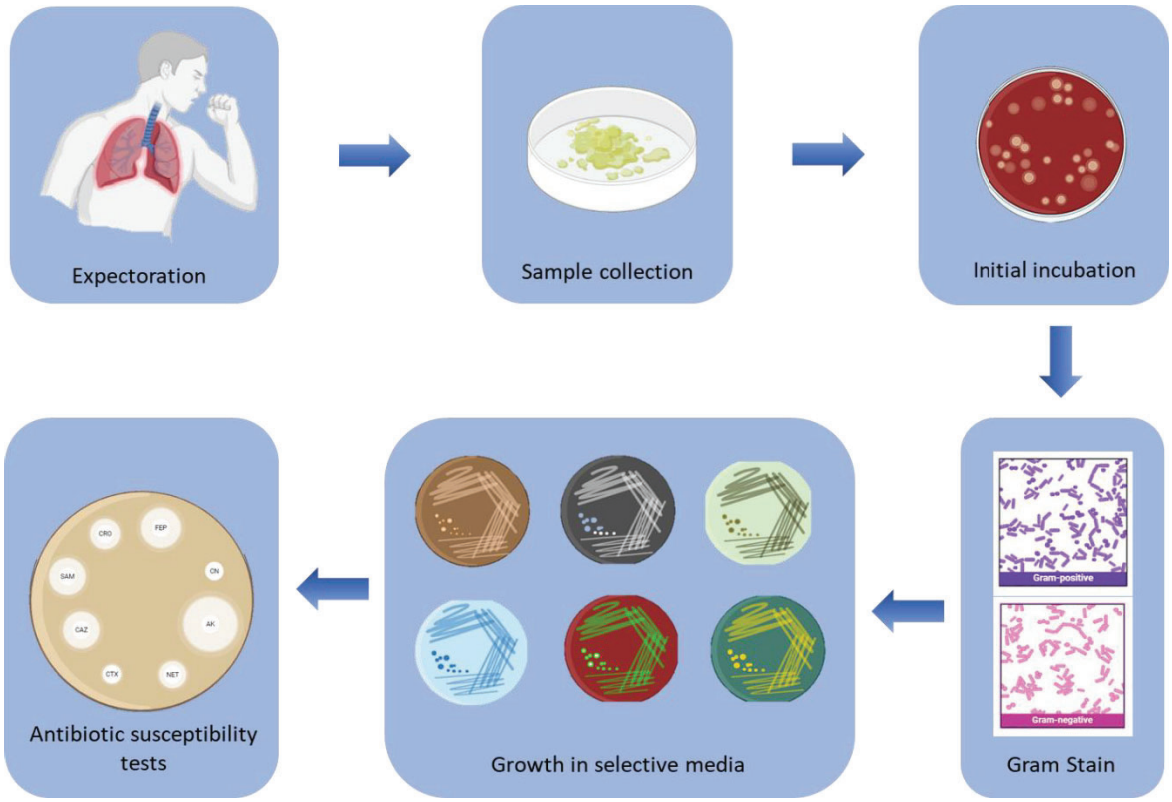

Figure 1.2: A flowchart outlining the diagnostic process utilizing specific culture media for diagnosing bacterial respiratory infections.

Simultaneously, antibiograms can be conducted, wherein the microorganism is cultured on plates with different antibiotics, enabling their diffusion through the medium and creating a concentration gradient. If the bacterium is susceptible to a specific antibiotic, a clear area forms around the antibiotic site, inhibiting bacterial growth. The diameter of this clear area helps determine the Minimum Inhibitory Concentration (MIC), the minimum concentration inhibiting bacterial growth. This technique yields information on the susceptibility of infectious agents to antibiotics, crucial for prescribing appropriate therapy and subsequent patient care[33].

The most notable drawback of these cell culture-based techniques is their lack of sensitivity and lengthy waiting times (a minimum of 48-72 hours) for identifying the infectious agent and determining antibiotic susceptibility. For slow-growing organisms like *Bartonella spp.*, *Francisella tularensis*, *Mycoplasma spp.*, and *Nocardia spp.*, as well as several molds or organisms that are challenging to cultivate through standard bacterial culture systems—such as *Coxiella burnetii*, *Rickettsia spp.*, *Chlamydophila pneumoniae*, and *Tropheryma whipplei*—it is preferable to identify them through immunodiagnostics or molecular techniques[34].

Additional downsides of this methodology arise from the diversity of microorganisms detectable in biological fluids, complicating cell culture protocols and needing different media based on microorganism type or culture conditions. Hence, established guidelines for cell cultures recommend collecting two to three sample sets for each infectious episode, separately stored under aerobic and anaerobic conditions to ensure the detection of all pathogens [5].

For these reasons, alternative diagnostic approaches have been assessed to develop methods that can detect pathogens and overcome the aforementioned drawbacks.

1.2.2 Alternative diagnostic (identification) techniques

The diagnostic methods based on DNA detection, protein detection, immunochemical techniques, or mass spectrometry systems are emerging to address the deficiencies presented by microbiological cultures. The primary goal of these new approaches is to minimize the time required for obtaining results compared to culture, improve sensitivity, and simultaneously maintain the specificity and simplicity of the technique[36].

These novel approaches also aim to provide other advantages, such as the ability to develop multiplexed systems capable of detecting more than one pathogen simultaneously or the development of portable systems that allow measurements to be taken near the patient like Point of Care (PoC) devices. In this latter case, ideally, the physician could obtain the result of the clinical test during the same consultation and prescribe treatment to the patient, significantly reducing the time and costs of diagnosis[37].

1.2.2.1 Mass spectrometry

The method of identifying harmful microorganisms from human specimen cultures has been completely transformed by the use of a mass spectrometer (MS) for microbial detection. Initially, clinical microbiologists were particularly interested in the application of matrix-assisted laser desorption/ionization time-of-flight mass spectrometry (MALDI-TOF MS) to bacteria that are challenging to identify using phenotypical assays[38]. Nowadays, MALDI-TOF- MS has become routine practice in may clinical laboratories. The introduction of this technology has brought more timely and accurate identification of microorganisms with subsequent improvement in diagnosis and reduction in the time to appropriate therapy.

The analytical technique MALDI-TOF MS was developed in the late 1980s for detecting large proteins. A few years later, findings were published that highlighted the potential of MALDI-TOF MS for differentiating and identifying unknown microorganisms. These studies revealed unique mass fingerprints specific to various bacterial species, suggesting the method's efficacy for rapid bacterial and fungal identification. Despite the proclaimed microbiological potential, MALDI-TOF MS did not make its way into clinical microbiology until 2007/2008, with the introduction of the MALDI Biotyper system by Bruker Daltonics[39].

To identify microorganisms from a single isolate colony on a culture plate, the target isolate is first prepared and introduced into a high-vacuum environment. A precise burst of laser ionizes the sample, releasing a "cloud" of proteins that are then accelerated by an electric charge. After passing through the electrode, the "time of flight" of the proteins are recorded using a formula based on the recorded time. A sensor detects the proteins, creating a spectrum that represents the proteomic fingerprint of each sample. The results are generated within a few minutes by matching the isolate to a library of microorganisms[40]. As the technology has evolved, the expansion of the databases containing spectra of known organisms has allowed for the identification of species with similar phenotypic, genotypic, and biochemical properties that was not previously possible.

Two MALDI-TOF MS systems have received approval from the Food and Drug Administration (FDA). The Vitek MS from bioMérieux , capable of identifying 1046 species, including

mycobacteria[41], and the MALDI Biotyper CA System from Bruker, which can detect 424 bacteria and yeast species[42].

The main drawbacks of this method arise from directly analyzing biological samples, primarily because of the presence of various other biomolecules. As a result, an initial stage of sample cultivation remains necessary before conducting subsequent analysis with MALDI-TOF MS. The critical step for successful microbial identification involves distinguishing microorganisms from host cells[43].

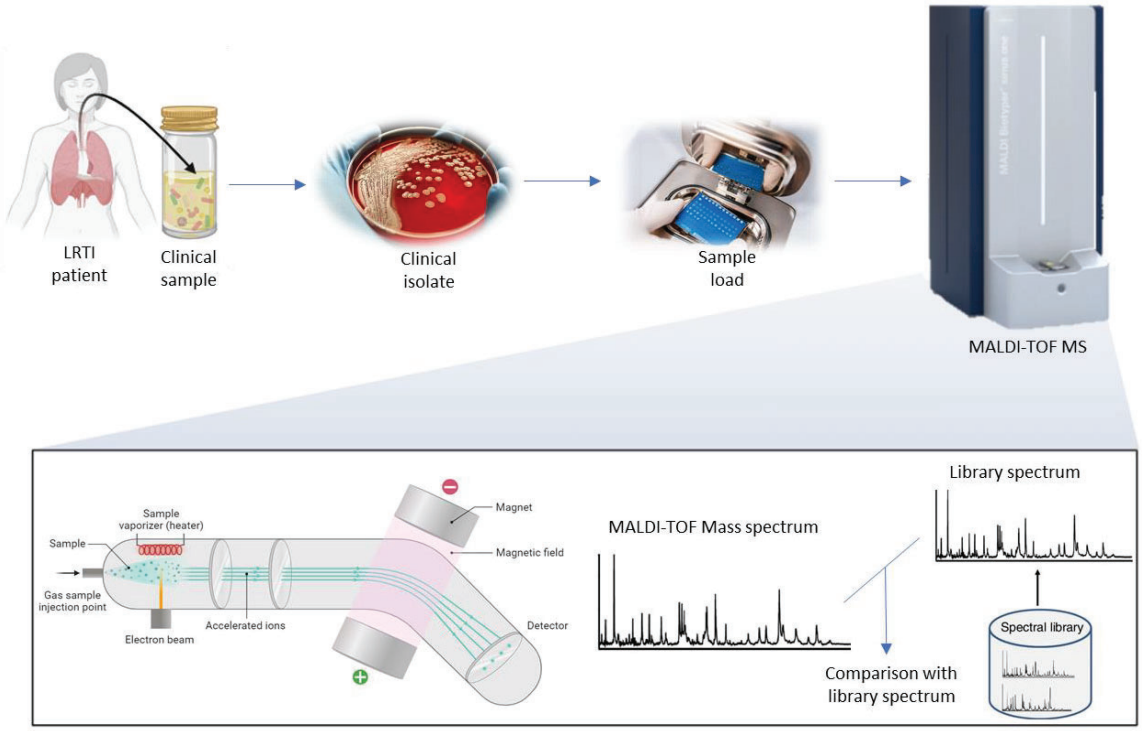

Figure 1.3: A colony is transferred from a culture plate to a location on a MALDI-TOF MS target plate (a reusable or disposable plate with several test spots) using a plastic or wooden stick, loop, or pipette tip. Testing can be done on one or many isolates at once. On the target plate, cells are subjected to formic acid treatment. After applying 1-2 µL of matrix, the area is dried. The plate is inserted into the MALDI-TOF MS's ionisation chamber. The programme creates a mass spectrum, which is then compared to a database of mass spectra to identify the organism.

Regarding blood culture samples, direct detection is indeed possible after a period of incubation, as they typically involve monomicrobial infections in the majority of cases. A positive blood culture bottle typically contains approximately 10^8 CFU·mL^{-1}, well exceeding the MALDI-TOF MS identification limit (10^4 to 10^5 CFU·mL^{-1})[44]. However, since MALDI-TOF MS discriminates only based on protein content size, it measures proteins from the blood culture, thereby reducing spectrum matching and lowering identification/confidence scores. A purification of bacterial cells can be easily performed to solve this problem[45].

As an exceptional case, some studies have investigated the direct application of MALDI-TOF MS technology to urine samples, showing promising results when the urine contains more than 10^5 CFU·mL^{-1} [44]. To enhance MALDI-TOF MS sensitivity with direct clinical samples, specific protocols involving membrane filtration and magnetic separation to collect bacteria and produce an enriched solution for MS analysis have been utilized, resulting in improved detection sensitivity of MALDI-TOF MS to 13 CFU·mL^{-1} [46]. However, challenges in reliably identifying

polymicrobial infections and database matching issues arising from urinary proteins such as defensins are limitations of this approach. Other sample types, like cerebrospinal fluid, may also undergo direct testing[40].

Nowadays, for organisms commonly encountered in the clinical laboratory, MALDI-TOF MS can accurately identify them. However, there are still some exceptions when there exists an inherent similarity between the microorganisms. For example, MALDI-TOF MS is currently unable to differentiate *E. coli* from *Shigella* which could be related to the fact that both microorganisms have been suggested to be the same according to taxonomists [47]. There have also been reported problems to distinguish between the *Mycobacterium tuberculosis* complex, *Mycobacterium abscessus complex*, and the *Mycobacterium avium complex*[48, 49].

Another challenge lies in the absence, up to this point, of implementing antimicrobial susceptibility identification through this technique. Due to heightened concerns surrounding strains like Methicillin-resistant *Staphylococcus aureus* (MRSA), certain studies have shifted focus towards identifying MRSA with MALDI-TOF MS and machine learning [50, 51]. For the case of *P. aeruginosa*, methods have recently been developed for detecting strains resistant to colistin using this technique. The test relies on detecting modified lipid A through the addition of 4-amino-l-arabinose (l-ara4N) molecules to one or two phosphate groups in colistin-resistant strains[52].

1.2.2.2 Polymerase chain reaction

Polymerase Chain Reaction (PCR) revolutionized molecular biology and diagnostics by providing a powerful and efficient method for amplifying DNA. Developed in the 1980s by Kary Mullis, PCR has become a fundamental technique with widespread applications in various scientific disciplines. This technology enables the exponential replication of specific DNA sequences, allowing the generation of an abundance of genetic material from small starting amounts[53].At its core, PCR involves a cyclic process of denaturation, annealing, and extension, driven by a heat-stable DNA polymerase enzyme. The denaturation step separates the DNA strands, annealing facilitates the binding of primers to the target sequence, and extension leads to the synthesis of complementary DNA strands. Through repeated cycles, the targeted DNA segment is exponentially amplified, creating a substantial quantity for subsequent analysis[53].

Quantitative PCR (q-PCR) involves monitoring the amount of obtained product using markers, typically fluorescent, to quantify the number of amplifications obtained. Between the drawbacks of this technology is that samples for DNA isolation may initially contain very low numbers of target bacteria, which may lead to false negative results. Pre-enrichment of sample in culture media could be placed prior to the qPCR to overcome this problem. On the other hand extraction of the DNA from the culture media is easier than that from the complex clinical samples, which are much more heterogeneous in terms of composition[54]. Finally, one of the most important disadvantages of qPCR, is its inherent incapability of distinguishing between live and dead cells.

Reverse transcriptase PCR (RT-PCR) is a technique that produces complementary DNA from RNA found in the sample. The susceptibility of mRNA to degradation allows the presence of mRNA sequences to act as an indicator of viable pathogens in the sample, providing a means to distinguish between viable and non-viable microorganisms and avoiding the detection of dead microorganisms[55].

Another variant, the multiplex PCR, enables the simultaneous detection of diverse microorganisms by introducing different primers to amplify specific DNA regions for each microorganism. Although multiplex PCR has so many advantages, also presents various drawbacks. As a result, self-inhibition may occur when using several sets of primers in the reaction. This implies that different target sequences' amplification may be hampered by certain primers, producing conflicting findings. Moreover, the effectiveness of multiplex PCR may vary depending on the target sequence or template used. For certain targets, variations in primer binding sites, GC content, or template complexity might impact amplification efficiency. The amplification efficiency of multiplex PCR reactions may be lower than that of singleplex PCR reactions. This is due to the possibility of competition for reaction components like dNTPs and enzymes when primer dimer sets are present in the same reaction. Multiplex PCR also requires a single set of amplification conditions for each PCR product, limiting flexibility in optimizing conditions for individual sequences[56].

Although most of the times PCR methods requires of a pre-culture of the sample, various FDA-approved devices based on PCR methodology can be found in the market for the identification of microorganisms. These devices can directly test a clinical sample without the need for performing a previous culture, saving a significant amount of time. They can analyse the clinical sample within less than 5 hours[57]. However, these techniques necessitate supplementary steps like pipetting, vortex mixing, and centrifugation. They also demand sophisticated equipment for temperature control and fluorescence detection, along with skilled professionals and intricate sample preparation protocols. Additionally, multiplex qPCR detection assays mandate costly probes for labeling individual target sequences[58].

The Unyvero A50 Molecular Diagnostic Platform by Curetis was FDA-approved in 2018. It can identify pathogens associated with over 90% of pneumonia cases in hospitalized patients, along with genetic antibiotic resistance markers in endotracheal aspirate samples[59]. The device demonstrates a specificity of 99.5% and a sensitivity of 91.4% across all LRTI panel pathogens[60]. There are plans to seek FDA approval for expanding the sample types to include bronchoalveolar lavage[61]. Additionally, the development of a smaller unit, Unyvero A30 RQ, is underway, promising faster results (within 90 minutes)[30].

Another PCR test, which was approved by the FDA in 2018, is the BIOFIRE FilmArray System (RT-PCR/nested multiplex PCR) Pneumonia Panel by bioMérieux. This assay employs sputum, endotracheal aspirate and bronchoalveolar lavage sample types, and within an hour it can detect 18 bacteria, 9 viruses that cause pneumonia and other LRTIs, and 7 genetic markers of antibiotic resistance. The specificity of the assay is 97% with a sensitivity of 96%[62].

As a consequence of the commercialization of these devices, numerous published studies have compared their performance to the gold standard, which is culture. Generally, these studies indicate that the Unyvero System demonstrates an overall sensitivity for bacterial detection ranging from 63.5% to 88.8% for respiratory panels[63-65]. In the case of the Filmarray, specifically with the pneumonia panel, sensitivities appear to be higher, ranging between 79.0% and 98.0% depending on the study[66, 67]. However, it seems that the high specificity of these devices ultimately leads to false positives. For instance, Young Yoo *et al.*[66], in a study involving 99 sputum and endotracheal aspirate samples, discovered discrepancies in 45 samples. These discrepancies arise because the Filmarray detects the presence of more bacteria than the culture does.

Therefore, although in most positive samples, both methods agree on one bacterium as the cause of the infection, the Filmarray indicates the presence of other bacteria in the sample, resulting in false positives. It is important to note that the majority of patients in this study had received antibiotics before sampling, potentially influencing the findings to show a higher sensitivity for detecting low levels of nucleic acids from organisms that are difficult to culture or nonviable organisms[68]. Nonetheless, distinguishing between colonizing organisms and pathogens remains challenging because levels of bacteria below the culture threshold can yield positive results in Filmarray.

Regarding the detection of resistance genes, there are several reported cases where the detection of a genetic marker of antimicrobial resistance cannot definitively be linked to the microorganisms detected. This is because there may be other organisms present that are not detectable with Filmarray pneumonia panel or are below the limit of detection of this assay. The inability to link a resistance gene with a pathogen was particularly noted for CTX-M and carbapenemase genes when Filmarray yielded two or more pathogens in the same sample that could potentially contain the resistance markers. Therefore, the results from Filmarray need to be used in conjunction with culture results to determine susceptibility or resistance[66, 67].

Despite the drawbacks of this technique, studies have indicated that it has allowed for modifications in the treatment administered to patients, such as changes in the escalation and de-escalation of antibiotics in suspected pneumonia cases. It was found that Filmarray results potentially guided antibiotic treatment changes in 51.0% and 41% of suspected pneumonia cases in the studies performed by Young Yoo *et al.* and Lee *et al.*[66, 67]. Notably, Filmarray may have prompted the discontinuation of antipseudomonal β-lactam antibiotics (piperacillin–tazobactam) when *P. aeruginosa* and *Acinetobacter* species were not detected by the assay.

1.2.2.3 Immunochemical assays

Immunochemical assays are designed to detect and quantify the presence of molecules in a solution, utilizing immunoglobulins or antibodies as specific recognition elements. The antibody's binding site recognizes an epitope on the antigen's surface. The analytical sensitivity of immunoassays largely depends on the affinity of the antibodies used and the type of labeling or transduction principle employed. The nature of labeling can be very diverse: radioisotopes, enzymes, fluorophores, chemiluminescent compounds, or magnetic markers[69].

One of the most widespreadly used immunochemical assays is the ELISA (enzyme-linked immunosorbent assay), which involves the combination of a solid support with the enzymatic labelling of one of the immunoreactants. The solid support often takes the form of a 96 or 384-well microplate, allowing high-throughput screening for the simultaneous processing of multiple samples, thereby enhancing the efficiency of the technique. It is currently consider as a gold standard technique for protein quantification reaching limits of detectability in the order of $pg \cdot mL^{-1}$ [70]. The choice of the ELISA format depends on the type of analyte being detected. Typically, the sandwich format is employed for larger analytes, while the competitive format is used for the detection of low molecular weight molecules. In competitive assays, the direct format is used when the Ag-Ab complex is detected through the labeling of one of the two immunoreactants, or indirect when the signal is generated by a labeled secondary antibody. In competitive formats, the signal is inversely proportional to the analyte concentration[71].

ELISAs find applications in various settings, serving as rapid screening tests for bacteria, viruses, fungi, autoimmune diseases, blood typing, food allergens, presence of the pregnancy hormone hCG, forensic toxicology, laboratory and clinical research, and numerous diagnostic scenarios[71]. ELISAs are also a valuable tool for the detection not only of antigens but also of antibodies, and, in this sense, many of the immunochemical techniques for detecting infectious diseases are based on serological studies aimed at detecting circulating antibodies in the blood.

One of the advantages that makes ELISAs one of the most widely used diagnostic tools in healthcare centers is their easy automation. Automated immunoassay analyzers, designed to conduct immunoassays autonomously, significantly reduce manual labor typically required in traditional diagnostic procedures. Automation drastically reduces sample processing time, leading to faster turnaround times and more accurate patient diagnoses, particularly crucial in emergency situations where timely findings can mean the difference between life and death. These analyzers ensure accuracy and precision by effectively managing incubation periods, volumes, and other variables, thus minimizing human error. Additionally, they have the capacity to perform multiple tests simultaneously on a single sample, enabling the concurrent detection of numerous markers or analytes in a single run. This not only saves time but also conserves valuable patient samples, enhancing efficiency and resource utilization[72].

One of the most commonly used ELISAs in clinical diagnosis is for the detection of the human immunodeficiency virus (HIV). There are several FDA-approved tests for its detection that combine serological and antigen tests. One of them is the ARCHITECT HIV Ag/Ab Combo by Abbott Diagnostics. The ARCHITECT HIV Ag/Ab Combo assay is a chemiluminescent microparticle immunoassay designed for the simultaneous qualitative detection of the viral capsid protein P24 from the virus and antibodies (IgG and IgM) to HIV type 1 and/or type 2. The detection can be done in less than 30 minutes and with only 150 µL of plasma or serum[73].

1.2.2.3.1 Lateral flow immunoassay (LFIA)

Other immunoassay format is the lateral flow immunoassays (LFIA), which have also had significant applications due to their simplicity and the advantage of being able to interpret the

result visually. It is a paper-based platform designed for the rapid detection and quantification of analytes in complex mixtures. In this method, the sample is applied to a test device, and the results are visible within 5 to 30 minutes. The cost-effectiveness and ease of production of LFIAs have led to their widespread application in various fields requiring rapid tests. These tests find extensive use in physician's offices, hospitals, and clinical laboratories, facilitating both quantitative and qualitative detection of specific antigens, antibodies, and products of gene amplification[74].

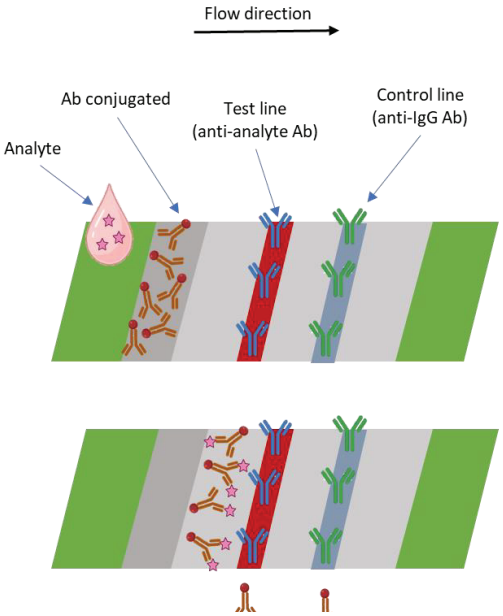

Figure 1.4: Illustration of the assay's mechanism: At the top, the sample is placed on the sample pad and moves towards the conjugate. In the middle, the conjugated antibodies attach to the target analyte, and at the bottom, they migrate to the test line where the captured target analyte is detected and to the control line.

The LFIA is based on the simple idea that a liquid sample, or its extract containing the analyte of interest, flows between different zones of polymeric strips through capillary action. The sample is applied to the absorbent sample pad, which is at the end of the strip. The conjugate release pad, which is filled with antibodies specific to the target analyte and conjugated to coloured or fluorescent particles (most often colloidal gold and latex microspheres), is passed through by the treated sample. The sample moves into the detection zone along the strip with the conjugated antibody attached to the target analyte. This zone consists of a porous membrane, often made of nitrocellulose, on which particular biological elements, primarily antigens or antibodies, have been immobilised in lines. Their job is to react with the antibody that has been conjugated to the analyte. While a response on the control line indicates appropriate liquid flow through the strip, recognition of the sample analyte produces a response on the test line. The read-out, which is shown by the lines in the detection zone, can be evaluated using a specialised reader or by eye (see Figure 1.4). Additional test lines containing antibodies specific to various analytes can be immobilised in an array configuration to allow testing of numerous analytes at the same time and under the same conditions[75].

Clinical diagnostic tests typically occur in central laboratories, often yielding results after hours or even days. Given the critical importance of timely decisions in many cases, the potential advantages of LFIA in the clinical settings are evident. LFIA can significantly contribute to screening, diagnosis, prognosis, monitoring, and surveillance, facilitating immediate clinical assessments that can profoundly impact disease management. This immediate assessment can reduce workload, streamline workflow, improve clinical care, enhance patient outcomes, and potentially lower costs. Furthermore, LFIA usage can enable patients to receive diagnosis and treatment within the same consultation, reducing clinical visits and addressing issues related to therapy delays. Long-term benefits include the ability of LFIA to distinguish between bacterial and viral infections, thereby reducing antibiotic misuse and mitigating antibiotic resistance[76].

LFIA's suitability for use outside laboratory settings makes them valuable not only in hospital laboratories but also in hospital wards, clinics, health centers, physicians' offices, and even for self-testing at home[77].

The success of LFIA in the clinical field can be attributed to its direct impact on human health and its initial applications for clinical purposes. Despite the relative complexity of biological fluids, the types of samples used are limited, including blood, saliva, urine, nasopharyngeal swabs, and stools. Once appropriate sample treatment is defined, analysis becomes relatively straightforward. Sample handling and treatment may involve various methods depending on the sample type, such as plasma separation, filtration, cellular lysis, mucin breakdown, or pH adjustment. In some cases, these treatments can be performed using specialized sample pads, eliminating additional steps[78].

Due to the COVID-19 pandemic, a large number of lateral flow tests have been approved by regulatory agencies for the detection of viral proteins. The first antigen test that did not require interpretation with an instrument and was approved by the FDA was the Abbott BinaxNOW COVID-19 Ag Card. This test was able to detect the nucleocapsid protein from the virus from a nasopharyngeal swab as a sample, providing a qualitative result in 15 minutes with a detection limit of 4.04×10^4 copies/swab[79].

In the market, a wide variety of lateral flow tests for the detection of pathogenic microorganisms can be found. However, most tests for bacterial detection are developed for the food industry and enable detection in matrices such as milk, juice, water, or extracts from various foods. Regarding detection in clinical samples, there is much less variety, and the majority of developed tests are targeted against viruses[80]. An example of a commercial lateral flow test for the bacterial detection of respiratory tract diseases is the detection of *Streptococcus pyogenes* with throat swabs. The BinaxNow StrepA, developed by Abbott, has a sensitivity of 92% and specificity of 100%, providing results in 6 minutes[81].

1.2.2.4 Biosensors

A biosensor is a specialized analytical device that combines a biological component (bioreceptor) with a physicochemical detector (transducer) to convert a biological response into a measurable signal. Every biosensor should consist of three fundamental components. Firstly, the biorecognition element, which is in direct contact with the target analyte and the sensing surface. Next, a transducer, which is responsible for converting the biological signal produced by the receptor-target interaction into a measurable output value. Lastly, a read-out system is needed to interpret and display the final data[82].

These devices can be classified based on the bio-recognition element or the transduction method. Depending on the bio-recognition element, there are catalytic biosensors, which are based on the catalytic properties of active enzymes, or affinity biosensors, which rely on the interaction of the analyte with the receptor, leading to the formation of a complex (analyte-receptor). In this type of receptors, nucleic acids, proteins, cells, microorganisms or tissues can be utilized [83]. Antibodies are frequently the biological units of these devices leading to immunosensors as one of the most relevant groups of biosensor devices.

On the other hand, considering the type of transducer employed, we encounter (i) electrochemical biosensors, which measure electric signal fluctuations resulting from the

interaction between the analyte and the receptor in contact with the surface of an electrode[84]. (ii) Piezoelectric biosensors enable the monitoring of changes in the frequency of a piezo element. These include bulk acoustic wave sensors, crystal quartz microbalances, and surface acoustic waves. Additionally, as part of physical transducers, thermometric sensors measure slight changes in temperature generated by the binding between the analyte and bioreceptor[85]. (iii) Optical biosensors measure photons, specifically detecting alterations in light properties due to the interaction of these photons with bioreceptors, triggered by biological, chemical, or physical responses[86]. Key examples include the evanescent wave, surface Raman spectroscopy, fluorescence, infrared, or plasmonic methods[69].

The goal of biosensors is to offer a fast, real-time, sensitive, and specific detection system. Ideally, it aims to be a compact, portable system requiring minimal or no sample treatment, capable of multi-detection, and with a low production cost. Biosensors can reduce even more the analysis time compared with an immunoassay, completing the analysis within minutes. However, the cost associated with the development of sophisticated equipment is one of the drawbacks[87].

In recent decades, a large number of biosensor systems have been developed for the detection of various pathogens. However, the number of biosensors capable of measuring in clinical samples is more limited. Table 1.1 displays different types of biosensors published for the detection of pathogenic bacteria.

Table 1.1: Different types of biosensors for the detection of pathogenic bacteria, classified according to the type of transduction

Transductor	Target analyte	Type	Bioreceptor	LOD/CFU · mL^{-1}	Matrix	References
Electrochemical biosensors	*S. aureus*	Amperometric	Ab	10^3	Yougurt and milk	88
	K. pneumoniae	Impedometric	Clavanin A peptide	10^3	Buffer	89
	E. coli	Impedometric	E. coli-specific phage (T4)	800	Buffer	90
Piezoelectric biosensors	*P. aeruginosa*	QCM	Aptamer	52	Simulated blood	91
	Listeria monocytogenes	AAP-EMSC	Ab	10^2	Milk	92
	Salmonella Typhimurium	QCB	Ab	10	Meat Extract	93
Optical biosensors	*S. Aureus*	SPR	Lectin	10^4	Serum	94
	E. Coli	SPR	Ab	10^4	Buffer	95
	S. aureus	SERS	Ab	10	Buffer	96

1.3 Pseudomonas aeruginosa

Pseudomonas aeruginosa, identified as a gram-negative bacterium, can provoke a diverse range of infections by adapting and thriving in challenging environments. This opportunistic pathogen takes advantage of breaches in tissue barriers, utilizing a variety of biological mechanisms to overcome the host immune system. This microorganism has developed an extensive adaptive response and significant resistance to both immune system and antibiotics, particularly in the context of chronic infections [97]. This is notably observed in individuals with cystic fibrosis (CF), a genetic disorder causing thick mucus production, and affecting the respiratory system. Individuals with CF often develop chronic lung infections, with *P. aeruginosa* being a common pathogen. This bacterium, known for its antibiotic multi-resistance profile, leads to persistent respiratory issues, causing progressive lung damage and declining function. Treatment involves aggressive antibiotic therapy, but eradicating *P. aeruginosa* infections is challenging[98].

P. aeruginosa, when in a biofilm state, exhibits resilience in hypoxic atmospheres and other exceptionally challenging environments. The treatment of *P. aeruginosa* infections poses considerable difficulties due to its rapid mutations and its ability to adapt, acquiring resistance to antibiotics[99]. Moreover, *P. aeruginosa* ranks among the primary pathogens responsible for hospital-acquired infections, particularly the ones related with medical devices like ventilation systems, where it thrives on moist surfaces [100]. Significantly, *P. aeruginosa* is classified as one of the multi-drug resistance (MDR) ESKAPE pathogens, part of the acronym representing *Enterococcus faecium*, *Staphylococcus aureus*, *Klebsiella pneumoniae*, *Acinetobacter baumannii*, *P. aeruginosa*, and *Enterobacter* (Figure 1.5). Notably, *P. aeruginosa*, especially with carbapenem resistance, has been categorized as "critical" by the WHO, emphasizing the urgent need for novel antibiotics in clinical settings. Novel antibiotics are urgently required to address the escalating challenge posed by MDR bacterial infections, which claim nearly 700,000 lives annually according to epidemiological studies[101]. In European populations, *P. aeruginosa*

exhibits a resistance rate of 12.9%, emphasizing its role as a significant contributor to hospital-acquired infections resistant to conventional antibiotics[102].

The 2016 "Estudio de prevalencia de las Infecciones Nosocomiales en España" (EPINE) survey highlights *E. coli* and *P. aeruginosa* as the leading causes of hospital-acquired infections in Spain, with *P. aeruginosa* accounting for 10.5% of clinically isolated bacterial infections in 2019[103]. In the context of community-acquired infections with intensive care unit (ICU) admission, it held the third position, followed by *E. coli* and *S. aureus*. In such settings, the mortality rate for *P. aeruginosa* bacteraemia infections is between 20-39%. Moreover, when it comes to ventilator-associated pneumonia (VAP) caused by *P. aeruginosa*, the mortality rate is notably higher, reaching 44% [104].

In the 2020 annual epidemiological report from the European Center for Disease Control and Prevention (ECDC) *P. aeruginosa* was found to be the fifth most common pathogen in European hospitals, causing 6.2 % of the infections[105]. Similarly, 7.1% of the healthcare-associated infections are caused by *P. aeruginosa* in the United States [106]. Moreover, data from the China Antimicrobial Surveillance Network (CHINET) identifies *P. aeruginosa* as the fourth most common nosocomial infection globally, accounting for 7.96% of clinically isolated pathogenic

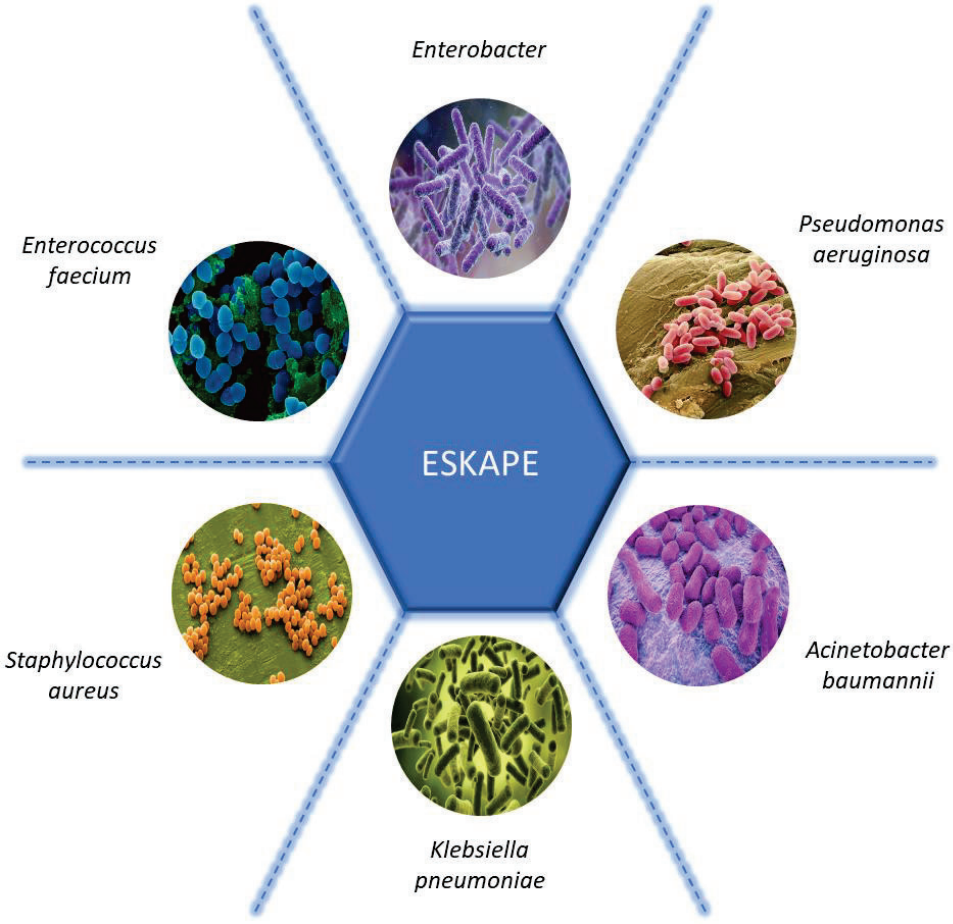

Figure 1.5: The ESKAPE pathogens (Enterococcus faecium, Staphylococcus aureus, Klebsiella pneumoniae, Acinetobacter baumannii, Pseudomonas aeruginosa, and Enterobacter species) are the leading cause of nosocomial infections throughout the world.

strains[107]. In summary, *P. aeruginosa* emerges as a global, rather than a localized, major threat to human health, necessitating immediate attention and novel antimicrobial strategies.

1.3.1 Diagnosis of *P. aeruginosa*

Rapid and accurate detection of *P. aeruginosa*, especially in the early stages of infection, is essential for adequate and appropriate patient treatment to avoid life-threatening conditions and stop the spread of antibiotic resistance[108]. Ideally, appropriate therapy should be given before biofilm has been established.

Traditional approaches for identifying *P. aeruginosa* rely on the bacterium's biological traits observed under specific culture conditions. These traits include determining its Gram-negative or Gram-positive status and evaluating the physicochemical activities of products produced by the bacteria like arginine dihydrolases, oxidases, acetamidases, and PYO[109].

Initially, a sample must be grown in a general medium so that any microorganism can grow. Then, selected colonies are grown in the corresponding selective medium (Figure 1.2). There are different types of selective media for the growth of *P. aeruginosa*. One of them is enriched media with 0.03% cetrimide; for example, the King's B medium supplemented with cetrimide (CTA 2). This media induces strong fluorescence when *P. aeruginosa* is incubated at 42°C due to the production of different fluorophores, while other bacteria are unable to produce fluorescence at these temperatures, making it suitable for the diagnosis of the bacterium [110]. Additionally, *P. aeruginosa* can produce ammonia by breaking down acetamide, by the action of acylamidases. The resulting ammonia production induces a pH change that can be detected using a pH indicator. Based on this mechanism, other media have been developed, exhibiting higher sensitivity and selectivity than cultures supplemented with cetrimide[111].

A wide range of immunochemical techniques has also been developed for the specific identification of *P. aeruginosa*. To achieve this, antibodies capable of detecting the bacterium had to be developed. In such case, as mentioned above, the limit of detection achieved rarely exceeds 10^3 CFUs in culture media. In most cases, antibodies have been developed against extracellular proteins such as exotoxin A, elastase, alkaline phosphatase, and phospholipase C[112]. Antibodies targeting alkaline protease exhibited the highest specificity, whereas those against elastase demonstrated the highest sensitivity. Despite specificity being a significant advantage of ELISA, numerous secreted proteins from *P. aeruginosa* share considerable homology with those of other bacteria, posing a risk of false-positive detection[113].

Serological studies have also been conducted as a diagnostic strategy for *P. aeruginosa* infections. The majority of these studies detect antibodies produced by the host against the lipopolysaccharides (LPS) of the bacterial surface. A study conducted with CF patients demonstrated that high levels of IgG and IgA can be detected at advanced stages of the infection. In contrast, IgM levels increase during the initial stage of the infection but remain stable in more advanced stages[114]. In another study conducted with CF patients, anti-LPS antibodies were detected in the saliva of 15 out of 17 patients and in the serum of all 13 patients tested, while none were found in the 37 healthy subjects[111]. The main disadvantages of this type of tests are related to the delay in the appearance of antibodies, which delays diagnosis, especially in the early stages. Antibody production varies between individuals, complicating diagnostic criteria. These tests may fail to detect low antibody levels and produce false positives due to cross-

reactivity. Despite the challenges, they are valuable when combined with other methods and considered alongside the patient's medical history and symptoms[115].

Regarding techniques based on molecular biology, over the years, a large number of PCR assays have been developed for the detection of *P. aeruginosa*. The most critical aspect of this process is deciding which fragment of genetic material to identify. The most commonly used targets include the following: 16S rRNA, *toxA*, *ecfX*, *algD* GDP mannose, *gyrB*, *fliC*, and *oprL*[116-118]. Specificity is crucial for the success of conventional PCR, but it is also the most common cause of failure in PCR detection. Several studies have demonstrated that the genes showing the highest specificity are *ecfX* and *gyrB*[119-122]. As an example, Tang and co-workers published a study in which they developed a biosensor that combines the PCR technique, targeting the *gyrB* gene, with magnetic nanoparticles and chemiluminescence, achieving a detection limit of 10 $CFU \cdot mL^{-1}$ in culture media with great selectivity[123].

Regarding detection through electrochemical methods, the majority of techniques are based on the detection of PYO or other quorum-sensing molecules due to their redox properties. An example is the one published by Webster and coworkers, who reported a disposable carbon electrode sensor capable of directly detecting PYO in cultures, blood, urine, sputum, and bronchoalveolar lavage (corresponding limit of detection (LOD) in µM respectively: 0.18, 0.16, 1.81, 0.13, and 0.14). Detection is carried out using square wave voltammetry and takes around 5 minutes without the need of sample treatment[124]. However, up to now these technologies have not been implemented on clinical laboratories.

Despite the existence of multiple techniques, only a few have made it to the market and received approval from regulatory agencies such as the FDA and European Medicines Agency (EMA). Table 1.2 lists assays approved by these agencies for the detection of *P. aeruginosa* in LRTI.

Table 1.2: Diagnostic methods for the detection of P. aeruginosa in LRTI approved by the FDA and CE.

Manufacturer	Assay name	Type of technology	Assay target	Sample types
ELITechGroup	Rapid Polymyxin Pseudomonas	Chemical/Biochemical	Growth/metabolism	Colony/plate
Curetis GmbH	Unyvero Hospitalized Pneumonia	Molecular	DNA	BAL, sputum
Curetis GmbH	Unyvero Lower Respiratory	Molecular	RNA	ETA
Ustar Biotechnologies (Hangzhou) Ltd.	MultNAT Pneumonia Panel	Molecular	DNA	Sputum
bioMérieux	BioFire FilmArray Pneumonia Panel	Molecular	RNA + DNA	BAL, ETA, sputum
Bruker Corporation	MICRONAUT-S Pseudomonas MIC	Growth based	Growth/metabolism	Colony/plate
Alifax	I-dOne	Biophysics	Microorganism	Colony/plate
bioMérieux	VITEK 2 ID and AST Cards	Growth based; Chemical/Biochemical	Growth/metabolism	Colony/plate
Becton, Dickinson and Company (BD)	BD Phoenix panels	Growth based; Chemical/Biochemical	Growth/metabolism	Colony/plate
Beckman Coulter Inc.	MicroScan Conventional Panels	Growth based; Chemical/Biochemical	Growth/metabolism	Colony/plate
Master Diagnóstica	Sepsis Flow Chip	Molecular	DNA	Blood Culture; Colony/plate; Rectal swab

The information in the table has been extracted from FIND diagnostics[125].

As can be seen in the table, the majority do not perform direct detection in the sample but instead require colony isolation first, using molecular techniques. This clearly indicates a significant gap in the market for the development of more technologies capable of rapid and

direct diagnosis in samples. Immunochemical techniques could play an important role in addressing this need.

1.4 The future of infection diagnosis

In the realm of bacterial disease diagnosis, there is a pressing need for a novel approach. Existing methods are either excessively time-consuming, prohibitively expensive, or require sophisticated equipment and expertise, rendering them impractical for widespread implementation across all types of laboratories. The reality is that traditional culture-based methods, while reliable, are notably slow in delivering results. In addition, it's crucial to acknowledge a significant drawback of current diagnostic techniques: their inability to reliably differentiate between bacterial colonization and active infection. This ambiguity can lead to unnecessary treatments or missed opportunities for intervention, ultimately impacting patient care. Hence, any novel diagnostic framework must not only focus on speed and accessibility but also on improving the accuracy of distinguishing between colonization and infection. Addressing this challenge will be pivotal in ensuring optimal patient management and combating the spread of bacterial diseases effectively.

To confront these challenges, a reimagined diagnostic framework is imperative. This framework must prioritize rapidity, affordability, and simplicity, enabling widespread adoption across diverse laboratory environments. By doing so, it would facilitate rapid and accurate identification of bacterial pathogens, thereby enhancing patient care and mitigating the spread of infections. One avenue for exploration lies in the development of novel diagnostic platforms that emphasize rapidity and ease of use. Such platforms could exploit innovative technologies and simplified workflows to achieve faster turnaround times without compromising accuracy. By democratizing access to diagnostic tools, this approach has the potential to transform the landscape of bacterial disease diagnosis, particularly in resource-constrained settings.

Furthermore, a shift towards decentralized diagnostic solutions could prove instrumental in addressing the limitations of centralized laboratory-based testing. Point-of-care testing devices, designed for use in clinical settings or even at home, could enable prompt diagnosis and treatment initiation, thereby reducing the burden on healthcare systems and improving patient outcomes. In essence, the need for a new approach to diagnosing bacterial diseases is clear. By prioritizing speed, affordability, and accessibility, empowering healthcare providers and improving patient outcomes worldwide.

1.5 References

1. Baker, R. E.; Mahmud, A. S.; Miller, I. F.; Rajeev, M.; Rasambainarivo, F.; Rice, B. L.; Takahashi, S.; Tatem, A. J.; Wagner, C. E.; Wang, L.-F.; Wesolowski, A.; Metcalf, C. J. E., Infectious disease in an era of global change. *Nature Reviews Microbiology* **2022,** *20* (4), 193-205.
2. Balkhy, H., Global Antimicrobial Resistance and Use Surveillance System (GLASS) Report 2022 **2022**.
3. Antibiotic resistance threats in the United States, 2019. **2019**.
4. Murray, C. J. L.; Ikuta, K. S.; Sharara, F.; Swetschinski, L.; Robles Aguilar, G.; Gray, A.; Han, C.; Bisignano, C.; Rao, P.; Wool, E.; Johnson, S. C.; Browne, A. J.; Chipeta, M. G.; Fell, F.; Hackett, S.; Haines-Woodhouse, G.; Kashef Hamadani, B. H.; Kumaran, E. A. P.; McManigal, B.; Achalapong, S.; Agarwal, R.; Akech, S.; Albertson, S.; Amuasi, J.; Andrews, J.; Aravkin, A.; Ashley, E.; Babin, F.-X.; Bailey, F.; Baker, S.; Basnyat, B.; Bekker, A.; Bender, R.; Berkley, J. A.; Bethou, A.; Bielicki, J.; Boonkasidecha, S.; Bukosia, J.; Carvalheiro, C.; Castañeda-Orjuela, C.; Chansamouth, V.; Chaurasia, S.; Chiurchiù, S.; Chowdhury, F.; Clotaire Donatien, R.; Cook, A. J.; Cooper, B.; Cressey, T. R.; Criollo-Mora, E.; Cunningham, M.; Darboe, S.; Day, N. P. J.; De Luca, M.; Dokova, K.; Dramowski, A.; Dunachie, S. J.; Duong Bich, T.; Eckmanns, T.; Eibach, D.; Emami, A.; Feasey, N.; Fisher-Pearson, N.; Forrest, K.; Garcia, C.; Garrett, D.; Gastmeier, P.; Giref, A. Z.; Greer, R. C.; Gupta, V.; Haller, S.; Haselbeck, A.; Hay, S. I.; Holm, M.; Hopkins, S.; Hsia, Y.; Iregbu, K. C.; Jacobs, J.; Jarovsky, D.; Javanmardi, F.; Jenney, A. W. J.; Khorana, M.; Khusuwan, S.; Kissoon, N.; Kobeissi, E.; Kostyanev, T.; Krapp, F.; Krumkamp, R.; Kumar, A.; Kyu, H. H.; Lim, C.; Lim, K.; Limmathurotsakul, D.; Loftus, M. J.; Lunn, M.; Ma, J.; Manoharan, A.; Marks, F.; May, J.; Mayxay, M.; Mturi, N.; Munera-Huertas, T.; Musicha, P.; Musila, L. A.; Mussi-Pinhata, M. M.; Naidu, R. N.; Nakamura, T.; Nanavati, R.; Nangia, S.; Newton, P.; Ngoun, C.; Novotney, A.; Nwakanma, D.; Obiero, C. W.; Ochoa, T. J.; Olivas-Martinez, A.; Olliaro, P.; Ooko, E.; Ortiz-Brizuela, E.; Ounchanum, P.; Pak, G. D.; Paredes, J. L.; Peleg, A. Y.; Perrone, C.; Phe, T.; Phommasone, K.; Plakkal, N.; Ponce-de-Leon, A.; Raad, M.; Ramdin, T.; Rattanavong, S.; Riddell, A.; Roberts, T.; Robotham, J. V.; Roca, A.; Rosenthal, V. D.; Rudd, K. E.; Russell, N.; Sader, H. S.; Saengchan, W.; Schnall, J.; Scott, J. A. G.; Seekaew, S.; Sharland, M.; Shivamallappa, M.; Sifuentes-Osornio, J.; Simpson, A. J.; Steenkeste, N.; Stewardson, A. J.; Stoeva, T.; Tasak, N.; Thaiprakong, A.; Thwaites, G.; Tigoi, C.; Turner, C.; Turner, P.; van Doorn, H. R.; Velaphi, S.; Vongpradith, A.; Vongsouvath, M.; Vu, H.; Walsh, T.; Walson, J. L.; Waner, S.; Wangrangsimakul, T.; Wannapinij, P.; Wozniak, T.; Young Sharma, T. E. M. W.; Yu, K. C.; Zheng, P.; Sartorius, B.; Lopez, A. D.; Stergachis, A.; Moore, C.; Dolecek, C.; Naghavi, M., Global burden of bacterial antimicrobial resistance in 2019: a systematic analysis. *The Lancet* **2022,** *399* (10325), 629-655.
5. Team, W. A. P., Lack of innovation set to undermine antibiotic performance and health gains. **22 June 2022**.
6. Butler, M. S.; Henderson, I. R.; Capon, R. J.; Blaskovich, M. A. T., Antibiotics in the clinical pipeline as of December 2022. *The Journal of Antibiotics* **2023,** *76* (8), 431-473.
7. Gigante, V., 2021 Antibacterial agents in clinical and preclinical development: an overview and analysis. **27 May 2022**.
8. Niederman, M. S.; Torres, A., Respiratory infections. *European Respiratory Review* **2022,** *31* (166), 220150.
9. WHO Coronovirus (COVID-19) Dashbaord, World Health Organization. https://covid19.who.int/ (accessed 14/12/2023).
10. Levine, S. M.; Marciniuk, D. D., Global Impact of Respiratory Disease: What Can We Do, Together, to Make a Difference? *CHEST* **2022,** *161* (5), 1153-1154.
11. Forum of International Respiratory Societies . 3rd Edition. European Respiratory Society; 2021. The Global Impact of Respiratory Disease. .

https://www.firsnet.org/images/publications/FIRS_Master_09202021.pdf (accessed 14/12/2023).
12. Quinton, L. J.; Walkey, A. J.; Mizgerd, J. P., Integrative Physiology of Pneumonia. *Physiological Reviews* **2018,** *98* (3), 1417-1464.
13. World Health Organization Global Tuberculosis Program. Global Tuberculosis Report 2020. World Health Organization; 2020. . https://www.who.int/teams/global-tuberculosis-programme/tb-reports/global-tuberculosis-report-2022/tb-disease-burden/2-3-drug-resistant-tb#fig--2-3-1 (accessed 14/12/2023).
14. Mahashur, A., Management of lower respiratory tract infection in outpatient settings: Focus on clarithromycin. *Lung India* **2018,** *35* (2), 143-149.
15. Stamm, W. E.; Norrby, S. R., Urinary tract infections: disease panorama and challenges. *J Infect Dis* **2001,** *183 Suppl 1*, S1-4.
16. Magill, S. S.; O'Leary, E.; Janelle, S. J.; Thompson, D. L.; Dumyati, G.; Nadle, J.; Wilson, L. E.; Kainer, M. A.; Lynfield, R.; Greissman, S.; Ray, S. M.; Beldavs, Z.; Gross, C.; Bamberg, W.; Sievers, M.; Concannon, C.; Buhr, N.; Warnke, L.; Maloney, M.; Ocampo, V.; Brooks, J.; Oyewumi, T.; Sharmin, S.; Richards, K.; Rainbow, J.; Samper, M.; Hancock, E. B.; Leaptrot, D.; Scalise, E.; Badrun, F.; Phelps, R.; Edwards, J. R., Changes in Prevalence of Health Care-Associated Infections in U.S. Hospitals. *N Engl J Med* **2018,** *379* (18), 1732-1744.
17. Klevens, R. M.; Edwards, J. R.; Richards, C. L., Jr.; Horan, T. C.; Gaynes, R. P.; Pollock, D. A.; Cardo, D. M., Estimating health care-associated infections and deaths in U.S. hospitals, 2002. *Public Health Rep* **2007,** *122* (2), 160-6.
18. Moragas Moreno, A.; Fernández-García, S.; Llor, C.; Ouchi, D.; García-Sangenís, A.; Monteagudo, M.; Monfà, R.; Giner-Soriano, M., Diagnostic and Therapeutic Management of Urinary Tract Infections in Catalonia, Spain: Protocol for an Observational Cohort Study. *JMIR Res Protoc* **2023,** *12*, e44244.
19. Flores-Mireles, A. L.; Walker, J. N.; Caparon, M.; Hultgren, S. J., Urinary tract infections: epidemiology, mechanisms of infection and treatment options. *Nat Rev Microbiol* **2015,** *13* (5), 269-84.
20. Josephs-Spaulding, J.; Krogh, T. J.; Rettig, H. C.; Lyng, M.; Chkonia, M.; Waschina, S.; Graspeuntner, S.; Rupp, J.; Møller-Jensen, J.; Kaleta, C., Recurrent Urinary Tract Infections: Unraveling the Complicated Environment of Uncomplicated rUTIs. *Frontiers in cellular and infection microbiology* **2021,** *11*, 562525.
21. Wagenlehner, F. M. E.; Bjerklund Johansen, T. E.; Cai, T.; Koves, B.; Kranz, J.; Pilatz, A.; Tandogdu, Z., Epidemiology, definition and treatment of complicated urinary tract infections. *Nat Rev Urol* **2020,** *17* (10), 586-600.
22. Lo, E.; Nicolle, L. E.; Coffin, S. E.; Gould, C.; Maragakis, L. L.; Meddings, J.; Pegues, D. A.; Pettis, A. M.; Saint, S.; Yokoe, D. S., Strategies to prevent catheter-associated urinary tract infections in acute care hospitals: 2014 update. *Infect Control Hosp Epidemiol* **2014,** *35* (5), 464-79.
23. Kollef, M. H., Broad-Spectrum Antimicrobials and the Treatment of Serious Bacterial Infections: Getting It Right Up Front. *Clinical Infectious Diseases* **2008,** *47* (Supplement_1), S3-S13.
24. Maxson, T.; Mitchell, D. A., Targeted Treatment for Bacterial Infections: Prospects for Pathogen-Specific Antibiotics Coupled with Rapid Diagnostics. *Tetrahedron* **2016,** *72* (25), 3609-3624.
25. Soler, N.; Torres, A., Significance of sputum purulence to guide antibiotic therapy in exacerbations of COPD. *European Respiratory Journal* **2013,** *41* (1), 248-249.
26. Loens, K.; Van Heirstraeten, L.; Malhotra-Kumar, S.; Goossens, H.; Ieven, M., Optimal sampling sites and methods for detection of pathogens possibly causing community-acquired lower respiratory tract infections. *J Clin Microbiol* **2009,** *47* (1), 21-31.

27. de Koff, E. M.; Man, W. H.; van Houten, M. A.; Jansen, N. J. G.; Arp, K.; Hasrat, R.; Sanders, E. A. M.; Bogaert, D., The respiratory microbiota during and following mechanical ventilation for respiratory infections in children. *Eur Respir J* **2021,** *57* (4).
28. In brief: Understanding urine tests. https://www.ncbi.nlm.nih.gov/books/NBK279350/.
29. Dadzie, I.; Quansah, E.; Puopelle Dakorah, M.; Abiade, V.; Takyi-Amuah, E.; Adusei, R., The Effectiveness of Dipstick for the Detection of Urinary Tract Infection. *Can J Infect Dis Med Microbiol* **2019,** *2019*, 8642628.
30. Noviello, S.; Huang, D. B., The Basics and the Advancements in Diagnosis of Bacterial Lower Respiratory Tract Infections. *Diagnostics (Basel)* **2019,** *9* (2).
31. Campbell, S.; Forbes, B. A., *The Clinical Microbiology Laboratory in the Diagnosis of Lower Respiratory Tract Infections*. J Clin Microbiol. 2011 Sep;49(9 Suppl):S30-3. doi: 10.1128/JCM.00789-11.: 2011.
32. Hunt, D. M., *Microbiology and Immunology On-line*. Hunt, R.C: 2015; Vol. INFECTIOUS DISEASE.
33. Truong, W. R.; Hidayat, L.; Bolaris, M. A.; Nguyen, L.; Yamaki, J., The antibiogram: key considerations for its development and utilization. *JAC-Antimicrobial Resistance* **2021,** *3* (2).
34. Mancini, N.; Carletti, S.; Ghidoli, N.; Cichero, P.; Burioni, R.; Clementi, M., The era of molecular and other non-culture-based methods in diagnosis of sepsis. *Clin Microbiol Rev* **2010,** *23* (1), 235-51.
35. Opota, O.; Croxatto, A.; Prod'hom, G.; Greub, G., Blood culture-based diagnosis of bacteraemia: state of the art. *Clinical Microbiology and Infection* **2015,** *21* (4), 313-322.
36. Rentschler, S.; Kaiser, L.; Deigner, H. P., Emerging Options for the Diagnosis of Bacterial Infections and the Characterization of Antimicrobial Resistance. *Int J Mol Sci* **2021,** *22* (1).
37. Reali, S.; Najib, E. Y.; Treuerné Balázs, K. E.; Chern Hui Tan, A.; Váradi, L.; Hibbs, D. E.; Groundwater, P. W., Novel diagnostics for point-of-care bacterial detection and identification. *RSC Advances* **2019,** *9* (37), 21486-21497.
38. Banerjee, S., Empowering Clinical Diagnostics with Mass Spectrometry. *ACS Omega* **2020,** *5* (5), 2041-2048.
39. Kostrzewa, M., Application of the MALDI Biotyper to clinical microbiology: progress and potential. *Expert Review of Proteomics* **2018,** *15* (3), 193-202.
40. Patel, R., MALDI-TOF MS for the diagnosis of infectious diseases. *Clin Chem* **2015,** *61* (1), 100-11.
41. Biomérieux Vitek MS. https://www.biomerieux.es/diagnostico-clinico/productos/vitekr-ms.
42. Bruker Microbial Identification. https://www.bruker.com/en/products-and-solutions/microbiology-and-diagnostics/microbial-identification.html (accessed 08/01/2024).
43. Haider, A.; Ringer, M.; Kotroczó, Z.; Mohácsi-Farkas, C.; Kocsis, T., The Current Level of MALDI-TOF MS Applications in the Detection of Microorganisms: A Short Review of Benefits and Limitations. *Microbiology Research* **2023,** *14* (1), 80-90.
44. Ferreira, L.; Sánchez-Juanes, F.; González-Avila, M.; Cembrero-Fuciños, D.; Herrero-Hernández, A.; González-Buitrago, J. M.; Muñoz-Bellido, J. L., Direct identification of urinary tract pathogens from urine samples by matrix-assisted laser desorption ionization-time of flight mass spectrometry. *J Clin Microbiol* **2010,** *48* (6), 2110-5.
45. Faron, M. L.; Buchan, B. W.; Ledeboer, N. A., Matrix-Assisted Laser Desorption Ionization-Time of Flight Mass Spectrometry for Use with Positive Blood Cultures: Methodology, Performance, and Optimization. *J Clin Microbiol* **2017,** *55* (12), 3328-3338.
46. Guo, Z.; Liu, Y.; Li, S.; Yang, Z., Interaction of bacteria and ion-exchange particles and its potential in separation for matrix-assisted laser desorption/ionization mass spectrometric identification of bacteria in water. *Rapid Commun Mass Spectrom* **2009,** *23* (24), 3983-93.
47. Pupo, G. M.; Lan, R.; Reeves, P. R., Multiple independent origins of Shigella clones of Escherichia coli and convergent evolution of many of their characteristics. *Proc Natl Acad Sci U S A* **2000,** *97* (19), 10567-72.

48. Neuschlova, M.; Vladarova, M.; Kompanikova, J.; Sadlonova, V.; Novakova, E., Identification of Mycobacterium Species by MALDI-TOF Mass Spectrometry. *Adv Exp Med Biol* **2017,** *1021*, 37-42.
49. Body, B. A.; Beard, M. A.; Slechta, E. S.; Hanson, K. E.; Barker, A. P.; Babady, N. E.; McMillen, T.; Tang, Y. W.; Brown-Elliott, B. A.; Iakhiaeva, E.; Vasireddy, R.; Vasireddy, S.; Smith, T.; Wallace, R. J., Jr.; Turner, S.; Curtis, L.; Butler-Wu, S.; Rychert, J., Evaluation of the Vitek MS v3.0 Matrix-Assisted Laser Desorption Ionization-Time of Flight Mass Spectrometry System for Identification of Mycobacterium and Nocardia Species. *J Clin Microbiol* **2018,** *56* (6).
50. Yu, J.; Tien, N.; Liu, Y. C.; Cho, D. Y.; Chen, J. W.; Tsai, Y. T.; Huang, Y. C.; Chao, H. J.; Chen, C. J., Rapid Identification of Methicillin-Resistant Staphylococcus aureus Using MALDI-TOF MS and Machine Learning from over 20,000 Clinical Isolates. *Microbiol Spectr* **2022,** *10* (2), e0048322.
51. Weis, C.; Cuénod, A.; Rieck, B.; Dubuis, O.; Graf, S.; Lang, C.; Oberle, M.; Brackmann, M.; Søgaard, K. K.; Osthoff, M.; Borgwardt, K.; Egli, A., Direct antimicrobial resistance prediction from clinical MALDI-TOF mass spectra using machine learning. *Nat Med* **2022,** *28* (1), 164-174.
52. Jeannot, K.; Hagart, K.; Dortet, L.; Kostrzewa, M.; Filloux, A.; Plesiat, P.; Larrouy-Maumus, G., Detection of Colistin Resistance in Pseudomonas aeruginosa Using the MALDIxin Test on the Routine MALDI Biotyper Sirius Mass Spectrometer. *Front Microbiol* **2021,** *12*, 725383.
53. Mingke Wang, J. C., Jinhong Chen, Jingwen Liu, Xiaoyu Geng, Xuelu Yu and Jishun Yang, *PCR Techniques and Their Clinical Applications*. 2023.
54. Margot, H.; Zwietering, M. H.; Joosten, H.; O'Mahony, E.; Stephan, R., Evaluation of different buffered peptone water (BPW) based enrichment broths for detection of Gram-negative foodborne pathogens from various food matrices. *Int J Food Microbiol* **2015,** *214*, 109-115.
55. Mo, Y.; Wan, R.; Zhang, Q., Application of reverse transcription-PCR and real-time PCR in nanotoxicity research. *Methods Mol Biol* **2012,** *926*, 99-112.
56. Parker, J.; Fowler, N.; Walmsley, M. L.; Schmidt, T.; Scharrer, J.; Kowaleski, J.; Grimes, T.; Hoyos, S.; Chen, J., Analytical Sensitivity Comparison between Singleplex Real-Time PCR and a Multiplex PCR Platform for Detecting Respiratory Viruses. *PLoS One* **2015,** *10* (11), e0143164.
57. Aydemir, O.; Aydemir, Y.; Ozdemir, M., The role of multiplex PCR test in identification of bacterial pathogens in lower respiratory tract infections. *Pak J Med Sci* **2014,** *30* (5), 1011-6.
58. Koo, B.; Kim, M. G.; Lee, K.; Kim, J. Y.; Lee, S.; Kim, S.-H.; Shin, Y., Automated sample-to-answer system for rapid and accurate diagnosis of emerging infectious diseases. *Sensors and Actuators B: Chemical* **2023,** *380*, 133382.
59. Curetis The Unyvero System. https://curetis.com/products/unyvero-a50-system/#:~:text=The%20Unyvero%20A50%20System%20is,answer%20within%204%2D5%20hours (accessed 08/01/2024).
60. Curetis Hospitalized Pneumonia. https://curetis.com/products/applications/#hpn (accessed 08/01/2024).
61. Klein, M.; Bacher, J.; Barth, S.; Atrzadeh, F.; Siebenhaller, K.; Ferreira, I.; Beisken, S.; Posch, A. E.; Carroll, K. C.; Wunderink, R. G.; Qi, C.; Wu, F.; Hardy, D. J.; Patel, R.; Sims, M. D., Multicenter Evaluation of the Unyvero Platform for Testing Bronchoalveolar Lavage Fluid. *J Clin Microbiol* **2021,** *59* (3).
62. Biomérieux BIOFIRE FILMARRAY Pneumonia Panel plus. https://www.biomerieux.es/diagnostico-clinico/productos/biofirer-filmarrayr-pneumonia-panel-plus (accessed 08/01/2024).
63. Gadsby, N. J.; McHugh, M. P.; Forbes, C.; MacKenzie, L.; Hamilton, S. K. D.; Griffith, D. M.; Templeton, K. E., Comparison of Unyvero P55 Pneumonia Cartridge, in-house PCR and culture for the identification of respiratory pathogens and antibiotic resistance in bronchoalveolar lavage fluids in the critical care setting. *Eur J Clin Microbiol Infect Dis* **2019,** *38* (6), 1171-1178.

64. Jamal, W.; Al Roomi, E.; AbdulAziz, L. R.; Rotimi, V. O., Evaluation of Curetis Unyvero, a multiplex PCR-based testing system, for rapid detection of bacteria and antibiotic resistance and impact of the assay on management of severe nosocomial pneumonia. *J Clin Microbiol* **2014,** *52* (7), 2487-92.
65. Ozongwu, C.; Personne, Y.; Platt, G.; Jeanes, C.; Aydin, S.; Kozato, N.; Gant, V.; O'Grady, J.; Enne, V. I., The Unyvero P55 'sample-in, answer-out' pneumonia assay: A performance evaluation. *Biomol Detect Quantif* **2017,** *13*, 1-6.
66. Yoo, I. Y.; Huh, K.; Shim, H. J.; Yun, S. A.; Chung, Y. N.; Kang, O. K.; Huh, H. J.; Lee, N. Y., Evaluation of the BioFire FilmArray Pneumonia Panel for rapid detection of respiratory bacterial pathogens and antibiotic resistance genes in sputum and endotracheal aspirate specimens. *Int J Infect Dis* **2020,** *95*, 326-331.
67. Lee, S. H.; Ruan, S. Y.; Pan, S. C.; Lee, T. F.; Chien, J. Y.; Hsueh, P. R., Performance of a multiplex PCR pneumonia panel for the identification of respiratory pathogens and the main determinants of resistance from the lower respiratory tract specimens of adult patients in intensive care units. *J Microbiol Immunol Infect* **2019,** *52* (6), 920-928.
68. Gadsby, N. J.; McHugh, M. P.; Russell, C. D.; Mark, H.; Conway Morris, A.; Laurenson, I. F.; Hill, A. T.; Templeton, K. E., Development of two real-time multiplex PCR assays for the detection and quantification of eight key bacterial pathogens in lower respiratory tract infections. *Clin Microbiol Infect* **2015,** *21* (8), 788.e1-788.e13.
69. Zhang, P.; Wang, R., Label-Free Biosensor. *Biosensors* **2023,** *13* (5).
70. Darwish, I. A., Immunoassay Methods and their Applications in Pharmaceutical Analysis: Basic Methodology and Recent Advances. *Int J Biomed Sci* **2006,** *2* (3), 217-35.
71. Alhajj M, Z. M., Farhana A. Enzyme Linked Immunosorbent Assay. https://www.ncbi.nlm.nih.gov/books/NBK555922/.
72. Chiba, R.; Miyakawa, K.; Aoki, K.; Morikawa, T. J.; Moriizumi, Y.; Degawa, T.; Arai, Y.; Segawa, O.; Tanaka, K.; Tajima, H.; Arai, S.; Yoshinaga, H.; Tsukada, R.; Tani, A.; Fuji, H.; Sato, A.; Ishii, Y.; Tateda, K.; Ryo, A.; Yoshimura, T., Development of a Fully Automated Desktop Analyzer and Ultrahigh Sensitivity Digital Immunoassay for SARS-CoV-2 Nucleocapsid Antigen Detection. *Biomedicines* **2022,** *10* (9).
73. Abbott, L. ARCHITECT HIV Ag/Ab Combo https://www.fda.gov/media/116836/download#:~:text=INTENDED%20USE-,The%20ARCHITECT%20HIV%20Ag%2FAb%20Combo%20assay%20is%20a%20chemiluminescent,plasma%20(EDTA%20and%20heparin). (accessed 08/01/2024).
74. Mak, W. C.; Beni, V.; Turner, A. P. F., Lateral-flow technology: From visual to instrumental. *TrAC Trends in Analytical Chemistry* **2016,** *79*, 297-305.
75. Koczula, K. M.; Gallotta, A., Lateral flow assays. *Essays Biochem* **2016,** *60* (1), 111-20.
76. Pai, N. P.; Vadnais, C.; Denkinger, C.; Engel, N.; Pai, M., Point-of-care testing for infectious diseases: diversity, complexity, and barriers in low- and middle-income countries. *PLoS Med* **2012,** *9* (9), e1001306.
77. Soh, J. H.; Chan, H.-M.; Ying, J. Y., Strategies for developing sensitive and specific nanoparticle-based lateral flow assays as point-of-care diagnostic device. *Nano Today* **2020,** *30*, 100831.
78. Kamiya, M.; Kobayashi, H.; Hama, Y.; Koyama, Y.; Bernardo, M.; Nagano, T.; Choyke, P. L.; Urano, Y., An Enzymatically Activated Fluorescence Probe for Targeted Tumor Imaging. *Journal of the American Chemical Society* **2007,** *129* (13), 3918-3929.
79. Filchakova, O.; Dossym, D.; Ilyas, A.; Kuanysheva, T.; Abdizhamil, A.; Bukasov, R., Review of COVID-19 testing and diagnostic methods. *Talanta* **2022,** *244*, 123409.
80. Akgönüllü, S.; Çimen, D.; Bakhshpour, M.; Bereli, N.; Yavuz, H.; Denizli, A., Chapter Five - Commercial sensors for pathogen detection. In *Commercial Biosensors and Their Applications*, Sezgintürk, M. K., Ed. Elsevier: 2020; pp 89-106.
81. Abbott BINAXNOW STREP A. https://www.globalpointofcare.abbott/es/es/product-details/binaxnow-strep-a.html (accessed 08/01/2024).

82. Mehrotra, P., Biosensors and their applications - A review. *J Oral Biol Craniofac Res* **2016,** *6* (2), 153-9.
83. Naresh, V.; Lee, N., A Review on Biosensors and Recent Development of Nanostructured Materials-Enabled Biosensors. *Sensors (Basel)* **2021,** *21* (4).
84. Cotchim, S.; Thavarungkul, P.; Kanatharana, P.; Limbut, W., Multiplexed label-free electrochemical immunosensor for breast cancer precision medicine. *Analytica Chimica Acta* **2020,** *1130*, 60-71.
85. Narita, F.; Wang, Z.; Kurita, H.; Li, Z.; Shi, Y.; Jia, Y.; Soutis, C., A Review of Piezoelectric and Magnetostrictive Biosensor Materials for Detection of COVID-19 and Other Viruses. *Advanced Materials* **2021,** *33* (1), 2005448.
86. Singh, A. K.; Mittal, S.; Das, M.; Saharia, A.; Tiwari, M., Optical biosensors: a decade in review. *Alexandria Engineering Journal* **2023,** *67*, 673-691.
87. Bhalla, N.; Jolly, P.; Formisano, N.; Estrela, P., Introduction to biosensors. *Essays Biochem* **2016,** *60* (1), 1-8.
88. Han, E.; Zhang, Y.; Cai, J.; Zhang, X., Development of Highly Sensitive Immunosensor for Detection of Staphylococcus aureus Based on AuPdPt Trimetallic Nanoparticles Functionalized Nanocomposite. *Micromachines (Basel)* **2021,** *12* (4).
89. Andrade, C. A. S.; Nascimento, J. M.; Oliveira, I. S.; de Oliveira, C. V. J.; de Melo, C. P.; Franco, O. L.; Oliveira, M. D. L., Nanostructured sensor based on carbon nanotubes and clavanin A for bacterial detection. *Colloids and Surfaces B: Biointerfaces* **2015,** *135*, 833-839.
90. Tlili, C.; Sokullu, E.; Safavieh, M.; Tolba, M.; Ahmed, M. U.; Zourob, M., Bacteria screening, viability, and confirmation assays using bacteriophage-impedimetric/loop-mediated isothermal amplification dual-response biosensors. *Anal Chem* **2013,** *85* (10), 4893-901.
91. Shi, X.; Zhang, J.; He, F., A new aptamer/polyadenylated DNA interdigitated gold electrode piezoelectric sensor for rapid detection of Pseudomonas aeruginosa. *Biosensors and Bioelectronics* **2019,** *132*, 224-229.
92. Sharma, H.; Mutharasan, R., Rapid and sensitive immunodetection of Listeria monocytogenes in milk using a novel piezoelectric cantilever sensor. *Biosensors and Bioelectronics* **2013,** *45*, 158-162.
93. Salam, F.; Uludag, Y.; Tothill, I. E., Real-time and sensitive detection of Salmonella Typhimurium using an automated quartz crystal microbalance (QCM) instrument with nanoparticles amplification. *Talanta* **2013,** *115*, 761-767.
94. Gasparyan, V. K.; Bazukyan, I. L., Lectin sensitized anisotropic silver nanoparticles for detection of some bacteria. *Anal Chim Acta* **2013,** *766*, 83-7.
95. Wang, Y.; Ye, Z.; Si, C.; Ying, Y., Subtractive inhibition assay for the detection of E. coli O157:H7 using surface plasmon resonance. *Sensors (Basel)* **2011,** *11* (3), 2728-39.
96. Wang, J.; Wu, X.; Wang, C.; Rong, Z.; Ding, H.; Li, H.; Li, S.; Shao, N.; Dong, P.; Xiao, R.; Wang, S., Facile Synthesis of Au-Coated Magnetic Nanoparticles and Their Application in Bacteria Detection via a SERS Method. *ACS Appl Mater Interfaces* **2016,** *8* (31), 19958-67.
97. Horcajada, J. P.; Montero, M.; Oliver, A.; Sorlí, L.; Luque, S.; Gómez-Zorrilla, S.; Benito, N.; Grau, S., Epidemiology and Treatment of Multidrug-Resistant and Extensively Drug-Resistant Pseudomonas aeruginosa Infections. *Clin Microbiol Rev* **2019,** *32* (4).
98. Grasemann, H.; Ratjen, F., Cystic Fibrosis. *New England Journal of Medicine* **2023,** *389* (18), 1693-1707.
99. Pang, Z.; Raudonis, R.; Glick, B. R.; Lin, T. J.; Cheng, Z., Antibiotic resistance in Pseudomonas aeruginosa: mechanisms and alternative therapeutic strategies. *Biotechnol Adv* **2019,** *37* (1), 177-192.
100. Jangra, V.; Sharma, N.; Chhillar, A. K., Therapeutic approaches for combating Pseudomonas aeruginosa infections. *Microbes Infect* **2022,** *24* (4), 104950.
101. Chinemerem Nwobodo, D.; Ugwu, M. C.; Oliseloke Anie, C.; Al-Ouqaili, M. T. S.; Chinedu Ikem, J.; Victor Chigozie, U.; Saki, M., Antibiotic resistance: The challenges and some emerging strategies for tackling a global menace. *J Clin Lab Anal* **2022,** *36* (9), e24655.

102. Botelho, J.; Grosso, F.; Peixe, L., Antibiotic resistance in Pseudomonas aeruginosa - Mechanisms, epidemiology and evolution. *Drug Resist Updat* **2019,** *44*, 100640.
103. López-Calleja, A. I.; Morilla Morales, E.; Nuñez Medina, R.; Fernández Esgueva, M.; Sahagún Pareja, J.; García-Lechuz Moya, J. M.; Ferrer Cerón, I.; Viñuelas Bayon, J.; Rezusta López, A., Antimicrobial activity of ceftolozane-tazobactam against multidrug-resistant and extensively drug-resistant Pseudomonas aeruginosa clinical isolates from a Spanish hospital. *Rev Esp Quimioter* **2019,** *32* (1), 68-72.
104. Mensa, J.; Barberán, J.; Soriano, A.; Llinares, P.; Marco, F.; Cantón, R.; Bou, G.; González Del Castillo, J.; Maseda, E.; Azanza, J. R.; Pasquau, J.; García-Vidal, C.; Reguera, J. M.; Sousa, D.; Gómez, J.; Montejo, M.; Borges, M.; Torres, A.; Alvarez-Lerma, F.; Salavert, M.; Zaragoza, R.; Oliver, A., Antibiotic selection in the treatment of acute invasive infections by Pseudomonas aeruginosa: Guidelines by the Spanish Society of Chemotherapy. *Rev Esp Quimioter* **2018,** *31* (1), 78-100.
105. Europe, W. R. O. f. E. E. C. f. D. P. a. C. C. W. R. O. f., Antimicrobial resistance surveillance in Europe 2022 – 2020 data. **2022**.
106. McCarthy, K. L.; Paterson, D. L., Increased risk of death with recurrent Pseudomonas aeruginosa bacteremia. *Diagnostic Microbiology and Infectious Disease* **2017,** *88* (2), 152-157.
107. Qin, S.; Xiao, W.; Zhou, C.; Pu, Q.; Deng, X.; Lan, L.; Liang, H.; Song, X.; Wu, M., Pseudomonas aeruginosa: pathogenesis, virulence factors, antibiotic resistance, interaction with host, technology advances and emerging therapeutics. *Signal Transduction and Targeted Therapy* **2022,** *7* (1), 199.
108. Llor, C.; Bjerrum, L., Antimicrobial resistance: risk associated with antibiotic overuse and initiatives to reduce the problem. *Therapeutic Advances in Drug Safety* **2014,** *5* (6), 229-241.
109. BH, I., *Medical Microbiology*. 4 th ed.; Galveston (TX), 1996; Vol. 27. Pseudomonas.
110. Brown, V. I.; Lowbury, E. J., Use of an improved cetrimide agar medium and other culture methods for Pseudomonas aeruginosa. *J Clin Pathol* **1965,** *18* (6), 752-6.
111. Szita, G.; Tabajdi, V.; Fábián, A.; Biró, G.; Reichart, O.; Körmöczy, P. S., A novel, selective synthetic acetamide containing culture medium for isolating Pseudomonas aeruginosa from milk. *Int J Food Microbiol* **1998,** *43* (1-2), 123-7.
112. Granström, M.; Wretlind, B.; Markman, B.; Pavlovskis, O. R.; Vasil, M. L., Enzyme-linked immunosorbent assay for detection of antibodies to Pseudomonas aeruginosa exoproteins. *Eur J Clin Microbiol* **1985,** *4* (2), 197-200.
113. Beutin, L.; Zimmermann, S.; Gleier, K., Pseudomonas aeruginosa can cause false-positive identification of verotoxin (Shiga-like toxin) production by a commercial enzyme immune assay system for the detection of Shiga-like toxins (SLTs). *Infection* **1996,** *24* (3), 267-268.
114. Fomsgaard, A.; Dinesen, B.; Shand, G. H.; Pressler, T.; Høiby, N., Antilipopolysaccharide antibodies and differential diagnosis of chronic Pseudomonas aeruginosa lung infection in cystic fibrosis. *J Clin Microbiol* **1989,** *27* (6), 1222-9.
115. Ohst, C.; Saschenbrecker, S.; Stiba, K.; Steinhagen, K.; Probst, C.; Radzimski, C.; Lattwein, E.; Komorowski, L.; Stöcker, W.; Schlumberger, W., Reliable Serological Testing for the Diagnosis of Emerging Infectious Diseases. *Adv Exp Med Biol* **2018,** *1062*, 19-43.
116. Kingsford, N. M.; Raadsma, H. W., Detection of Pseudomonas aeruginosa from ovine fleece washings by PCR amplification of 16S ribosomal RNA. *Vet Microbiol* **1995,** *47* (1-2), 61-70.
117. Khan, A. A.; Cerniglia, C. E., Detection of Pseudomonas aeruginosa from clinical and environmental samples by amplification of the exotoxin A gene using PCR. *Appl Environ Microbiol* **1994,** *60* (10), 3739-3745.
118. Deschaght, P.; Van Daele, S.; De Baets, F.; Vaneechoutte, M., PCR and the detection of Pseudomonas aeruginosa in respiratory samples of CF patients. A literature review. *J Cyst Fibros* **2011,** *10* (5), 293-7.
119. Anuj, S. N.; Whiley, D. M.; Kidd, T. J.; Ramsay, K. A.; Bell, S. C.; Syrmis, M. W.; Grimwood, K.; Wainwright, C. E.; Nissen, M. D.; Sloots, T. P., Rapid single-nucleotide polymorphism-based identification of clonal Pseudomonas aeruginosa isolates from patients

with cystic fibrosis by the use of real-time PCR and high-resolution melting curve analysis. *Clin Microbiol Infect* **2011,** *17* (9), 1403-8.
120. Qin, X.; Emerson, J.; Stapp, J.; Stapp, L.; Abe, P.; Burns, J. L., Use of Real-Time PCR with Multiple Targets To Identify *Pseudomonas aeruginosa* and Other Nonfermenting Gram-Negative Bacilli from Patients with Cystic Fibrosis. **2003,** *41* (9), 4312-4317.
121. Anuj, S. N.; Whiley, D. M.; Kidd, T. J.; Bell, S. C.; Wainwright, C. E.; Nissen, M. D.; Sloots, T. P., Identification of Pseudomonas aeruginosa by a duplex real-time polymerase chain reaction assay targeting the ecfX and the gyrB genes. *Diagn Microbiol Infect Dis* **2009,** *63* (2), 127-31.
122. Motoshima, M.; Yanagihara, K.; Fukushima, K.; Matsuda, J.; Sugahara, K.; Hirakata, Y.; Yamada, Y.; Kohno, S.; Kamihira, S., Rapid and accurate detection of Pseudomonas aeruginosa by real-time polymerase chain reaction with melting curve analysis targeting gyrB gene. *Diagn Microbiol Infect Dis* **2007,** *58* (1), 53-8.
123. Tang, Y.; Zou, J.; Ma, C.; Ali, Z.; Li, Z.; Li, X.; Ma, N.; Mou, X.; Deng, Y.; Zhang, L.; Li, K.; Lu, G.; Yang, H.; He, N., Highly sensitive and rapid detection of Pseudomonas aeruginosa based on magnetic enrichment and magnetic separation. *Theranostics* **2013,** *3* (2), 85-92.
124. Webster, T. A.; Sismaet, H. J.; Conte, J. L.; Chan, I. p. J.; Goluch, E. D., Electrochemical detection of Pseudomonas aeruginosa in human fluid samples via pyocyanin. *Biosensors and Bioelectronics* **2014,** *60*, 265-270.
125. AMR test directory. https://www.finddx.org/tools-and-resources/dxconnect/test-directories/amr-test-directory/.

2. OBJECTIVES AND THESIS STRUCTURE

2.1 General Objective

In light of the scenario described in Chapter 1, this PhD thesis project has focused on developing new diagnostic strategies to improve the diagnostic efficiency of infectious diseases and consequently mitigate the growing concern of antimicrobial resistance. Antibiotic prescription without knowing the microorganisms causing the diseases is still a common practice. Ideally, diagnostic technologies should provide results in a short time, particularly for infectious diseases. Turnaround times (TAT, the amount of time invested to deliver the result) of minutes or at least less than one hour would significantly improve the situation. Moreover, the identification of the microorganism would allow for the administration of specific therapies instead of broad-spectrum antibiotics and help avoid unnecessary prescriptions, such as in the case of viral infections. Additionally, distinguishing between colonization and infection is also key to preventing needless antibiotic treatment.

With all these requirements in mind, we have focused on bacterial Quorum Sensing (QS), an intercommunication system that allows bacteria to exchange information on cell density and regulate various processes such as population growth, biofilm formation, and pathogenicity. Its role in pathogenesis makes this system an interesting target for both the development of new therapeutic strategies and for diagnosis. While for the first case, there are numerous articles that support the interest of pursuing the QS system, there are only few cases in which the QS has been contemplated as a potential target for developing new diagnostic approaches.

We have centred our attention on the lower respiratory tract (LRT) and urinary tract (UT) infections as representative diseases based on their importance and worldwide prevalence. In this context, and as described in Chapter 1, *Pseudomonas aeruginosa* is a highly relevant, virulent, and multidrug-resistant microorganism involved in these infections, among others.

2.2Quorum Sensing

Bacteria were initially believed to be capable only of simple processes and single-celled life. However, there is now a growing appreciation for their ability to engage in collective behaviours within multi-cellular groups. These coordinated actions involve a variety of processes, such as virulence factors production, bioluminescence, competence for DNA uptake, secondary metabolite production, and biofilm formation. Importantly, these processes are ineffective when undertaken by individual bacteria in isolation; success needs the coordination of individual cells[1].

To achieve this orchestration of collective behaviours, bacteria employ a cell-to-cell communication process known as Quorum Sensing (QS). QS involves the production, release, accumulation, and group-wide detection of extracellular signalling molecules called autoinducers (AI)[2]. These AIs are released into the extracellular space, and as the bacterial population grows, the AI concentration increases. Bacteria, equipped with specialized receptors, detect the AI, and when a specific threshold is reached, initiate a collective response by modulating the expression of specific genes (see Figure 2.1). This orchestrated genetic regulation triggers synchronized behaviours such us virulence, luminescence, motility and biofilm formation[3].

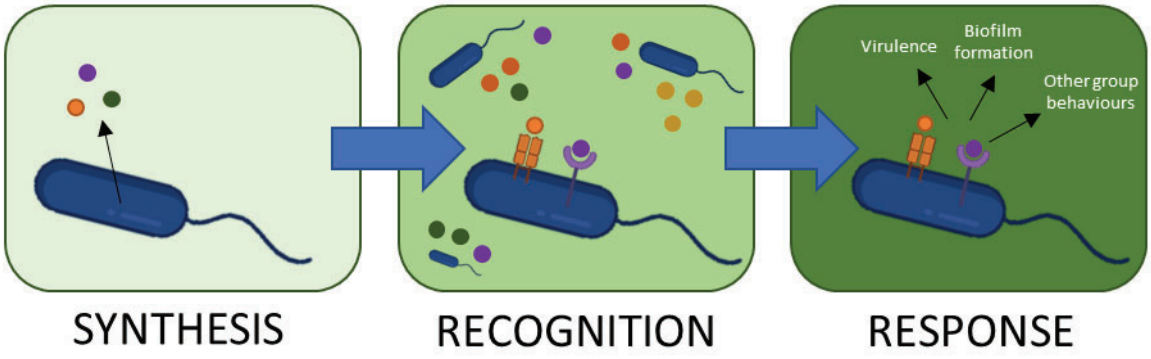

Figure 2.1: The Quorum Sensing process can be divided into three key phases: the production of signaling molecules through biosynthesis, their detection by neighboring bacteria, and the subsequent response triggered upon reaching a defined threshold limit.

The initial indications of QS emerged in the late 1960s when researchers demonstrated that genetic competence in *Streptococcus pneumoniae*[4] and bioluminescence in species of marine bacteria relied on the production of extracellular molecules[5]. These molecules were proposed as agents for cell-cell signalling, representing a form of chemical communication. However, these early findings faced skepticism and were largely overlooked for the subsequent 10–20 years. The 1980s marked two important discoveries: firstly, the identification of the luminescence (*lux*) genes in the marine bacterium *Vibrio fischeri*, with *luxI* and *luxR* identified as the genes responsible for QS, which regulates the transcription of *lux* gene[6]. Secondly, the QS signal from *V. fischeri* was identified as N-(3-oxohexanoyl)-L-homoserine lactone (3-oxo-C6-HSL)[7]. The *luxI* gene encodes the AI synthase essential for 3-oxo-C6-HSL production, while *luxR* codes for a 3-oxo-C6-HSL-responsive transcriptional activator of the *lux* genes[8].

Gram-negative QS bacteria utilize low molecular weight molecules as AIs, and two types of receptors to detect them: transmembrane two-component histidine sensor kinases or

cytoplasmic transcription factors. In both cases, receptor complexes direct the expression of QS-dependent target genes[9].

In contrast, Gram-positive bacteria usually use oligopeptides as AIs, with partner receptors being transmembrane two-component histidine protein kinases[10]. AI–receptor complexes in this case often activate the expression of the gene encoding the AI synthase, leading to an increase in extracellular AI concentration. This feedforward autoinduction loop is believed to synchronize behaviours across the bacterial population[11].

2.2.1 Quorum sensing of *P. aeruginosa*

Due to the significance of *P. aeruginosa* as a pathogenic microorganism, considerable attention has been devoted to studying its QS. It exhibits a finely tuned and intricate network in which four interconnected systems (Las, Rhl, Pqs, and Iqs) function hierarchically (See Figure 2.2). Each of these systems generates and responds to a specific AI, which enters the cytoplasm and binds to its corresponding cognate transcriptional activator (LasR, RhlR, PqsR, and an unidentified receptor for the *iqs* system). Subsequently, upon binding to gene promoters, the complexes initiate the expression of associated regulons for their biosynthesis (LasI, RhlI, PqsABCDH, and PchABCDEF, respectively). This process establishes an auto-induction loop, significantly amplifying the number of AIs. Moreover, each transcriptional activator-AI complex exerts control over the expression of a diverse array of genes related to virulence, biofilm formation, and secondary metabolism (Malešević *et al.*, 2019).

Over 25 years ago, Pearson and collaborators elucidated the structure of the initial chemical signal of *P. aeruginosa*, identified as N-(3-oxododecanoyl)-L-homoserine lactone (3-oxo-C12-HSL)[12]. This molecule is a part of the Las signalling system, positioned at the top of the regulatory network, where it exerts positive control over other systems. Subsequently, the Rhl system was identified as another player in *P. aeruginosa's* QS, featuring a structurally related AI recognized as N-butyryl-L-homoserine lactone (C4-HSL), by Ochsner et al[13]. The two systems oversee the regulation of intersecting sets of genes, playing a central role in the pathogenicity of *P. aeruginosa*. Approximately 11% of the genes within the *P. aeruginosa* genome respond to the homoserine lactone (HSL) signals[14, 15]. The activity of various cellular and secreted virulence factors, such as rhamnolipids, alkaline proteases, LasA proteases, elastases, lipases, phospholipases C, pyocyanin (PYO), exotoxin A, and lectins, are under the control of both the Las and Rhl systems. In addition, the C4-HSL-RhlR complex negatively regulates a third system, later named Pqs[16].

The significance of the Pqs system, along with the role of 2-heptyl-3-hydroxy-4(1H)-quinolone, also known as Pseudomonas quinolone signal (PQS), were reported for the first time by Pesci *et al.* in 1999. They discovered that the *lasB'-lacZ* reporter construct was clearly induced in a *lasR* mutant by the culture supernatant of wild-type *P. aeruginosa* PAO1 cells, nearly deactivating the Las and Rhl signalling pathways and making it impossible to reverse the induction by adding the AIs 3-oxo-C12-HSL or C4-HSL[17]. Following the identification of the PQS signal, the receptor PqsR (formerly known as MvfR) was implicated in the regulation of PQS production. PqsR, a LysR-type transcriptional regulator, binds to the promoter region of the *pqsABCDE* operon, orchestrating an immediate auto-regulatory loop to control its expression[18]. The expression of *pqsR* is subsequently modulated by LasR[19]. PqsR interacts with two ligands, HHQ (the PQS precursor) and PQS, initiating its binding to the *pqsABCDE* promoter region, with PQS exhibiting

higher affinity than HHQ and being approximately 100-fold more active[20]. PqsR-PQS complex regulates positively the production of PYO, elastase, exoproteins, biofilm and 3-oxo-C12-HSL[18, 21].

The involvement of the Pqs signalling system in promoting infection and regulating virulence factors has been extensively examined in various studies. Null mutants of the Pqs system exhibit diminished biofilm formation and reduced production of virulence factors, including PYO, elastase, lectin, and rhamnolipids[22, 23]. The Pqs system is crucial for the complete virulence of *P. aeruginosa* towards plants[18], nematodes[21], and mice[24]. Additionally, PQS has been detected in the sputum of cystic fibrosis patients infected with *P. aeruginosa*[25].

The identification of the aforementioned systems occurred within a relatively brief timeframe; however, the elucidation of the final system involved in *P. aeruginosa* QS and its functions was resolved more than 10 years later[26]. The integrated quorum sensing (Iqs) system serves as a link between the central Las system and the phosphate stress response, connecting with the downstream regulatory systems Pqs and Rhl. The distinctive signalling molecule of the Iqs QS system is 2-(2-hydroxyphenyl)-thiazole-4-carbaldehyde, known as IQS. Notably, the structure and production of IQS by *P. aeruginosa* had been uncovered many years prior to understanding its role in the communication architecture[27]. Initially, it was perceived as a by-product of the biosynthesis of the siderophore pyochelin from aeruginoic acid. However, the genes implicated in the biosynthesis and production of IQS have sparked a contentious debate between the pyochelin-related production route and the *ambBCDE* cluster gene, believed to be responsible for the synthesis of the 2-amino-4-methoxy-trans-3-butenoic acid (AMB) antimetabolite[28].

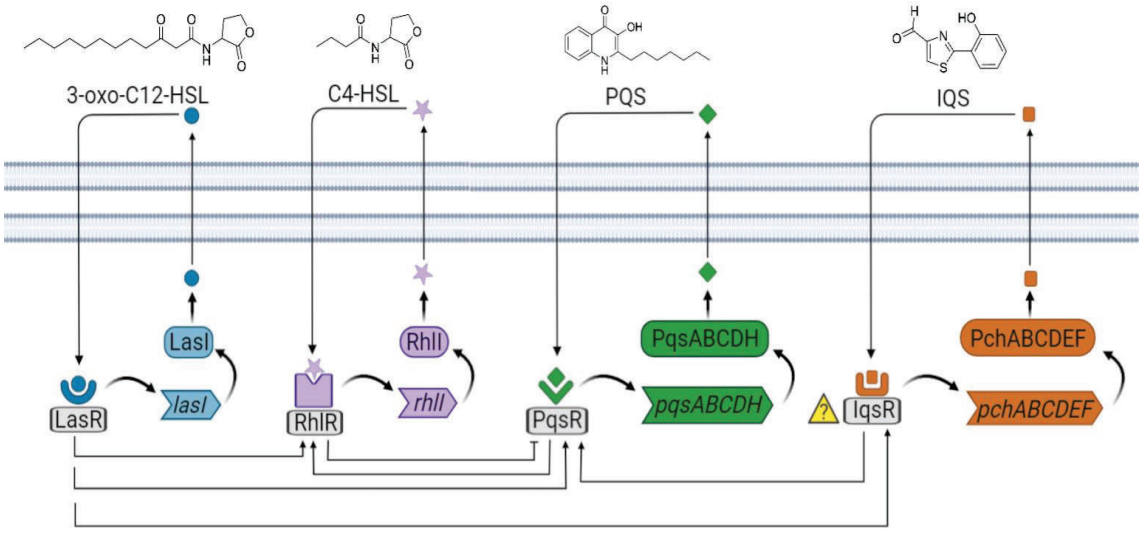

Figure 2.2: Schematic representation of the four QS networks in P. aeruginosa. The four autoinducer synthases produce the autoinducers, 3-oxo-C12-HSL, C4-HSL, PQS and IQS. 3-oxo-C12-HSL, C4-HSL and PQS, are recognized by the receptors placed in the cytoplasm. The receptor for IQS is currently unknown.

2.2.2 QS as diagnosis biomarker in *P. aeruginosa*

Bacterial QS has recently emerged as a compelling target for the development of innovative therapeutic and diagnostic approaches. The signaling molecules of the QS are released into the extracellular space to facilitate communication and regulation. Consequently, these molecules, due to their chemical nature, can be detected in biological fluids such as sputum, urine, or

plasma[29-34]. Moreover, as they occur in the very early stages of the infection, they could allow the detection of small concentrations of bacteria at the beginning of the infection[31]. Additionally, our group has demonstrated that these molecules can not only provide information about the presence or absence of infection caused by *P. aeruginosa* but also offer insights into the infection's status or the behavior of the bacteria. Hence, the concentration levels of some of these QS molecules significantly differ when the patient is having an acute or a chronic infection[35-38]. Similarly, Michalet *et al.*[39] have reported differentiation in the levels of AIs produced by primo-colonized strains and chronic strains infecting CF patients. Therefore, AIs have the potential to function as biomarkers of infection, supplying pertinent information to aid clinicians in decision-making for the management of infected patients.

Detecting QS signals rather than the bacteria itself offers significant advantages in bacterial infection diagnostics. Firstly, QS molecules are often produced in larger quantities compared to the bacteria, enhancing the sensitivity of detection methods. This heightened sensitivity enables the detection of bacterial presence even at low levels, thereby improving the accuracy of diagnosis[32]. Moreover, QS molecules are generated early in the bacterial growth cycle, sometimes before the bacteria reach detectable levels. This early production allows for timely detection of infections, facilitating prompt treatment and potentially preventing the progression of the infection[32].

Another advantage lies in the specificity of QS molecules, which are specific to particular bacterial species or strains. This specificity enables differentiation between different types of bacterial infections, reducing the likelihood of false positive results and ensuring precise diagnosis[40].

Lastly, monitoring QS molecules can provide valuable insights into bacterial behaviour and the development of antibiotic resistance. Changes in QS molecule production can indicate the emergence of resistant bacteria, allowing clinicians to adjust treatment strategies accordingly[41-43].

2.3 Thesis hypothesis and objectives

The main hypothesis of this PhD project has been the idea that the QS molecular signature of the bacteria could provide valuable and comprehensive information regarding the stage of colonization or infection, the mechanisms involved in pathology, and guiding on the application of more appropriate treatments. Furthermore, QS molecules could be used as biomarkers to diagnose infection at an early stage more efficiently.

To probe this hypothesis, we have proposed an immunochemical approach for detecting the main molecules of QS and virulence factors of *P. aeruginosa* in clinical samples or in the culture media of bacterial isolates obtained from patients diagnosed with LRTI or UTI.

The key factor has been having access to antibodies with high affinity and specificity against these molecules. However, implementing this approach in the analysis of complex clinical samples has also been a fundamental issue. Hence, the specific objectives addressed in this PhD thesis are listed below.

1. Development of antibodies against molecules of the QS of *P. aeruginosa* to achieve detection of the complete panel of all the AIs of the three main QS systems. Previously, Dr. Enrique Montagut developed pAbs for the detection of AQs (PQS, HHQ and HQNO)

from the Pqs system. Within this thesis we have been addressing the development of mAbs for the specific detection of PQS, the main autoinducer of the Pqs system, and pAbs for the detection of 3-oxo-C12-HSL and C4-HSL of the Las and RhI systems, respectively.

2. Establishment and optimization of robust microplate-based ELISAs to detect all these molecules in buffer and in MH culture medium with enough detectability to monitor QS profiles on samples from patients at different disease stages.

3. Assessment of the QS and virulence factors profiles of *P. aeruginosa* clinical isolates from patients with lower respiratory tract (LRT) and urinary tract (UT) infections by ELISA. Analysis of the data using bioinformatics approaches to identify potential relationships between the levels of these molecules and the clinical status of the patient.

4. Implementation of the developed assays to the direct detection of QS molecules and virulence factors of *P. aeruginosa* in complex clinical samples.

2.4Thesis structure.

The structure of this thesis follows the scheme detailed below:

- Antibody production and ELISA development.
    - *Chapter 3* describes the production of monoclonal antibodies against PQS and the development of ELISA for its detection in buffer and in MH culture medium.
    - *Chapter 4* describes the production of polyclonal antibodies against the signaling molecules of the Las and Rhl systems of *P. aeruginosa*. These molecules are 3-oxo-C12-HSL and C4-HSL, respectively. It also details the development and optimization of the ELISAs for their detection in buffer and MH culture medium.

- Detection of QS molecules and virulence factors in clinical biological samples.
    - Chapter 5 describes the optimization of the ELISA assay format for the detection of previously studied molecules in sputum samples.

- QS profiling in clinical isolates.
    - *Chapter 6* describes the quantification of QS molecules and virulence factors of *P. aeruginosa* produced by clinical isolates from respiratory and urinary infections. Additionally, it includes a bioinformatic study where the correlation between the levels of these biomarkers and the clinical status of the patients is obtained.
- In the annex, two publications related to the thesis topic, which have been carried out within the context of this doctoral thesis, are included.
    - Publication 1: During the work of this thesis, some of the experiments included in this publication were conducted. "Montagut EJ, Raya J, Martin-Gomez MT, Vilaplana L, Rodriguez-Urretavizcaya B, Marco MP. An Immunochemical Approach to Detect the Quorum Sensing-Regulated Virulence Factor 2-Heptyl-4-Quinoline N-Oxide (HQNO) Produced by Pseudomonas aeruginosa Clinical Isolates. Microbiol Spectr. 2022 Aug 31;10(4)

- Publication 2: During this thesis, a bibliographic review has also been conducted that discusses the controversy surrounding the Iqs system as a potential fourth QS system in *P. aeruginosa* and its connection with the established QS systems. The paper has been submitted and at the time to write this thesis it is under review.

2.5 Context of the research

The thesis presented herein has been performed thanks to State Training Program within the State Plan for Scientific and Technical Reseach and Innovation 2021-2023 through the predoctoral fellowship PRE2019-087542, and has evolved through the framework of three different research projects.

- ***Quorum Sensing as an alternative for the management of cystic fibrosis (QS4CF project).*** (ref # RTI2018-096278-B-C21, 01/01/2019 - 30/06/2022, co-funded by "Ministerio de Ciencia, Innovación y Universidades (MICIU)" and "Fondo Europeo de Desarrollo Regional" (FEDER)). The QS4CF project is the continuation of a previously granted project, Immuno-QS. The two projects share similar objectives that can be divided into two parts. The development of immunochemical methods to obtain the expression profile of different molecules of QS in order to understand the mechanisms that regulate the virulence of two of the main bacteria in respiratory tract infections: *P. aeruginosa* and *S. aureus*. The aim is to develop antibodies against relevant QS signaling molecules that regulate the production of the main virulence factors and biofilm formation. With these antibodies, the goal is to evaluate their potential value as biomarkers of these molecules by obtaining their production profile. The other objective is to evaluate the potential therapeutic effect of antibodies generated against QS molecules and virulence factors of *P. aeruginosa* and *S. aureus* and to use them as quorum quenchers in a way that would interrupt communication between them and therefore the production of virulence factors, as well as directly quenching virulence factors. To ensure the translational nature of this project, two clinical groups are included: 1. HGTiP, Microbiology Laboratory (Hospital Germans Trias i Pujol, Badalona, Spain) and 2. HUVH, Microbiology Laboratories and Respiratory Units of the Hospital Vall d'Hebrón (Hospital Vall d'Hebron, Barcelona, Spain). Patients suffering from CF are identified as a priority based on the prevalence of infection by these bacteria and their impact on life expectancy. In this context, the development of a POC is considered an important need for routine monitoring of CF patients. For this reason, the project collaborates with the Bioanalysis and Biosensors group of the University of Alcalá de Henares.
- ***Quorum Sensing as potential biomarker targets to diagnose bacterial infections (QS-MOTION project).*** (ref # FMTV3-201824-30-31, 11/7/2019 - 30/7/2022, funded by "Fundació La Marató de TV3"). This project is focuses in the diagnostic part. The main objective is the development of immunochemical techniques for the rapid and accurate diagnosis of *S. aureus* and *P. aeruginosa*, as well as obtaining the complete molecular profile of QS molecules from both pathogens. To achieve this, the plan includes the development of more specific Abs against QS molecules of the mentioned pathogens and the optimization of techniques for their detection with the lowest possible LOD. Additionally, the detection of these molecules directly in biological samples from patients is proposed for rapid diagnosis.

- ***Towards Improved Diagnostic and Therapeutic Strategies for Infectious Diseases Targeting Quorum Sensing (TARGETING-QS project*).** (ref # PID2021-126257OB-C21, 01/09/2022-31/08/2025, co-funded by "Ministerio de Ciencia e Innovación (MICIN)" and FEDER). The primary aim of this proposal is to clinically validate the QS molecular signatures obtained in the QS4CF project for clinical isolates of *P. aeruginosa*. The goal is to bring the developed QS technologies and the knowledge provided by the QSome to the market for clinical use. This project will primarily focus on analyzing cultured media of representative clinical isolates from well-characterized and selected patients infected by *P. aeruginosa*. The potential benefits of conducting these studies directly on clinical samples, despite the challenges posed by the complex matrix of sputum, are being considered. Therefore, alternative clinical samples such as plasma or urine are being evaluated. Meanwhile, the potential interest of recording QS molecular signatures from clinical isolates is recognized, constituting the main objective of the proposed scientific activities.

2.6 References

1. Mukherjee, S.; Bassler, B. L., Bacterial quorum sensing in complex and dynamically changing environments. *Nature Reviews Microbiology* **2019,** *17* (6), 371-382.
2. Rutherford, S. T.; Bassler, B. L., Bacterial quorum sensing: its role in virulence and possibilities for its control. *Cold Spring Harb Perspect Med* **2012,** *2* (11).
3. Waters, C. M.; Bassler, B. L., Quorum sensing: cell-to-cell communication in bacteria. *Annu Rev Cell Dev Biol* **2005,** *21*, 319-46.
4. Tomasz, A., Control of the Competent State in Pneumococcus by a Hormone-Like Cell Product: An Example for a New Type of Regulatory Mechanism in Bacteria. *Nature* **1965,** *208* (5006), 155-159.
5. Nealson, K. H.; Platt, T.; Hastings, J. W., Cellular control of the synthesis and activity of the bacterial luminescent system. *J Bacteriol* **1970,** *104* (1), 313-22.
6. Greenberg, E. P.; Hastings, J. W.; Ulitzur, S., Induction of luciferase synthesis in Beneckea harveyi by other marine bacteria. *Archives of Microbiology* **1979,** *120* (2), 87-91.
7. Eberhard, A.; Burlingame, A. L.; Eberhard, C.; Kenyon, G. L.; Nealson, K. H.; Oppenheimer, N. J., Structural identification of autoinducer of Photobacterium fischeri luciferase. *Biochemistry* **1981,** *20* (9), 2444-9.
8. Whiteley, M.; Diggle, S. P.; Greenberg, E. P., Progress in and promise of bacterial quorum sensing research. *Nature* **2017,** *551* (7680), 313-320.
9. Papenfort, K.; Bassler, B. L., Quorum sensing signal-response systems in Gram-negative bacteria. *Nat Rev Microbiol* **2016,** *14* (9), 576-88.
10. Novick, R. P.; Geisinger, E., Quorum sensing in staphylococci. *Annu Rev Genet* **2008,** *42*, 541-64.
11. Miller, M. B.; Bassler, B. L., Quorum Sensing in Bacteria. *Annual Review of Microbiology* **2001,** *55* (1), 165-199.
12. Pearson, J. P.; Gray, K. M.; Passador, L.; Tucker, K. D.; Eberhard, A.; Iglewski, B. H.; Greenberg, E. P., Structure of the autoinducer required for expression of Pseudomonas aeruginosa virulence genes. *Proc Natl Acad Sci U S A* **1994,** *91* (1), 197-201.
13. Ochsner, U. A.; Vasil, A. I.; Vasil, M. L., Role of the ferric uptake regulator of Pseudomonas aeruginosa in the regulation of siderophores and exotoxin A expression: purification and activity on iron-regulated promoters. *Journal of bacteriology* **1995,** *177* (24), 7194-7201.
14. Wagner, V. E.; Bushnell, D.; Passador, L.; Brooks, A. I.; Iglewski, B. H., Microarray analysis of Pseudomonas aeruginosa quorum-sensing regulons: effects of growth phase and environment. *J Bacteriol* **2003,** *185* (7), 2080-95.
15. Schuster, M.; Lostroh, C. P.; Ogi, T.; Greenberg, E. P., Identification, timing, and signal specificity of Pseudomonas aeruginosa quorum-controlled genes: a transcriptome analysis. *J Bacteriol* **2003,** *185* (7), 2066-79.
16. Duan, K.; Surette, M. G., Environmental Regulation of Pseudomonas aeruginosa PAO1 Las and Rhl Quorum-Sensing Systems. **2007,** *189* (13), 4827-4836.
17. Pesci, E. C.; Milbank, J. B.; Pearson, J. P.; McKnight, S.; Kende, A. S.; Greenberg, E. P.; Iglewski, B. H., Quinolone signaling in the cell-to-cell communication system of Pseudomonas aeruginosa. *Proc Natl Acad Sci U S A* **1999,** *96* (20), 11229-34.
18. Cao, H.; Krishnan, G.; Goumnerov, B.; Tsongalis, J.; Tompkins, R.; Rahme, L. G., A quorum sensing-associated virulence gene of Pseudomonas aeruginosa encodes a LysR-like transcription regulator with a unique self-regulatory mechanism. *Proc Natl Acad Sci U S A* **2001,** *98* (25), 14613-8.
19. Camilli, A.; Bassler, B. L., Bacterial Small-Molecule Signaling Pathways. *Science* **2006,** *311* (5764), 1113-1116.

20. Xiao, G.; Déziel, E.; He, J.; Lépine, F.; Lesic, B.; Castonguay, M. H.; Milot, S.; Tampakaki, A. P.; Stachel, S. E.; Rahme, L. G., MvfR, a key Pseudomonas aeruginosa pathogenicity LTTR-class regulatory protein, has dual ligands. *Mol Microbiol* **2006,** *62* (6), 1689-99.
21. Gallagher, L. A.; McKnight, S. L.; Kuznetsova, M. S.; Pesci, E. C.; Manoil, C., Functions required for extracellular quinolone signaling by Pseudomonas aeruginosa. *J Bacteriol* **2002,** *184* (23), 6472-80.
22. Diggle, S. P.; Winzer, K.; Chhabra, S. R.; Worrall, K. E.; Cámara, M.; Williams, P., The Pseudomonas aeruginosa quinolone signal molecule overcomes the cell density-dependency of the quorum sensing hierarchy, regulates rhl-dependent genes at the onset of stationary phase and can be produced in the absence of LasR. *Mol Microbiol* **2003,** *50* (1), 29-43.
23. Bala, A.; Kumar, L.; Chhibber, S.; Harjai, K., Augmentation of virulence related traits of pqs mutants by Pseudomonas quinolone signal through membrane vesicles. *J Basic Microbiol* **2015,** *55* (5), 566-78.
24. Lau, G. W.; Ran, H.; Kong, F.; Hassett, D. J.; Mavrodi, D., Pseudomonas aeruginosa pyocyanin is critical for lung infection in mice. *Infect Immun* **2004,** *72* (7), 4275-8.
25. Abdalla, M. Y.; Hoke, T.; Seravalli, J.; Switzer, B. L.; Bavitz, M.; Fliege, J. D.; Murphy, P. J.; Britigan, B. E., Pseudomonas Quinolone Signal Induces Oxidative Stress and Inhibits Heme Oxygenase-1 Expression in Lung Epithelial Cells. *Infect Immun* **2017,** *85* (9).
26. Lee, J.; Wu, J.; Deng, Y.; Wang, J.; Wang, C.; Wang, J.; Chang, C.; Dong, Y.; Williams, P.; Zhang, L. H., A cell-cell communication signal integrates quorum sensing and stress response. *Nat Chem Biol* **2013,** *9* (5), 339-43.
27. Yang, W.; Dostal, L.; Rosazza, J. P., Aeruginol [2-(2'-hydroxyphenyl)-4-hydroxymethylthiazole], a new secondary metabolite from Pseudomonas aeruginosa. *Journal of natural products* **1993,** *56* (11), 1993-4.
28. Cornelis, P., Putting an end to the Pseudomonas aeruginosa IQS controversy. *Microbiologyopen* **2020,** *9* (2), e962.
29. Capatina, D.; Lupoi, T.; Feier, B.; Olah, D.; Cristea, C.; Oprean, R., Highly Sensitive Detection of PQS Quorum Sensing in Pseudomonas Aeruginosa Using Screen-Printed Electrodes Modified with Nanomaterials. *Biosensors* **2022,** *12* (8).
30. Barr, H. L.; Halliday, N.; Camara, M.; Barrett, D. A.; Williams, P.; Forrester, D. L.; Simms, R.; Smyth, A. R.; Honeybourne, D.; Whitehouse, J. L.; Nash, E. F.; Dewar, J.; Clayton, A.; Knox, A. J.; Fogarty, A. W., Pseudomonas aeruginosa quorum sensing molecules correlate with clinical status in cystic fibrosis. *Eur Respir J* **2015,** *46* (4), 1046-54.
31. Barr, H. L.; Halliday, N.; Barrett, D. A.; Williams, P.; Forrester, D. L.; Peckham, D.; Williams, K.; Smyth, A. R.; Honeybourne, D.; L Whitehouse, J.; Nash, E. F.; Dewar, J.; Clayton, A.; Knox, A. J.; Cámara, M.; Fogarty, A. W., Diagnostic and prognostic significance of systemic alkyl quinolones for *P. aeruginosa* in cystic fibrosis: A longitudinal study. *Journal of cystic fibrosis : official journal of the European Cystic Fibrosis Society* **2017,** *16* (2), 230-238.
32. Miller, C.; Gilmore, J., Detection of Quorum-Sensing Molecules for Pathogenic Molecules Using Cell-Based and Cell-Free Biosensors. *Antibiotics (Basel)* **2020,** *9* (5).
33. Dal Bello, F.; Zorzi, M.; Aigotti, R.; Medica, D.; Fanelli, V.; Cantaluppi, V.; Amante, E.; Orlandi, V. T.; Medana, C., Targeted and untargeted quantification of quorum sensing signalling molecules in bacterial cultures and biological samples via HPLC-TQ MS techniques. *Analytical and Bioanalytical Chemistry* **2021,** *413* (3), 853-864.
34. Singh, P. K.; Schaefer, A. L.; Parsek, M. R.; Moninger, T. O.; Welsh, M. J.; Greenberg, E. P., Quorum-sensing signals indicate that cystic fibrosis lungs are infected with bacterial biofilms. *Nature* **2000,** *407* (6805), 762-4.
35. Montagut, E. J.; Raya, J.; Martin-Gomez, M.-T.; Vilaplana, L.; Rodriguez-Urretavizcaya, B.; Marco, M.-P., An Immunochemical Approach to Detect the Quorum Sensing-Regulated Virulence Factor 2-Heptyl-4-Quinoline N-Oxide (HQNO) Produced by Pseudomonas aeruginosa Clinical Isolates. *Microbiology Spectrum* **2022,** *10* (4), e01073-21.

36. Montagut, E. J.; Marco, M. P., Biological and clinical significance of quorum sensing alkylquinolones: current analytical and bioanalytical methods for their quantification. *Anal Bioanal Chem* **2021**.
37. Montagut, E. J.; Vilaplana, L.; Martin-Gomez, M. T.; Marco, M. P., High-Throughput Immunochemical Method to Assess the 2-Heptyl-4-quinolone Quorum Sensing Molecule as a Potential Biomarker of Pseudomonas aeruginosa Infections. *ACS Infectious Diseases* **2020,** *6* (12), 3237-3246.
38. Rodriguez-Urretavizcaya, B.; Pascual, N.; Pastells, C.; Martin-Gomez, M. T.; Vilaplana, L.; Marco, M. P., Diagnosis and Stratification of Pseudomonas aeruginosa Infected Patients by Immunochemical Quantitative Determination of Pyocyanin From Clinical Bacterial Isolates. *Frontiers in cellular and infection microbiology* **2021,** *11*, 786929.
39. Michalet, S.; Allard, P.-M.; Commun, C.; Ngoc, V. T. N.; Nouwade, K.; Gioia, B.; Dijoux-Franca, M.-G.; Wolfender, J.-L.; Doléans-Jordheim, A., Alkyl-Quinolones derivatives as potential biomarkers for Pseudomonas aeruginosa infection chronicity in Cystic Fibrosis. *Scientific Reports* **2021,** *11* (1), 20722.
40. Hawver, L. A.; Jung, S. A.; Ng, W.-L., Specificity and complexity in bacterial quorum-sensing systems. *FEMS Microbiology Reviews* **2016,** *40* (5), 738-752.
41. Zhao, X.; Yu, Z.; Ding, T., Quorum-Sensing Regulation of Antimicrobial Resistance in Bacteria. *Microorganisms* **2020,** *8* (3).
42. Sikdar, R.; Elias, M. H., Evidence for Complex Interplay between Quorum Sensing and Antibiotic Resistance in Pseudomonas aeruginosa. *Microbiol Spectr* **2022,** *10* (6), e0126922.
43. Hemmati, J.; Nazari, M.; Abolhasani, F. S.; Ahmadi, A.; Asghari, B., In vitro investigation of relationship between quorum-sensing system genes, biofilm forming ability, and drug resistance in clinical isolates of Pseudomonas aeruginosa. *BMC Microbiology* **2024,** *24* (1), 99.

3. The Pqs System: DEVELOPMENT OF AN IMMUNOCHEMICAL ASSAY FOR PQS

3.1 Chapter presentation

This chapter describes the development of a monoclonal antibody that specifically detects the molecule 2-heptyl-3-hydroxy-4-quinolone or PQS, the main signaling molecule of the Pqs system in *P. aeruginosa* QS. Hellen Barr (School of Medicine, University of Nottingham, UK) suggested that this molecule, along with other alkylquinolones of the Pqs system, could be potential biomarkers for infections caused by these bacteria[1, 2]. Additionally, the chapter outlines the optimization of a microplate-based ELISA for PQS detection in buffer and in Mueller-Hinton (MH) culture media. The chapter's structure is depicted in Figure 3.1.

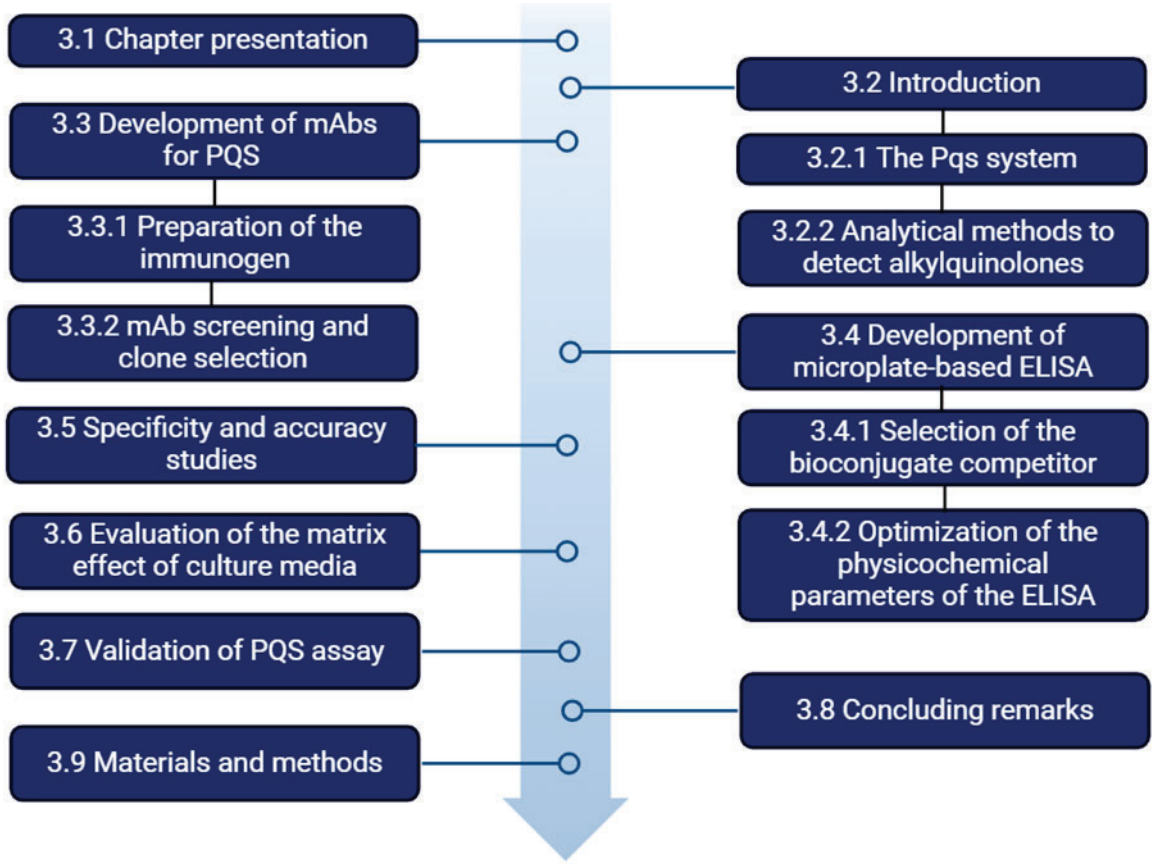

Figure 3.1: Structure of Chapter 3.1

3.2 Introduction

3.2.1 The Pqs system

The quinolone-based Pqs system, which regulates virulence factors such as PYO, elastase, lectin, and rhamnolipids, has gained significant attention from the scientific community. This system exhibits both QS-dependent and independent functions. The primary signaling molecule, PQS, specific to *P. aeruginosa*, plays crucial roles beyond its signaling activity. For instance, PQS is involved in mediating cytotoxicity and has been implicated in balancing the growth and death within *P. aeruginosa* populations[3]. PQS plays an important role in iron acquisition due to its strong chelating properties, prompting the expression of genes related to the biosynthesis of the siderophores pyoverdine and pyochelin. It has also been found that PQS promotes the formation of outer membrane vesicles owing to its pronounced lipophilic character. Moreover, PQS has been discovered to modulate the host immune response by dysregulating various defense mechanisms and cytokine expression[3].

The biosynthesis of alkylquinolones requires several genes (see Figure 3.2). The genes *pqsABCDE* are located in an operon, and alongside them are the genes *phnAB* and *pqsR*. The genes *pqsL* and *pqsH* are also responsible for biosynthesis but are located in another position on the chromosome. The first step in the biosynthesis requires the condensation of anthranilic acid with coenzyme A by PqsA, an anthranilate coenzyme A ligase. The activated thioester product (anthraniloy-CoA) is transferred to the active site of PqsD. An activated malonyl-CoA reacts with the thioester linked to PqsD to produce 2-aminobenzoylacetyl-CoA (2-ABA-CoA) through decarboxylation. In the next step, PqsE, a thioesterase generates 2-aminobenzoylacetate (2-ABA). The quinolone core is formed by the action of the heterodimeric complex PqsBC. This time, CoA-activated octanoic acid is linked to PqsC at the active site through a cysteine. The fatty acid condenses with 2-ABA to obtain 4-hydroxy-2-heptylquinoline (HHQ) through a decarboxylative condensation. Finally, PQS is produced by the hydroxylation of position 3 by the NADH-dependent flavin monooxygenase PqsH[4].

The biosynthetic cascade is also responsible for related metabolites like 2,4-dihydroxyquinoline (DHQ), 2-aminoacetophenone (2-AA), and 2-heptyl-4-quinoline N-oxide (HQNO), as well as other quinolones with different alkyl chain lengths. The previously mentioned PqsL is needed for the production of HQNO since it forms the substrate N-oxidized 2-hydroxy-aminobenzoylacetate (2-HABA), which reacts with PqsBC, condensing the N-oxide with octanoyl-CoA to yield HQNO[5].

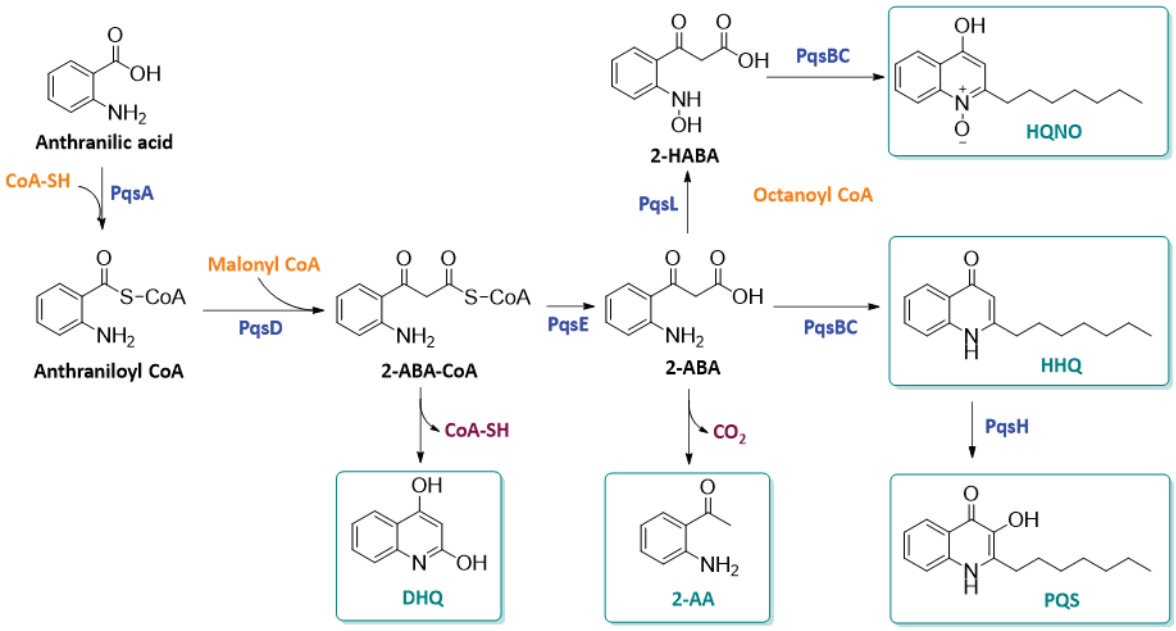

Figure 3.2: Schematic representation of biosynthetic pathway of PQS in P. aeruginosa.

3.2.2 Analytical methods to detect alkylquinolones

Due to the biological interest in molecules involved in the PQS system, multiple methods have been developed for their detection, both in culture media and in clinical samples. Ortori *et al.* developed an HPLC-MS method for PQS detection in culture media, with a quantification limit of 0.6 nM. The method exhibited recovery issues, possibly attributed to the extraction methods required for quantification[6]. Barr *et al.* conducted several studies quantifying different alkyl quinolones produced by *P. aeruginosa* in sputum, plasma, and urine samples from CF patients. The analysis was performed using HPLC-MS, requiring pre-treatment with extraction and concentration in organic solvent. They observed a correlation of the quinolone levels across the three clinical samples[1, 7, 8]. Another study by Abdalla *et al.* utilized HPLC-MS with multiple reaction monitoring to detect PQS in sputum samples from CF patients. A total of 22 samples were analyzed, with 11 being from patients whose sputum tested negative via culture and 11 from those testing positive. Among the 11 positive samples, after extraction of sputum with organic solvent and concentration of the extracted sample by 10-fold, HPLC-MS analysis was conducted. PQS was detected only in samples that had tested positive via culture, with values ranging between 0.34 and 26 nM[9].

Regarding optical or electrochemical methods, it appears that the best option for PQS detection is the boron-doped diamond electrode (BDDE)[10, 11]. Using this type of electrode, PQS has been detected in culture media. However, its detection requires extraction from the culture medium using an organic solvent, followed by evaporation to remove this solvent, and then reconstitution in an aqueous buffer for purification through solid-phase extraction columns. The method is specific enough to distinguish between PQS and HHQ and achieves a LOD of 1 nM. This electrode has also successfully detected PQS in sputum samples from CF patients following chloroform extraction, solvent evaporation, and resuspension in buffer. The recovery for PQS is 58%, showing a detection limit of 1.25 µM[12, 13].

Recently our group has reported the development of antibodies of immunochemical assays to detect different molecules within the Pqs system[14]. Hence, Montagut *et al.* reported the development of polyclonal antibodies for PQS, HHQ, and HQNO achieving detection limits of 3.6 nM, 0.17 nM, and 0.6 nM, respectively, in MH culture medium. Despite the structural similarity among these three molecules, the developed antibodies are quite specific, with only small cross-reactivity between them[15-17]. The assays were used to analyze culture media from clinical isolates obtained from patients with different respiratory diseases at different stages of the disease.

Understanding the functioning of PQS system is essential for comprehending the pathogenesis of *P. aeruginosa*. It has been proven that the PQS molecule is specific to *P. aeruginosa*, making it a potential biomarker for infection. Research has also shown that PQS levels can be used to stratify patients between acute and chronic infections or, in the case of CF patients, between chronic infections and initial colonizations[17, 18]. Therefore, if we can quantify this molecule and correlate its levels with different infection states, this information could assist clinicians in making decisions regarding the application of more appropriate treatments for their patients' conditions.

The primary method for detecting *P. aeruginosa* still relies on growth in culture media, but unfortunately, this method is very slow. For this reason, multiple alternative methods have been developed for the diagnosis of *P. aeruginosa*. Taking advantage of the specificity of the PQS molecule to *P. aeruginosa*, if this molecule can be detected in biological fluids, it could serve as a biomarker for infection [19]. Furthermore, as mentioned earlier, the levels of this molecule could provide additional information related to the diseases. Multiple techniques have been developed so far for the detection of PQS in biological fluids; unfortunately, most of these techniques are based on mass spectrometry, which is not suitable for PoC diagnostics, routine clinical analysis or high-throughput testing. Moreover, as mentioned above, usually require tedious sample treatment procedures before reliable quantification with recovery values not always quantitative.

In recent years, biosensors and PoC devices have emerged as an alternative for faster and more efficient biomarker detection. The majority of these devices utilize antibodies as a detection method due to their high specificity and affinity. Our research group was the first to develop polyclonal antibodies against PQS[17] despite its low molecular weight. The polyclonal antibodies against PQS were previously generated in New Zealand white rabbits. The synthesized PQS immunizing hapten, designed and synthesized in-house, was conjugated to the lysines of the Keyhole Limpet Hemocyanin (KLH) protein using the mixed anhydride method. Subsequently, it was emulsified with Freud's adjuvant, and the rabbits were immunized once a month for six months. Finally, rabbit serum was extracted and used as antiserum for conducting the ELISAs in an indirect competitive format. The optimized microplate-based ELISA has a half maximal inhibitory concentration (IC_{50}) of 3.87 nM and cross-reactivity of 13% with HHQ and 2% with HQNO (Figure 3.3).

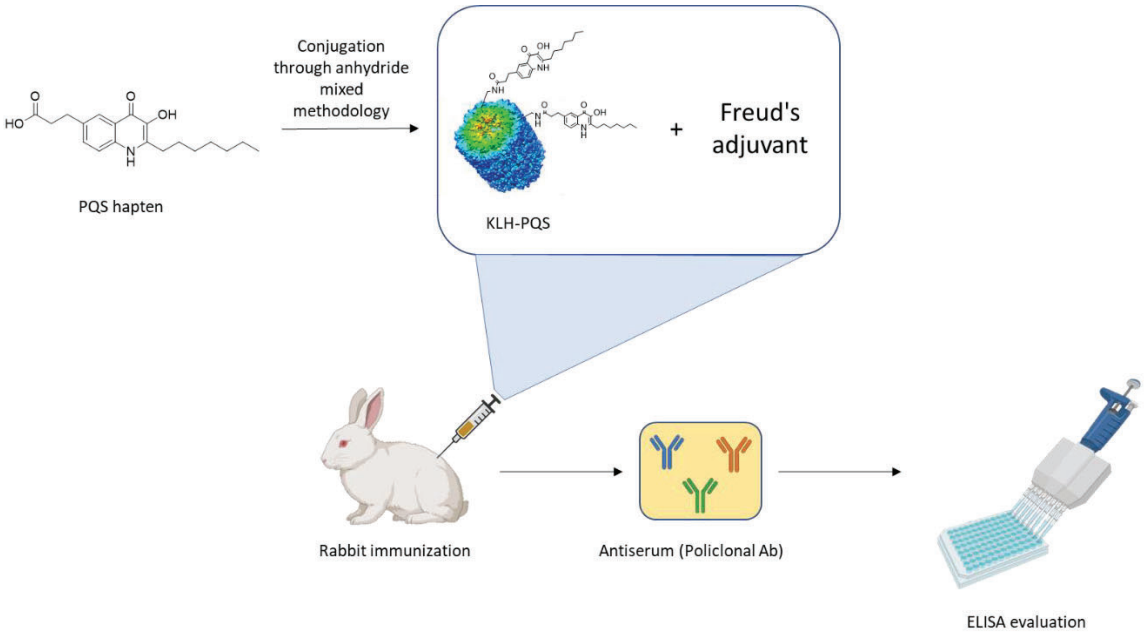

Figure 3.3: Schematic representation of the process followed for the production of polyclonal antibodies against PQS

The antibodies were proven to have excellent features in terms of avidity for the target analyte and therefore showed excellent detectability when used on ELISA. However, exhibited certain cross-reactivity with the other alkylquinolones (AQs) of the Pqs system due to the structural similarity. Moreover, a limited quantity of antibody was available owed the procedure use to obtain polyclonal antibodies; the antisera of one animal is unique and often difficult to reproduce with exactly the same features. This drawback does not prevent, but difficult their commercialization, particularly if they have to be used on diagnostic devices, which have to be approved by the regulatory authorities.

With this scenario, in this thesis presents, for the first time, the development of monoclonal antibody that recognize PQS with high sensitivity and specificity. This not only has resolved the issues of cross-reactivity with other quinolones thanks to careful screening assays but also allows for infinite production as long as the cell clone is alive and does not suffer any critical mutation. Because of the unique nature of the monoclonal antibodies (single and identical IgGs) their availability opens the possibility to use them more efficiently to biofunctionalized materials (biosensors or other nanobiotechnological approaches) as well as for in vivo and in vitro studies addressed to assess their potential for therapeutic purposes.

3.3 Development of mAbs against the PQS molecule

3.3.1 Preparation of the Immunogen

The same PQS hapten (see structure in Figure 3.4) designed and synthesized by Montagut *et al.* was used to prepare the immunogen using the mixed anhydride method. Briefly, the carboxylic group of the hapten reacted with isopropyl chloroformate to form an anhydride which reacts with the amino groups from the lysine residues of the protein to obtain the desired bioconjugate (Figure 3.4). The evaluation of the obtained bioconjugate was done using MALDI-TOF MS. With this technique, it can be verified whether there is an increase in the mass of the bioconjugate compared to the unconjugated protein, indicating that the reaction has taken place and providing information about the hapten density of the bioconjugate.

Due to the high molecular weight of KLH (390 kDa), the KLH conjugate could not be evaluated by MALDI-TOF MS for which reason, the same reaction was performed in parallel and under the same conditions with bovine serum albumin (BSA Mw 66.5 KDa). The BSA conjugate could then be analyzed by MALDI-TOF, assuming that if the reaction occurred with BSA, it would also have occurred with KLH.

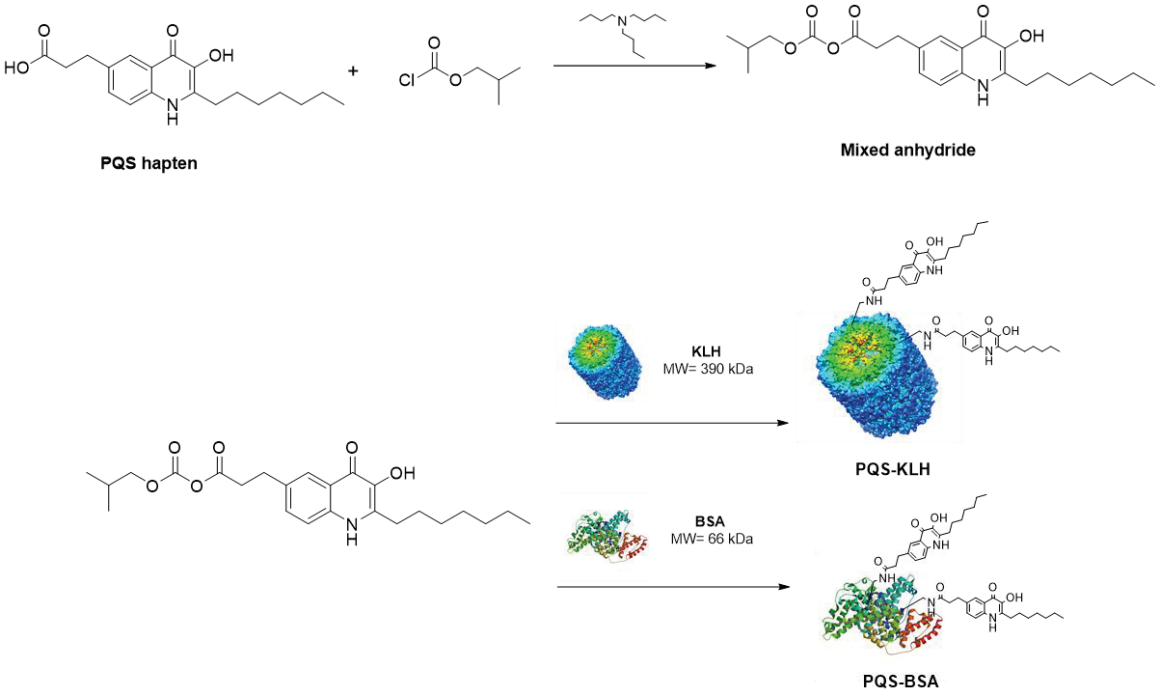

Figure 3.4: Conjugation of the PQS hapten to BSA and KLH using the mixed anhydride method.

The MALDI-TOF MS spectrum obtained when analyzing the BSA conjugate is shown in Figure 3.5.

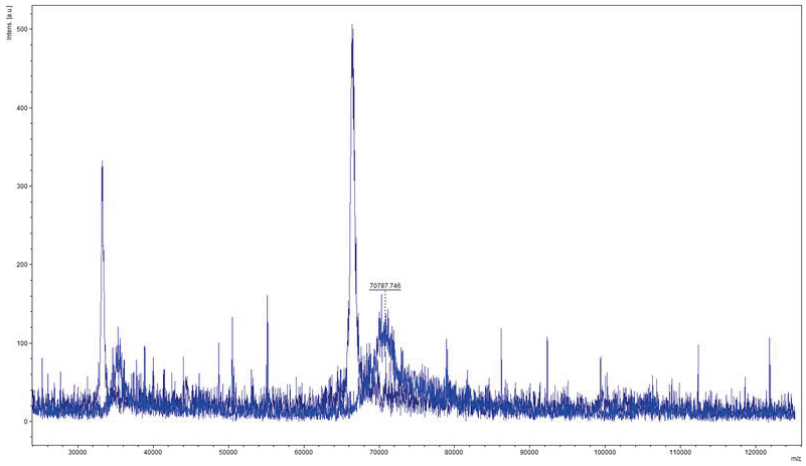

Figure 3.5: MALDI-TOF MS spectrum. In dark blue, the spectrum of BSA; in light blue, the spectrum of the BSA conjugate. The MALDI-TOF MS analysis provides information about the mass of the bioconjugate, enabling the calculation of the hapten density of the bioconjugate, in this case, 23.

In dark blue, the spectrum of BSA is displayed, and in light blue, the spectrum of the BSA bioconjugate. It can be observed that conjugation has taken place, yielding an average hapten density (HD) of 23 haptens per protein. As mentioned earlier, since both reactions have been carried out in parallel under exactly the same conditions, it is assumed that the reaction has also occurred for the KLH conjugate. 4.87 mg of the BSA conjugate were obtained with a yield of 93%, and 4.32 mg of the KLH conjugate were obtained with a yield of 88%.

3.3.2 mAb screening and clone selection

In monoclonal antibody technology, B-lymphocytes were fused with an immortal myeloma cell line lacking the hypoxanthine-guanine-phosphoribosyltransferase (HGPRT) gene to create hybridoma cells, which inherit the immortality of the myeloma cells. These hybridoma cells were then cultured in a selective medium (i.e., containing hypoxanthine-aminopterin-thymidine), where only the hybridomas survive. The myeloma cells lack HGPRT and therefore cannot synthesize nucleotides de novo, a process inhibited by aminopterin in the selective medium.

The initial culture of hybridomas contains a mixture of antibody-producing cells derived from the many different primary B-lymphocyte clones, each secreting its own individual specific antibody into the culture medium (i.e. the antibodies are still polyclonal). Each individual clone was then separated by dilution into different culture wells and culture medium screened to select those hybridoma cells producing the desired antibodies. The positive wells were re-cloned and retested for activity until single-cell clones producing the desired antibody with optimal sensitivity and specificity for the target analyte—PQS in this case—were selected. Finally, the antibodies were purified and characterized.

Hence, in this work, three female BALB/c mice and three Wistar rats were immunized with the PQS-KLH bioconjugate to obtain B-lymphocytes from the spleen of the animals. On a first instance, it was necessary to choose the best mouse or rat to collect their spleen cells for the fusion with the myeloma cells. To do this, the avidities of the antisera from the final blood of each animal towards the PQS-BSA bioconjugate were evaluated through an indirect competitive

ELISA, by adding serial dilutions of the antisera to PQS-BSA coated microplates. The experiment was conducted by assessing in parallel the response of the antisera in the absence and presence of PQS (1 µM solution) in the microwells. Table 3.1 shows the absorbances (Abs) obtained under non-competitive and competitive (presence of PQS) conditions, along with the percentage of inhibition produced by the binding of the antibody to the target analyte.

Table 3.1: Signal obtained with each of the antisera against under non-competitive and competitive conditions.

Animal	#	Abs PQS-BSA	Abs PQS-BSA + PQS	Competition rate %
Mice As dilution (1/32000)	1	1,1069	0,4973	55
	2	1,5475	0,4665	70
	3	1,1841	0,6009	49
	4	0,7468	0,3399	54
Rats As dilution (1/16000)	1	1,1091	0,6349	43
	2	0,4802	0,1429	70
	3	1,0815	0,3004	72
	4	1,0301	0,1975	81

The table displays the results for the 4 mice and 4 rats immunized with the PQS hapten. It shows the absorbance obtained for each antiserum after the final immunization in an ELISA assay. The bioconjugates were coated at 1 µg/mL and the competitor PQS was added at 1 µM. For mice, a 1/32000 dilution was used, and for rats, a 1/16000 dilution. The percentage of competition was calculated by taking the difference between the two absorbances, dividing it by the absorbance obtained without competition, and then multiplying by 100.

The antibody concentration displayed in the table is that for which the absorbance without competition was closest to one. In the case of mice, the antiserum could be more diluted, indicating a higher antibody titer compared to rats, where a more concentrated antiserum was required to achieve the same absorbance. Mice 2 and rats 3 and 4 were the animals providing the antisera with the best features. At the light of these results, it was decided to perform the spleen fusion of mouse 2 since it exhibits the highest absorbance (1.547) in the absence of PQS and the highest inhibition rate (70%) in its the presence. For the rats, it was decided to proceed with rat 4, as its antisera also showed a high antibody titer (absorbance 1.031) and the highest recognition to PQS (percentage of inhibition, 81%). The spleen of the other animals was also extracted and frozen, in case they were needed later.

3.3.2.1 Strategy of the monoclonal antibody screening

The objective of the monoclonal antibody screening in this case was to be able to select antibodies showing maximum recognition for PQS (high detectability) minimum recognition of the two other AQs of the Pqs system, despite the similar chemical structures. Hence, after performing the fusion, various rounds of screening and cloning were conducted, evaluating the avidity of antibodies for the PQS-BSA bioconjugate and the PQS analyte. Additionally, the avidity for HHQ, and HQNO was also evaluated aiming at being able to isolate a cell clone producing specific antibodies with minimum cross-reactivity for the other analytes. Table 3.2 shows the

competition rate of the three AQs on the ELISA carried out with the antibodies produced by the selected hybridomas in the third round of cloning.

Table 3.2: Percentage of competition of PQS, HHQ and HQNO with each selected hybridoma

Clone	Competition rate against PQS	Competition rate against HHQ	Competition rate against HQNO
3.2.1	96	42	18
5.4.2	93	13	2
6.1.1	96	65	26
7.1.4	96	56	9
7.5.2	79	20	7
8.5.2	67	7	7
10.1.3	96	97	34
10.4.2	90	96	2
10.5.1	89	94	3

The table shows the 9 hybridomas selected in the third cloning round. The plates were coated with PQS-BSA at a concentration of 1 µg/mL and the competitors were added at a concentration of 1 µM. The competition rates is defined as the difference between the absorbance with competition and without competition, divided by the absorbance without competition, multiplied by 100.

As it can be observed the hybridomas selected showed different profiles of recognition for the three AQs. For this reason, it was decided to select hybridomas with three different recognition profiles for the final cloning. These were hybridoma 5.4.2, which exhibits a very high recognition of PQS (high competition rate percentage) but very low for HHQ and HQNO; hybridoma 6.1.1, which shows a very high recognition of PQS and partial recognition for HHQ and HQNO; and hybridoma 10.1.3, which equally recognizes PQS and HHQ, and partially HQNO.

On the final cloning step, three cell clones were again selected (5.4.2.3, 6.1.1.5 and 10.1.3.2), each of them coming from hybridomas previously chosen, which maintained the same profiles of recognition as their parent hybridoma cells. The antibodies produced by these three clones were purified and then used to repeat the assay to assess cross-reactivity. Figure 3.6 shows that the three mAbs maintain the same recognition profiles. All of them exhibit high affinity for PQS, but the mAb 5.4.2.3 does not recognize HHQ or HQNO. The mAb 6.1.1.5 partially recognizes HHQ, and the mAb 10.1.3.2 equally recognizes PQS and HHQ while showing much lower affinity for HQNO.

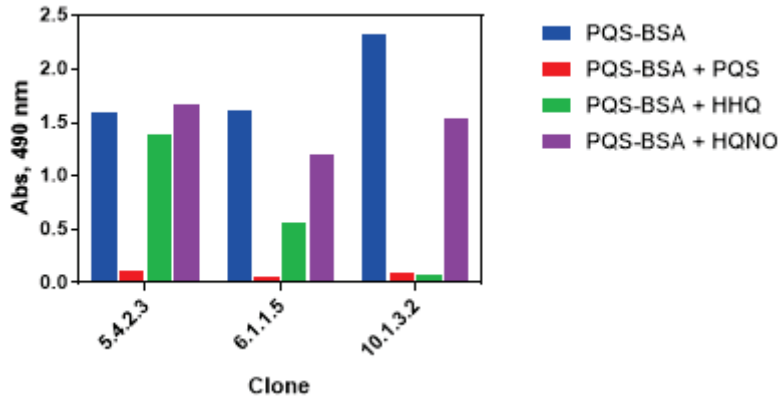

Figure 3.6: The result of the competitive indirect ELISA of the three selected clones is shown. In blue corresponds to the conditions without competition, while the red, green, and purple correspond to competition with PQS, HHQ, and HQNO respectively.

3.4 Development of microplate-based ELISAs

During the development of a competitive immunochemical assay, we determined the ability of the analyte (in this case PQS) to compete with the formation of the hapten-bioconjugate competitor in this case (PQS-BSA)-Ab complex. Two equilibrium reactions take place simultaneously leading to the analyte−Ab (K_a) and hapten-bioconjugate−Ab (K'_a) immunocomplexes (see Figure 3.7). In such assays, the ratio between both affinity constants is the key to obtain a good immunoassay with very low detection limits. To our knowledge the optimum value of K_a/K'_a ratio has never been exhaustively determined. However, it seems clear that K'_a lower than K_a would favor the equilibrium towards the formation of the analyte-Ab complex.

While a high K_a can be theoretically achieved based on an appropriate hapten design using molecular modelling and theoretical studies and monoclonal antibody screening strategy, the value of K'_a could be modulated by introducing variations on the bioconjugate competitor[20, 21]. The objective is to decrease the K'_a value to favor the formation of the analyte-Ab complex, instead of the hapten-bioconjugate complex. Hence, there are different options such as modifying the chemical structure of the competitor hapten in respect to the immunizing (hapten heterology), the attachment site of the spacer arm (site heterology), the chemical structure of the linker (linker heterology) or the chemical bioconjugation strategy (coupling method heterology). Another reported strategy to increase recognition of the analyte is to play with the hapten density of the bioconjugate competitor[22].

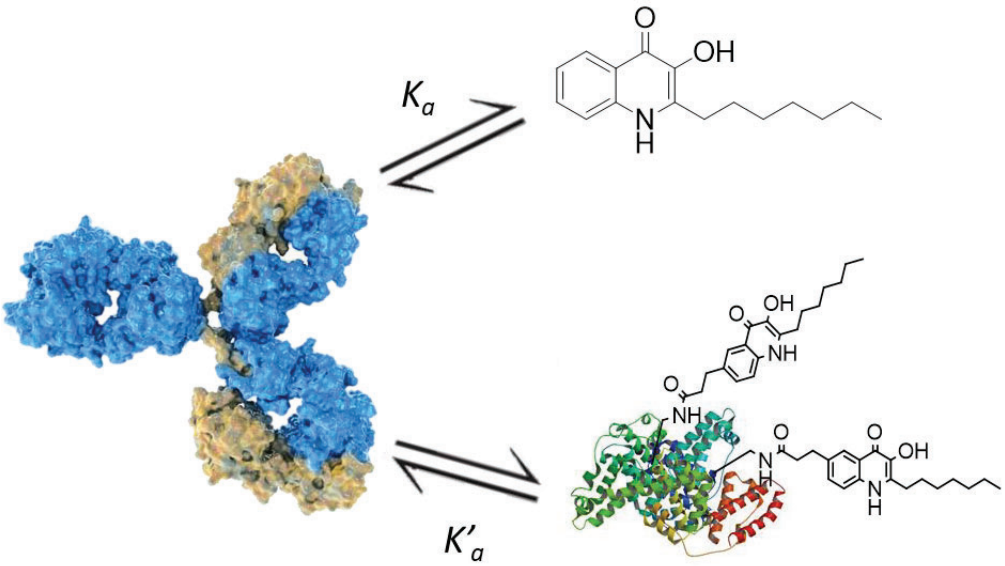

Figure 3.7: Representation of the antibody competition phenomenon against the analyte and bioconjugate.

3.4.1 Selection of the bioconjugate competitor

Different bioconjugate competitors were synthesized using different haptens and proteins at varying hapten densities, and employing different conjugation methods in order to increase the sensibility of the assay (see Table 3.3 for a complete list of the bioconjugates used in this study).

Hapten heterology. The haptens used included the one corresponding to PQS, which had been used for immunizations, and the hapten corresponding to HHQ (see Figure 3.8). Testing a different hapten than PQS was aimed at introducing heterology into the system. This strategy facilitates an increase in the value of K_a/K'_a ratio, ultimately resulting in a more sensitive assay.

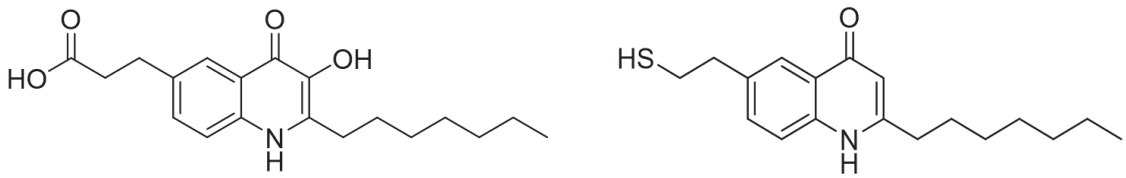

Figure 3.8: Chemical structures of the PQS and HHQ haptens.

Bioconjugation heterology. The conjugation method can also introduce heterology into the system, thereby shifting the K_a/K'_a constant towards analyte recognition, resulting in increased assay sensitivity. The immunogen was conjugated using the mixed anhydride method as described in Figure 3.4. In order to introduce heterology into the assay, different conjugation methods were tested. One of them is the active ester method. In this method, the acid group of the hapten was activated by a carbodiimide and then by an N-hydroxysuccinimide group. Finally, the lysines of the proteins attacked the activated carbonyl of the hapten to form the bioconjugate. For the HHQ bioconjugates, since the hapten has a thiol group, conjugation was performed through the reaction of the crosslinker succinimidyl iodoacetate (SIA) with the lysines

of the protein, resulting in an iodinated protein. Subsequently, the thiol of the hapten reacted with the alpha carbon of iodine through an elimination mechanism to form the bioconjugate.

Protein heterology. Another parameter that can be modified is the protein of the bioconjugate. It's crucial for this protein to be as different as possible from the immunization protein, which in this case is KLH, in order to introduce maximal heterology. The structural and physico-chemical features of the protein may introduce changes in the way the hapten is exposed for recognition by the antibody. Hence, in this study, three different proteins were used: BSA, conalbumin (CONA), and HRP. An indirect ELISA format was conducted for BSA and CONA bioconjugates, whereas the direct format was used for HRP bioconjugate.

The last parameter assessed for the bioconjugates was the ***hapten density***. When the hapten density of the bioconjugate decreases, the antibody's affinity for it also decreases, resulting in an increase in K_a/K'_a. For this reason, different bioconjugates with varying hapten densities were synthesized.

Once all the bioconjugates were produced and purified, two-dimensional titration experiments were conducted to assess the avidity of the antibodies towards the array of bioconjugate competitors prepared. In these experiments, serial dilutions of the antibodies were evaluated against a defined range of concentrations of the bioconjugate competitor. This allowed for the determination of the most appropriate concentrations to be used in the competitive assay to promote competition of the analyte while achieving a maximum absorbance of around 1 and minimal background noise. Subsequently, competitive indirect ELISAs were performed to determine the IC_{50} values achieved for each Ab/bioconjugate competitor combination.

A total of 39 ELISAs were obtained resulting from evaluating 13 bioconjugate competitors against the 3 monoclonal antibodies selected for their ability to recognize PQS. Table 3.3 shows the analytical parameters of the best Ab/bioconjugate competitor combinations found as result of the screening of competitive assays performed. The assays for further evaluation were selected based on their analytical parameters (IC_{50}<20 nM, slope 0.8-1.0, A_{max} near 1 unit, and low background noise).

Table 3.3: Detectability achieved (in terms of IC_{50}) with the different bioconjugates produced.

#	Conjugate	Hapten density	Conjugation method	mAb 5.4.2.3 IC_{50} / nM	mAb 6.1.1.5 IC_{50} / nM	mAb 10.1.3.2 IC_{50} / nM
1	PQS-BSA	3	Mixed anhydride	19,23	10,20	10,89
2	PQS-BSA	4	Active ester	27,24	21,57	21,28
3	PQS-BSA	6	Mixed anhydride	32,34	21,52	20,51
4	PQS-BSA	11	Mixed anhydride	33,44	23,34	25,83
5	PQS-BSA	12	Active ester	33,59	25,08	25,04
6	PQS-BSA	23	Mixed anhydride	44,00	31,80	33,12
7	PQS-CONA	1	Active ester	52,84	23,90	35,28
8	PQS-CONA	2	Active ester	62,11	53,38	50,35
9	PQS-HRP	2	Active ester	45,78	40,22	35,78
10	HHQ-BSA	7	SIA	21,12	13,97	40,67
11	HHQ-BSA	10	SIA	26,24	20,03	49,09
12	HHQ-BSA	14	SIA	27,74	25,71	44,74
13	HHQ-HRP	2	SIA	29,23	16,59	13,75

The table displays the detectability achieved (in terms of IC_{50}) with different bioconjugates produced, the obtained hapten density, the conjugation method used, and the IC_{50} obtained for each of the mAbs. Only those bioconjugates showing acceptable analytical parameters (IC_{50}<20 nM, slope 0.8-1.0, A_{max} near 1 unit, and low background noise) are shown. The IC_{50} values were obtained using concentrations of immunoreagents previously selected to achieve a maximum absorbance of the calibration curve of 1. mAb 5.4.2.3 PQS specific, mAb 6.1.1.5 partially recognizes HHQ, and mAb 10.1.3.2 equally recognizes PQS and HHQ showing much lower affinity for HQNO.

In order to assess whether the introduction of heterology provided by the use of the HHQ hapten has influenced the assay, bioconjugates of the same protein and similar hapten density needed to be compared. In that respect variation of the hapten chemical structure (***hapten heterology)*** did not result in a significant improvement in assay sensitivity. For example, the bioconjugate 4 (PQS hapten) shows IC_{50} values between 23 and 33 nM, while those of the bioconjugate 11 (HHQ hapten) range between 20 and 49 nM, depending on the mAb used. In the case of whether better results were obtained with CONA or BSA protein (***protein heterology***), when comparing bioconjugate 2 with bioconjugate 8, both of which have the PQS hapten and were conjugated using the active ester method, it was observed that the IC_{50} values for bioconjugate 2 (BSA) were considerably lower (around 20 nM, with the three mAbs) compared to those for bioconjugate 8 (CONA, around 50 nM with the three mAbs), even though the hapten density was lower in this case (4 vs 2). Regarding the conjugation method (***bioconjugation strategy heterology***), we can compare bioconjugates 4 and 5, which differ only in the conjugation method used, with very similar hapten densities. It can be observed that the active ester method does not decrease the IC_{50} compared to the mixed anhydride method, as both have IC_{50} values between 25 and 30 nM, despite being different conjugation methods than that of the immunogen. In contrast, a very clear trend is observed in the relationship between assay IC_{50} and ***hapten density***. Thus, when comparing the results obtained with bioconjugates 1 to 6, it can be observed that the IC_{50} gradually decreases. It decreases from around 30 nM for a hapten density of 23 to approximately 10 nM for a hapten density of 3 for the three antibodies. At the light of these results, it was decided to select bioconjugate number 1, PQS-BSA with a hapten density of 3 and conjugated using the mixed anhydride method, for the subsequent optimization steps because it exhibits the lowest IC_{50} values for all three mAbs.

3.4.2 Optimization of the physicochemical parameters of the ELISA

Other important parameters that can significantly influence the sensitivity of the assay are the physicochemical conditions during the competition stage. The first parameter evaluated was the **pre-incubation time**. The sensitivity of the ELISA can be improved by first incubating the antibody with the analyte, and then adding the mixture onto the well were the biocompetitor has been immobilized. In this way, preference is given to the antibody to interact with the analyte before interacting with the biocompetitor, thereby enhancing the detectability of the assay. Figure 3.9 shows the obtained IC_{50} and the maximum absorbance of the curve when performing the competitive indirect ELISA with different pre-incubation times.

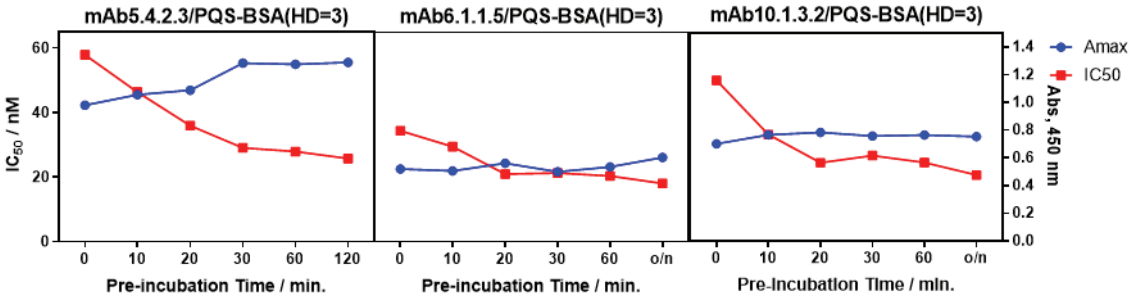

Figure 3.9: Graphs showing the effect of pre-incubation time between the analyte and the antibody on the maximum absorbance (right axis) and the IC_{50} values (left axis) of three immunochemical assays selected for optimization. In this experiment, the antibody and analyte were pre-incubated separately before the competitive step on a different microplate, each for varying durations. Subsequently, they were added to the assay microplate coated with the bioconjugate competitor and allowed to compete for 30 minutes. The absorbance and IC_{50} values presented were extracted from the four-parameter logistic equation used to calibrate the microplates. The PQS standards used to construct the calibration curve were measured in duplicate wells.

The impact of different pre-incubation times was assessed using the same microplate for each immunochemical assay. As shown in Figure 3.9, a reduction in the IC_{50} values is evident across all three assays with a pre-incubation time of 30 minutes. This effect is particularly pronounced in the assays mAb5.4.2.9/PQS-BSA(H=3) and mAb10.1.3.2/PQS-BSA(H=3), where the IC_{50} values decrease from 58 nM (no pre-incubation) to 31 nM and from 55 nM to 30 nM, respectively. Although less pronounced, there is also an improvement in detectability observed in the assay mAb6.1.1.5/PQS-BSA(H=3). In contrast, the maximum absorbance remains relatively stable regardless of pre-incubation time, except for the assay mAb5.4.2.9/PQS-BSA(H=3), where a slight increase in signal is observed (from 1.03 to 1.26). This behavior has been reported by other authors; for example, Montagut *et al.* reported an improvement in IC_{50} in an ELISA developed

for the detection of the autoinducer peptide IV of *Staphylococcus aureus* from 4.9 nM to 3.7 nM with a pre-incubation of 10 minutes[23].

The next parameter evaluated was the **competition time**. In this case, the three species antibody-analyte-bioconjugate competitor, in the mixture were allowed to interact during different time intervals.

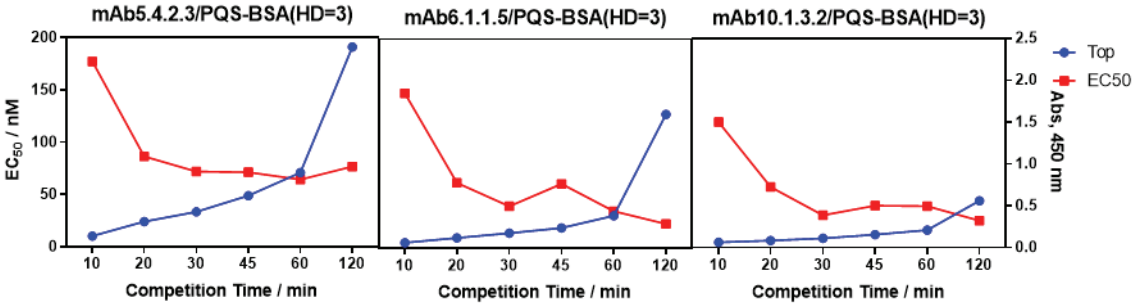

Figure 3.10: Graphs depicting the impact of competition time between the antibody-analyte-bioconjugate on the maximum absorbance (right axis) and IC_{50} values (left axis) of three immunochemical assays selected for optimization. In this experiment, the antibody, analyte, and bioconjugate were mixed simultaneously, allowing them to compete for varying time intervals. The absorbance and IC_{50} values presented were derived from the four-parameter logistic equation utilized to calibrate the microplates. PQS standards employed to construct the calibration curve were measured in duplicate wells.

Figure 3.10 shows that with a longer competition time, the IC_{50} values decreases, indicating an improvement in detectability. However, this improvement typically reaches a plateau after about 30 minutes, which is the standard competition time established in our research group. Therefore, there was no need to change the conditions based solely on detectability. However, due to the observed increase in maximum absorbance at competition times exceeding 30 minutes, it was deemed interesting to investigate whether this observation could lead to a reduction in the concentration of immunoreactants and an overall improvement in the performance of the immunochemical assay. It has often been observed that detectability increases when immunoreagents are used at lower concentrations. However, since our objective is to optimize the immunochemical assay features within the shortest possible time frame, an attempt was made to enhance the kinetics of the competition stage by conducting the assay at **37°C instead of at room temperature (RT)**, as usual. The following graphs compare the calibration curves of the competitive indirect ELISAs conducted at RT with a competition time of 2 hours and at 37°C with a competition time of 30 minutes, after adjusting the concentrations to achieve a maximum absorbance of approximately 1 (see Figure 3.11).

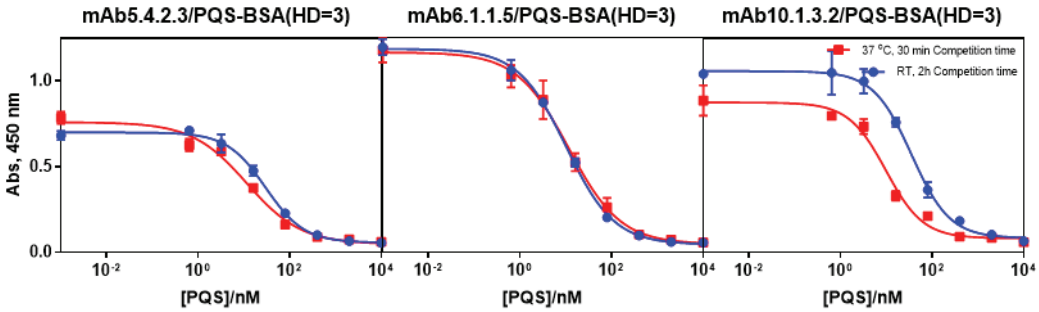

Figure 3.11: Calibration curves of the three immunochemical assays performed under different incubation times and temperature conditions. In red, a competition time of 30 minutes at 37°C; in blue, a competition time of 2 hours at room temperature. The data shown in graphs correspond to the average and standard deviation of the response of the calibrators measured using three-well-replicates.

As it can be observed, all three ELISAs had very similar analytical features (IC_{50}, slope, maximum absorbances and background noise) independently from whether the competition stage was conducted at RT for two hours or at 37°C for 30 minutes. Only on the case of the assay mAb10.1.3.2/PQS-BSA(HD=3) it was observed a slight improvement of the detectability when run at 37 ºC (see Figure 3.11) where the IC_{50} shifts from 35 nM to 10 nM. Therefore, at the light of these results it was proposed to pursuit with the optimization conducting the assays with a competition stage of 30 min at 37°C.

Subsequently, the effect of parameters such as the **conductivity, concentration of Tween 20,** and **the pH** of the buffer used in the competitive stage were evaluated (see Figure 3.12).

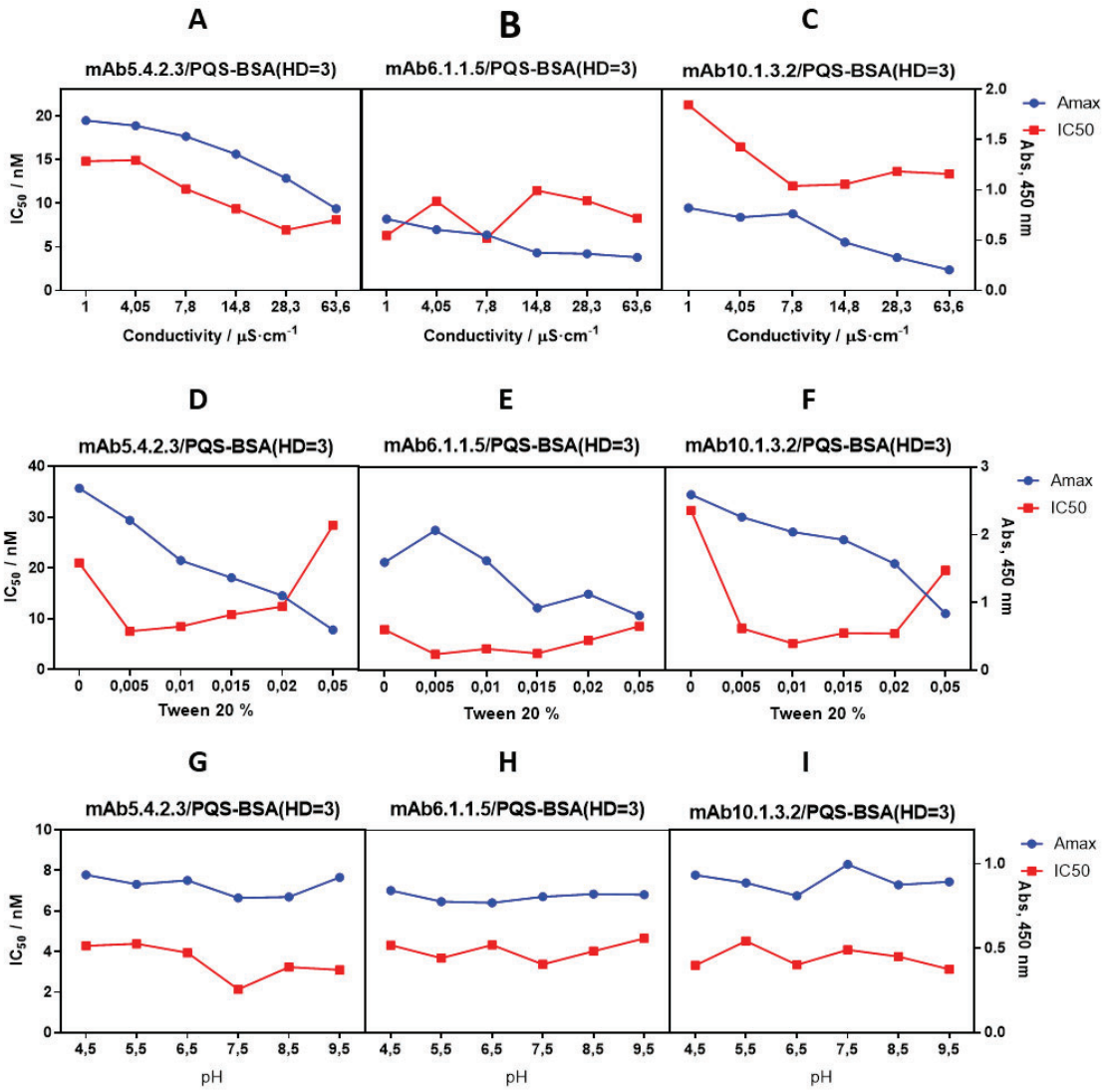

Figure 3.12: The figure shows the maximum absorbance and the IC_{50} of the calibration curves for the three mAbs under different conditions of conductivity, Tween 20, and pH. The absorbance and IC_{50} values presented were derived from the four-parameter logistic equation utilized to calibrate the microplates. PQS standards employed to construct the calibration curve were measured in duplicate wells.

The conductivity of the standard buffer used for the assays, PBS at a concentration of 10 mM, was 15 µS·cm^{-1}. It can be observed (graphs A, B, and C) that there is no significant improvement for any of the three assays when varying the conductivity. Tween 20, a detergent that reduces nonspecific interactions, such as those that may occur between proteins, was also investigated. It is noted that at zero concentration of Tween 20, the sensitivity of the assay worsens significantly in assays mAb5.4.2.3/PQS-BSA(HD=3) and mAb10.1.3.2/PQS-BSA(HD=3) (see graphs D and F, respectively). The same trend occurs in these assays when the concentration of Tween 20 exceeds 0.02%. Between 0.005% and 0.02% of Tween 20, the assays were found to be quite robust. In contrast, the detectability of the assay mAb6.1.1.5/PQS-BSA(HD=3) (see graph E) was found not to be significantly affected by the range of Tween 20 concentrations studied.

Regarding the maximum absorbance, an increase in the concentration of Tween 20 generally led to a decrease in the signal. Based on these results, 0.005% of Tween 20 was selected as the

most appropriate concentration for these assays. Finally, regarding **pH**, the assays were observed to be robust across a range of 4.5 to 9.5, as shown in graphs G, H, and I from Figure 3.12.

Due to the reported **chelating capacity** of PQS[24], it was deemed appropriate to add ethylenediaminetetraacetic acid (EDTA) to the buffer, as PQS might be interacting with traces of metals that could be present in the buffer, potentially hindering its recognition. For this reason, different concentrations of EDTA were added to the buffer of the competitive stage to see if an improvement was observed.

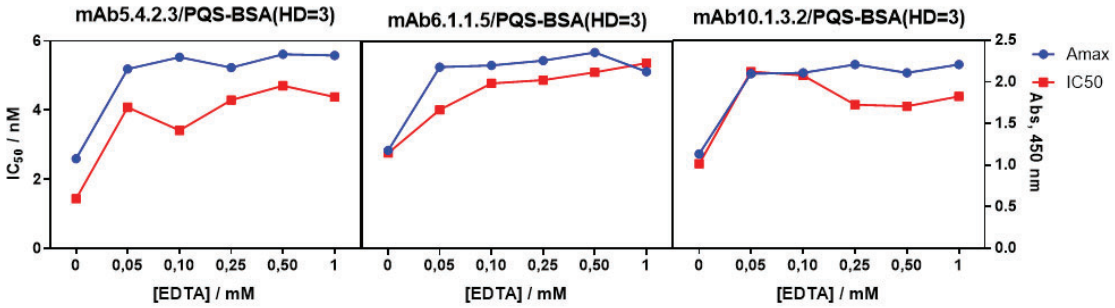

Figure 3.13: The maximum absorbance and IC_{50} of the calibration curve are shown when adding different concentrations of EDTA to the buffer in the competition stage

It can be observed in Figure 3.13 both, the maximum absorbance and the IC_{50} values increase significantly when adding small amounts of EDTA, indicating that a greater binding of the antibodies to the bioconjugate competitor coating the microwells. However, the increase of the signal allowed to perhaps dilute the immunoreagents and a potential subsequent improvement of the assay detectability. For this reason, it was decided to add 0.1 mM of EDTA to the competition buffer. As it is shown below, this fact allowed to reduce the concentration of the immunoreagents and as expected the detectability increased.

Table 3.4 summarizes the optimized physicochemical parameters for the competition stage and the ELISA conditions discussed earlier. The primary enhancement occurred through the reduction in Tween 20 concentration, an increase in temperature, and the addition of EDTA. These adjustments enabled a decrease in the concentration of immunoreagents, resulting in improved assay sensitivity.

Table 3.4: Concentration of immunoreactants and conditions chosen to run the PQS ELISAs[a]

	mAb5.4.2.3/PQS-BSA(HD=3)	mAb6.1.1.5/PQS-BSA(HD=3)	mAb10.1.3.2/PQS-BSA(HD=3)
[mAb] / µg·mL^{-1}	0.50	0.08	0.50
[PQS-BSA] / µg·mL^{-1} HD=3	0.20	0.16	0.50
pH	7.5	7.5	7.5
Conductivity / µS·cm^{-1}	15	15	15
Tween 20 / %	0.005	0.005	0.005
Competition Time / min	30	30	30
Pre-Incubation Time / min	0	0	0
Temperature / ºC	37	37	37
EDTA / mM	0.1	0.1	0.1

[a] The parameters shown are those selected from the studies of the effect of the different physico-chemical parameters described in section 3.4.2. The analytical parameters were extracted from the four-parameter logistic equation used to fit the standard curve.

The introduction of all these variations allowed to improve the performance of the three assays accomplishing IC_{50} and LOD in the low nM range. The analytical parameters of the three assays after the optimization are shown in Table 3.5. As it can be observed all of them showed excellent features in respect of the A_{max}, A_{min}, slope, IC_{50} and LOD values. Moreover, the regression coefficient resulting from the adjustment of the curve to a four-parameter logistic equation is also very good (R^2 >0.98), indicating the excellent correlation between the concentration values and the response provided by the assays.

Table 3.5: Main parameters of the calibration curves obtained for each of the optimized competitive indirect ELISAs.

	mAb5.4.2.3/PQS-BSA(HD=3)	mAb6.1.1.5/PQS-BSA(HD=3)	mAb10.1.3.2/PQS-BSA(HD=3)
A_{min}	0,06 ± 0,01	0,05 ± 0,01	0,04 ± 0,01
A_{max}	1,03 ± 0,08	0,92 ± 0,07	0,98 ± 0,10
Slope	-1,46 ± 0,11	-1,21 ± 0,09	-1,11 ± 0,13
IC_{50} / nM	4,16 ± 0,30	6,26 ± 0,27	7,28 ± 0,33
Dynamic Range / nM	10,68 ± 2,21 to 1,53 ± 0,08	12,31 ± 1,54 to 1,94 ± 0,06	15,30 ± 2,43 to 2,08 ± 0,09
LOD / nM	0,83 ± 0,05	0,95 ± 0,05	0,99 ± 0,04
R^2	0,997 ± 0,002	0,98 ± 0,006	0,997 ± 0,002

The data shown have been extracted from four-parameter logistic equation used to fit the standard curve. The values are the average and standard deviations of three assays performed on three different days. On each assay the calibrators were measured using three well replicates. The analytical parameters were extracted from the four-parameter logistic equation used to fit the standard curve.

3.5 Specificity and accuracy studies

As stated in section 3.2.2, one of the main goals in developing mAbs against PQS was to minimize the cross-reactivity towards other Pqs AQs with very similar structures, such as HHQ, HQNO or DHQ. HHQ differs from PQS only in the oxidation state of the C-3 in the molecule. Regarding HQNO, it differs solely in the oxidation state of the C-3 and contains a N-oxide group. Finally, DHQ also possesses the characteristic double ring of quinolones but lacks the alkyl chain at C-4 (See structures in Figure 3.14).

The monoclonal screening process was designed for, on each step, being able to select those hybridomas with the best features and the highest specificity. Once the three best antibodies were selected and the ELISAs established, our objective was now to probe that under competitive homologous (biocompetitor contains the same hapten used for immunizing) ELISA the specificity was, as expected, very high. These studies were conducted only with the ELISA mAb5.4.2.3/PQS-BSA(HD=3) since the specificity profile initially shown by the antibodies during the mAb screening was more useful for our purposes.

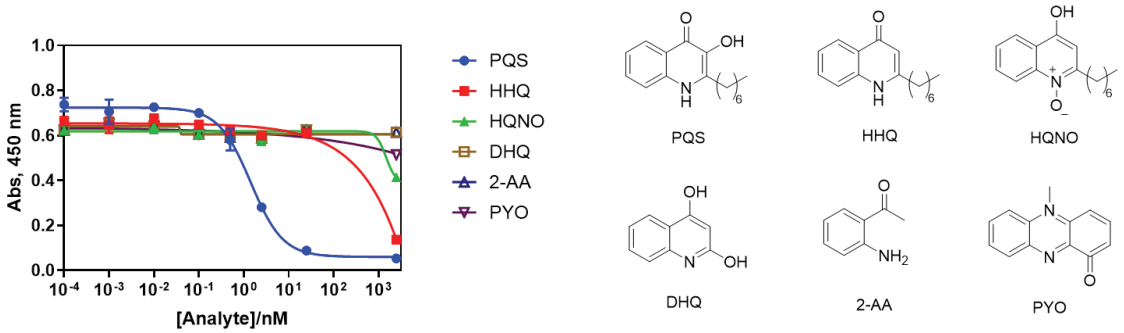

Figure 3.14: Graph showing the calibration curves of PQS, HHQ, HQNO, DHQ, 2-AA, and PYO as analytes run in the optimized ELISA mAb5.4.2.3/PQS-BSA(HD=3) using. As it can be observed only PQS is recognized while the response of the other analytes is negligible. All the curves were run in the same ELISA microplate. The data shown are the average and standard deviation of the response of calibrators measured using two-well replicates. The IC_{50} recorded for the PQS in this experiment was 4.37 ± 0.24 nM.

Figure 3.14 shows the results of the study in which the response of the ELISA mAb5.4.2.3/PQS-BSA(HD=3) towards PQS, and other quinolones with similar structures also produced by *P. aeruginosa*, as well as 2-AA and PYO, two metabolites also produced by the bacteria, were evaluated. For this purpose, calibration curves were built for each of these analytes and run in the ELISA.

As can be seen in Figure 3.14, the analytes under investigation did show very low or no response at all within the range of concentrations tested (from 2000 nM until 0.128 nM). Only HHQ was found to interact but only at the highest concentration studied. These data demonstrate the high specificity of the of mAb5.4.2.3/PQS-BSA (HD=3) optimized ELISA.

To demonstrate the accurate quantification capability of the optimized ELISA, an accuracy study was conducted. This study was conducted blindly, where samples containing PQS were prepared in buffer and analyzed using the optimized mAb5.4.2.3/PQS-BSA(HD=3) ELISA.

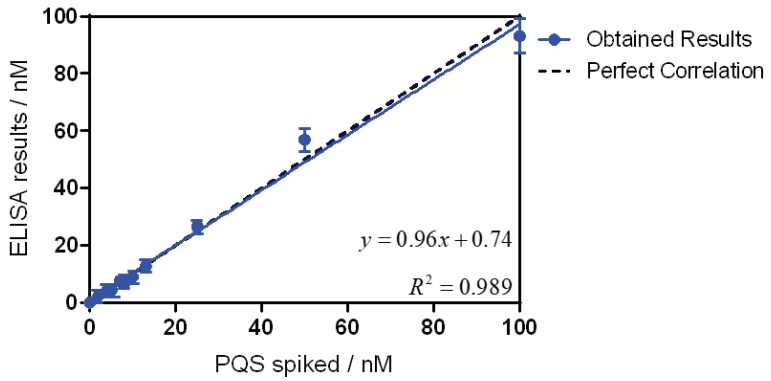

Figure 3.15: Results from the accuracy study. The graph shows the linear regression analysis of PQS spiked concentration and the concentration measured with the mAb5.4.2.3/PQS-BSA(HD=3) ELISA. Assays were run using the optimized conditions described in table 3.4. Each calibration point was measured in triplicates on the same ELISA plate and the data shown is the average and standard deviation.

As observed in Figure 3.15, the correlation coefficient between the blind spiked samples and the ELISA results is excellent (R^2=0.989), and the linear regression curve is close to 1 (slope = 0.96), indicating nearly a perfect match between the spiked concentration and the measured

concentration. This demonstrates that the assay can be utilized to measure samples with high accuracy.

3.6 Evaluation of the matrix effect of culture media

One of the most commonly used mediums for the growth of *P. aeruginosa* is the MH medium. This medium is quite complex since it is composed by the necessary nutrients for the bacteria to growth efficiently. Hence, it contains 2 % of beef infusion solids, around 17.5 % of casein hydrolysate, and 1.5 % of starch. Before measuring PQS in this complex medium, we assessed the potential nonspecific interactions caused by the media (matrix effect) to ensure it would not interfere with the PQS measurements. For this purpose, calibration curves were then generated in undiluted medium and diluted several times in the assay buffer. Figure 3.16 displays the obtained calibration curves.

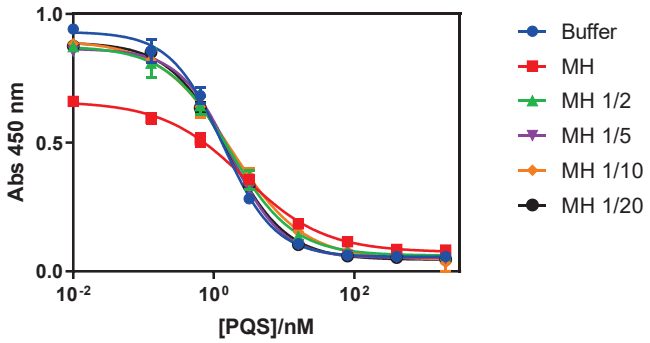

Figure 3.16: Matrix effect of undiluted MH, diluted one half, one fifth, one tenth, and one twentieth with the optimized assay buffer. Calibration curves obtained from the competitive indirect ELISA with mAb5.4.2.3/PQS-BSA HD=3 are shown. The assays were run in the same microplate. Each point of the curves is the average and standard deviation two replicates.

It can be observed that while undiluted media introduces some variation in the analytical parameters (such as a lower slope and higher IC_{50}) compared to the assay conducted in buffer, diluting only half of the culture medium with the assay buffer results in a curve closely resembling that of the buffer. Subsequent dilutions of the media do not significantly alter the analytical features of the assay. These results suggest the robustness of the ELISA for quantifying PQS in complex media such as MH medium. However, since the calibration curve of the undiluted MH still exhibits good detectability (8.47 nM vs. 4.16 m; in 1/2MH and 4.03 nM in buffer), we considered the possibility of performing measurements in undiluted MH to avoid decreasing detectability due to the dilution of the culture medium (resulting in an increase in the LOD value). Consequently, efforts were directed toward improving the assay's performance in undiluted MH media by conducting a two-dimensional assay to adjust the concentrations of immunoreactants in such media.

After fine-tuning the conditions, the calibration curve obtained in undiluted MH was very similar to that obtained in buffer (see Figure 3.17). Table 3.6 shows that the concentrations of immunoreactants are slightly higher for the MH curve; however, most parameters, including the IC_{50} and the LOD, are very similar for both curves. A detection limit below 1 nM was achieved without the need for sample purification or pre-treatment of the medium. Importantly, there was no need to dilute the complex MH culture medium to carry out the assay.

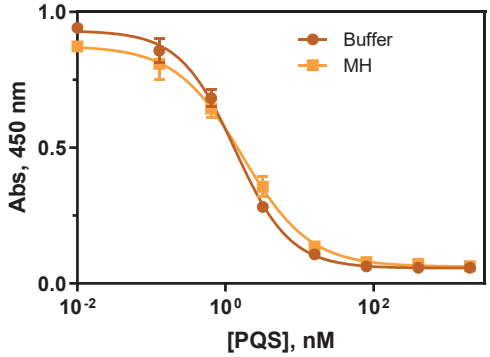

Figure 3.17: Calibration curves of the ELISA mAb5.4.2.3/PQS-BSA HD=3 in the optimized buffer and in MH. The concentrations of immunoreactants are optimized for each of the curves and shown in Table 3.6. The assays were run in the same microplate. The data shown is the average and standard deviation three replicates.

Table 3.6: Optimal concentrations of the immunoreactants and analytical parametersobtained of the ELISA mAb5.4.2.3/PQS-BSA HD=3 in buffer and in MH[a]

	Buffer	MH
[mAb 5.4.2.3] / µg·mL^{-1}	0.50	0.80
[PQS-BSA] / µg·mL^{-1} HD=3	0.20	0.875
A_{min}	0,06 ± 0,02	0,06 ± 0,01
A_{max}	0.93 ± 0,05	0,87 ± 0,05
Slope	-1,16 ± 0,10	-0,96 ± 0,11
IC_{50} / nM	1,34 ± 0,25	1,70 ± 0,20
Dynamic Range / nM	4,34 ± 0,67 to 0,38 ± 0,03	7,11 ± 0,95 to 0,41 ± 0,08
LOD / nM	0,18 ± 0,03	0,17 ± 0,05
R^2	0,998 ± 0,005	0,996 ± 0,01

[a] The data shown are the analytical parameters extracted from the four-parameter logistic equation used to fit the standard curves shown in figure 3.17. The data shown are the average an standard deviations of three assays performed on three different days. On each assay the calibrators were measured using three well replicates. The analytical parameters were extracted from the four-parameter logistic equation used to fit the standard curve.

The detectability achieved is greater than that of other techniques such as bioreporter assays[17, 25] or electrochemical detection approaches[13, 26]. Compared to HLPC-MS methods, the ELISA presented in this study yields similar or even higher detectability without necessitating additional sample treatment or pre-concentration steps. These latter methods typically entail the use of organic solvents and/or solid-phase extraction steps, often requiring a 20-fold sample concentration to achieve the reported LODs[6, 27]. Conversely, it has been documented that alkylquinolones are released into culture growth media at concentrations in the µM

range[6, 17, 25, 27, 28]. Hence, the detectability achieved by the PQS ELISA presented here indicates its strong potential for quantifying PQS in bacterial cultures and evaluating QS activation during early stages of bacterial growth. Furthermore, the achieved LOD is lower than the concentration values reported in sputum samples by Abdalla and colleagues (up to 36 nM)[9], suggesting the potential utility of this ELISA for quantifying PQS in clinical samples as well.

3.7 Validation of the PQS ELISA (mAb5.4.2.3/PQS-BSA(HD=3)) with mutant strains

As a validation method for the ELISA developed to measure PQS in MH culture medium, a reference strain of *P. aeruginosa*, PAO1, and different strains provided by Son Espases Hospital, which have been genetically characterized and confirmed to have the Pqs system mutated, were cultured. Since these strains have the Pqs system mutated, they are unable to produce the PQS molecule, and therefore, nothing should be detected with the ELISA, unlike the reference strain PAO1, which does produce PQS. For this purpose, the strains were grown in MH medium under the same time, temperature, and agitation conditions. The concentration of PQS of the obtained supernatants was measured with the ELISA developed in section 3.6. The values are shown in Table 3.7.

Table 3.7: Concentrations of PQS obtained from P. aeruginosa PAO1 and PqsR mutants

Strain	Mutation in PqsR	[PQS] / nM
PAO1	-	1945
Mutant 1	Ser199Arg	LLOD
Mutant 2	Ser199Arg	LLOD
Mutant 3	Ser199Arg	LLOD
Mutant 4	Pro238Leu	LLOD

Concentrations of PQS in the supernatants of PAO1 and PqsR mutants after 16 h of growth in MH. The supernatants were analyzed with the mAb5.4.2.3/PQS-BSA(HD=3) ELISA with the conditions described in section 3.6.

As can be observed in Table 3.7, PQS was not detected in any of the supernatants in which strains with mutations in PqsR were grown. However, as expected, levels of 1945 nM were detected in the supernatant of the reference strain of *P. aeruginosa* PAO1. This indicates that there is no interference derived from bacterial growth that influences the detection of PQS.

3.8 Concluding remarks

- For the first time, high quality mAbs against the PQS molecule of *P. aeruginosa* QS were obtained. The appropriately designed screening strategy conducted to select clones with different profiles of specificity. Particulary, mAb 5.4.2.3 was found to be highly specific to the PQS molecule which was one of our main goals for this study. The other mAbs selected may found application on further studies in which detection of other QS molecules of the Pqs system may be required.

- The mAb 5.4.2.3 against PQS was used to develop an ELISA enabling the quantification of PQS with a detection limit of 0.18±0.03 nM in buffer. Furthermore, the ELISA exhibits high specificity towards PQS, superior to that reported by Montagut *et al.*[17] with a pAb. The assay functions across a wide range of physicochemical conditions, demonstrating its high robustness. Additionally, it shows excellent accuracy, allowing reliable measurement of the target analyte.

- The mAb5.4.2.3/PQS-BSA(HD=3) ELISA was optimized for the detection of PQS in the complex MH culture medium. A LOD of 0.17±0.05 nM was achieved in this culture medium, a value much lower than the reported PQS values in bacterial cultures. This enables the quantification of PQS in *P. aeruginosa* bacterial cultures, facilitating the study of the complex QS mechanism of the bacteria and its detection in healthcare institutions, which can provide significant value to clinicians' decisions.

3.9 Materials and methods

3.9.1 Chemicals and Biochemicals

All chemical substances and proteins used have been purchased from Sigma-Aldrich. The synthesis of PQS and HHQ haptens is described in the following publications[15, 17] .
MH broth (Sigma Aldrich) was prepared by dissolving 21 g of MH powder in 1 L of deionized water, following the manufacturer's instructions. The resulting liquid medium was then autoclaved at 121 ^{o}C for 15 minutes.

3.9.2 Equipment

The pH and conductivity of all buffers and solutions were measured using a pH-meter pH 540 GLP and a conductimeter LF 340 (WTW, Weilheim, Germany) respectively. Polystyrene microtiter plates (Maxisorp, Roskilde, Denmark) were employed for the ELISAs, while dilution plates were procured from Nirco (Barberà del Vallés, Spain). Washing steps were conducted using a Biotek ELx465 (Biotek Inc.). Absorbances were recorded at 450 nm using a Thermo Scientific MultiSkan GO (Thermo Fisher Scientific, Waltham, MA, USA) in single wavelength mode. Competitive curves were analyzed using a four-parameter logistic equation in GraphPad Prism 7.0 software (GraphPad Software Inc., San Diego, CA, USA) according to the formula: y = B(A−B)/[1 − (x/C)D], where A represents the maximum absorbance, B the minimum absorbance, C the concentration producing 50% of the maximal absorbance, and D the slope at the inflection point of the sigmoid curve. Unless stated otherwise, presented data represent the average of at least two well replicates. The autoclave is the Presoclave II 75 from Selecta and the centrifuge is the 5810 R from Eppendorf.

3.9.3 Buffers

Phosphate buffer saline (PBS): 10mM phosphate buffer and 0.8% saline solution (pH 7,5). ***Coating buffer:*** 50 mM bicarbonate-carbonate buffer (pH 9,6). ***PBST:*** PBS with 0,05% Tween 20 (pH 7,5). ***Citrate buffer***: 40 mM sodium citrate solution (pH 5,5). ***Substrate solution:*** 0,01% of 3,3',5,5'- tetramethylbenzidine (TMB) and 0,004% H_2O_2 prepared in citrate buffer. ***Borate buffer***: 0,2 M sodium borate/boric acid (pH 8,7).

All buffers were prepared using ultra-pure Milli-Q® water with a resistivity between 16-18 MΩ·cm.

3.9.4 Purification procedures

The purification of conjugates was conducted using ÄKTA Prime Plus equipment with two HiTrap desalting columns from GE Healthcare. Alternatively, purification was carried out through dialysis using Spectra/Por membranes sourced from Spectrumlabs with a molecular weight cut-off of 12-14 kDa.

3.9.5 MALDI-TOF MS analysis and HD calculation

The MALDI-TOF MS instrument utilized for this study was a Bruker autoflex III Smartbeam spectrometer. HD of the conjugates were determined using MALDI-TOF-MS, comparing the molecular weights obtained from the MALDI spectra of the native proteins with the bioconjugates. To achieve this, the bioconjugates were combined with a freshly prepared matrix (trans-3,5-dimethoxy-4-hydroxycinnamic acid, 10 mg·mL^{-1} in 70:30 ACN/H_2O with 0.1% HCOOH) following the 'sandwich' sample preparation method. The bioconjugate aliquot was diluted by half using ACN with 0.2% HCOOH. Subsequently, 2 µL of the matrix was applied to the MALDI

plate and dried, followed by the addition of the bioconjugate solution (2 µL, 2 to 5 mg·mL^{-1} in 1:1 ACN/H_2O, 0.1% HCOOH), allowed to dry again, and finally, 2 µL of the matrix solution was reapplied. The resulting dried spot underwent analysis by MALDI-TOF-MS.

HD was calculated using the equation: [MW(conjugate) − MW(native protein)]/[MW(hapten)-MW(lost atoms)].

3.9.6 Synthesis of bioconjugates

Synthesis of bioconjugate PQS-KLH and PQS-BSA through mixed anhydride method: The PQS hapten (2.42 mg, 7.30 µmol) was dissolved in 400 µL of anhydrous DMF. While stirring in an ice bath, 2.09 µL (9 µmol, 1.2 eq.) of tributylamine and 1.14 µL (9 µmol, 1.2 eq.) of isobutyl chloroformate were added. The reaction was stirred on ice for 15 minutes and then for an additional 30 minutes at room temperature. Then, 200 µL of the reaction were added dropwise to a protein solution (BSA or KLH, 2.5 mg mL^{-1}, 2 mL in 10 mM PBS, pH 7.5). The reaction was left stirring for 1.5 hours. The bioconjugates were purified by dialysis against 0.5 mM PBS (5 x 5 L) and against Milli-Q water (1 x 5 L). A 20 µL fraction was reserved for MALDI-TOF MS analysis. Subsequently, it was frozen at -80°C and lyophilized. A total of 4.87 mg of the BSA conjugate and 4.32 mg of KLH conjugate were obtained.

Synthesis of bioconjugates PQS-BSA of HD=3, 6, and 11 through mixed anhydride method: The PQS hapten (1.3 mg, 4 µmol) was dissolved in 600 µL of anhydrous DMF. While stirring in an ice bath, 1.11 µL (4.8 µmol, 1.2 eq.) of tributylamine and 0.608 µL (4.8 µmol, 1.2 eq.) of isobutyl chloroformate are added. The reaction was stirred on ice for 15 minutes and then for an additional 30 minutes at room temperature. Three different BSA solutions (2.5 mg·mL^{-1}, 2 mL in 10 mM PBS, pH 7.5) were then prepared, and of the reaction crude were added dropwise (346 µL, 173 µL, and 80 µL, respectively) to the protein solution under agitation. The reaction was left stirring for 1.5 hours. The bioconjugates were purified by dialysis against 0.5 mM PBS (5 x 5 L) and against Milli-Q water (1 x 5 L). A fraction (20 µL) was reserved for MALDI-TOF MS analysis. Subsequently, it was frozen at -80°C and lyophilized. A total of 4.88 mg, 4.95 mg, and 4.83 mg were obtained with HD of 11, 6, and 3, respectively. The bioconjugates were stored freeze-dried at -40 ºC. Working aliquots(50 µL, 1 mg·mL^{-1}) were prepared at and stored frozen until use. Once unfrozen there were kept a 4ºC for about 2 weeks.

Synthesis of PQS-BSA bioconjugates through the active ester method: 2.19 mg (2.63 µmol) of PQS hapten was weighed and dissolved in 400 µL of anhydrous DMF. 0.76 mg (3.7 µmol, 1.5 eq.) of N,N'-dicyclohexylcarbodiimide (DCC) and 0.43 mg (3.7 µmol, 1.5 eq.) of N-hydroxysuccinimide (NHS) were added. The mixture was stirred for one hour at room temperature. A suspension was formed due to the insoluble urea. It was centrifuged at 10,000 rpm for 10 minutes. Two solutions of 5 mg BSA in 2 mL borate buffer were prepared. 300 µL and 100 µL of the supernatant were added dropwise to the protein solutions. The mixture was stirred for 4 h at RT. The bioconjugates were purified by dialysis against 0.5 mM PBS (5 x 5 L) and against Milli-Q water (1 x 5 L). A 20 µL fraction was reserved for MALDI-TOF MS analysis. Subsequently, it was frozen at -80°C and lyophilized. A total of 4.33 mg and 4.25 mg were obtained with HD of 12 and 4, respectively.

Synthesis of bioconjugates PQS-CONA through the active ester method: The same procedure as before was followed, but instead of using BSA, conalbumin (CONA) was utilized. Densities of hapten 1 and 2 yielded 4.66 mg and 4.25 mg, respectively.

Synthesis of bioconjugates PQS-HRP through the active ester method: The same procedure as for BSA conjugates was followed, but horseradish peroxidase (HRP) was used. Densities of hapten 2 resulted in 4.33 mg and 4.55 mg, respectively.

Synthesis of bioconjugates HHQ-HRP through the SIA method: A solution with 15 mg of BSA in 4.5 mL of borate buffer and another with 5 mg of HRP in 1.8 mL of borate buffer were prepared. 3.75 mg of SIA were weighed and dissolved in 700 µL of anhydrous DMF. 500 µL and 200 µL were added dropwise to the BSA and HRP solutions, respectively, with agitation. The mixture was left stirring for 4 hours at room temperature. The solutions were purified using a HiTrap size exclusion desalting column and borate as the eluting buffer, to isolate the protein-SIA intermediates. A fraction (20 µL) of the BSA-SIA bioconjugate was kept for MALDI-TOF MS analysis. 3.20 mg (10.4 µmol) of HHQ hapten were weighed and dissolved in 800 µL of anhydrous DMF. The purified BSA-SIA was divided into three fractions of 3 mL each. 267 µL, 178 µL, and 87 µL of the hapten solution were added to each BSA solution. 267 µL of the hapten solution was added to 4 mL of the HRP-SIA solution. The bioconjugates were purified by dialysis against 0.5 mM PBS (5 x 5 L) and Milli-Q water (1 x 5 L) and stored freeze-dried at -80 ºC. A small fraction (20 µL) of the conjugates was kept for MALDI-TOF-MS analysis. 4.13 mg, 4.02 mg, and 3.98 mg with hapten densities of 14, 10, and 7, respectively, were obtained for HHQ-BSA, and 3.96 mg of HHQ-HRP with a hapten density of 2.

3.9.7 Immunochemistry

3.9.7.1 Antibody production

All the here presented mAbs have been produced by the Custom Antibody Service (CAbS) Unit which belongs to CIBER in Bioengineering, Biomaterials and Nanomedicne (CIBER-BBN at the IQAC−CSIC) [17].

Female BALB/c mice and Wistar rats aged 8-10 weeks were immunized with PQS-BSA. The initial dose comprised 100 µg of the conjugate administered intraperitoneally as an emulsion of PBS and complete Freund's adjuvant. Subsequently, three booster injections were administered at 3-week intervals, utilizing the same immunogen dose emulsified in incomplete Freund's adjuvant. Animals chosen as spleen donors for hybridoma production received a concluding injection of 100 µg of the antigen in PBS four days prior to the fusion process.

P3-X63/Ag 8.653 murine myeloma cells (ATCC, Rockville, MD) were cultivated in supplemented Dulbecco's Modified Eagle Medium (high-glucose DMEM with 2 mM alanylglutamine, 1 mM minimum nonessential amino acids, and 25 $\mu g \cdot mL^{-1}$ gentamicin supplemented with 10% (v/v) fetal bovine serum (FBS)). Animal spleen lymphocytes were fused with myeloma cells at a 4:1 ratio using PEG 1500 (Roche Applied Science) as the fusing agent. The resulting fused cells were cultured in 96-well culture plates at a density of 2 x 10^5 cells/100 µl of 15% FBS supplemented DMEM per well. After 24 hours, hypoxanthine-aminopterin-thymidine (HAT) selection medium (10% FBS supplemented DMEM with 100 µM hypoxanthine, 0.4 µM aminopterin, 16 µM thymidine, 2% Hybridoma Fusion and Cloning Supplement (HFCS, Roche)) was added (100 $\mu l \cdot well^{-1}$) [29]. Subsequently, 10 days post-cell fusion, culture supernatants were screened through

indirect ELISA assays. Plates were coated with 1.0 µg·mL^{-1} of the PQS-BSA conjugate to select hybridomas capable of recognizing PQS with high affinity. The selected hybridomas were then cloned using the limiting dilution method, employing HAT medium without aminopterin (HT) supplemented with 15% FBS and 1% HFCS. Finally, stable antibody-producing clones were expanded, cryopreserved in liquid nitrogen, and the resulting supernatants containing mAbs were purified via protein G affinity chromatography (See Figure 3.18).

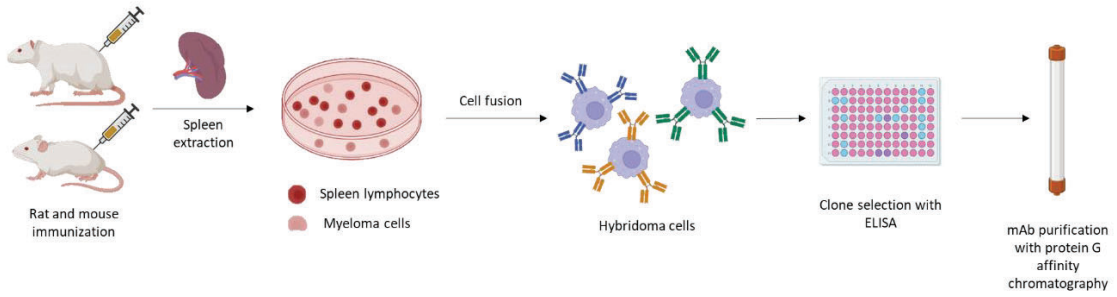

Figure 3.18: Schematic representation of the process of monoclonal antibody production and purification

3.9.7.2 ELISA

Non-competitive indirect two-dimensional titration experiments were conducted with the aim of determining the optimal concentrations of the coating antigen (CA) and mAb dilutions for subsequent competitive assays. A microtiter plate was coated with varying concentrations of the corresponding CA, ensuring that each row contained a different concentration (ranging from 5 µg·mL^{-1} to 5 ng·mL^{-1}, and zero in coating buffer, 100 µL·well^{-1}). The plate was left overnight at 4ºC. Subsequently, the plate was washed (4 x 300 µL, PBST), and different concentrations of mAb were added, ensuring that each column contained a different concentration (ranging from 5 µg·mL^{-1} to 78 ng·mL^{-1}, and zero in the assay buffer, 100 µL·well^{-1}). The plate was incubated for 30 minutes at room temperature, followed by a washing step (4 x 300 µL, PBST). Next, 100 µL/well of goat anti-mouse IgG or rabbit anti-rat IgG labeled with HRP (1/6000 in PBST) was added, and the plate was incubated for an additional 30 minutes at RT. Subsequently, the plate was washed (4 x 300 µL, PBST), and the substrate solution (100 µL/well) was added, incubating another 30 minutes at room temperature, shielded from light. The enzymatic reaction was stopped by adding 4M H_2SO_4 (50 µL·well^{-1}), and the absorbance was finally read at 450 nm.

Non-direct Competitive ELISA. Microtiter plates were coated with CA in coating buffer overnight at 4ºC. The following day, the plates were washed (4 x 300 µL, PBST), and solutions of PQS standards (ranging from 2 µM to 0.13 nM in PBST, 50 µL·well^{-1}) were added. Subsequently, the solution of mAb was added, and the microplates was left for 30 minutes at room temperature. After another round of washing (4 x 300 µL, PBST), a solution of goat anti-mouse IgG labeled with HRP (1/6000 in PBST) was added and incubated for an additional 30 minutes at room temperature. Following another wash (4 x 300 µL, PBST), the substrate solution (100 µL) was added and left for 30 minutes at room temperature in the dark. The enzymatic reaction was halted by the addition of 4N H_2SO_4 solution (50 µL·well^{-1}), and the absorbance was measured at 450 nm.

ELISA mAb5.4.2.3/PQS-BSA (HD=3) for the detection of PQS in buffer. Microtiter plates were coated with 0.20 µg·mL^{-1} of PQS-BSA HD=3 in coating buffer and left overnight at 4ºC. The

following day, the plates were washed (4 x 300 µL, PBST), and solutions of PQS standards (ranging from 2 µM to 0.13 nM in sterile MH, 50 µL·well-1) and the samples were added. Subsequently, the solution of mAb5.4.2.3 was added (0.50 µg·mL^{-1}, and the microplate was left for 30 minutes at 37 ºC. After another round of washing (4 x 300 µL, PBST), a solution of goat anti-mouse IgG labeled with HRP (1/6000 in PBST) was added and incubated for an additional 30 minutes at room temperature. Following another wash (4 x 300 µL, PBST), the substrate solution (100 µL) was added and left for 30 minutes at room temperature in the dark. The enzymatic reaction was halted by the addition of 4N H_2SO_4 solution (50 µL·well^{-1}), and the absorbance was measured at 450 nm.

Cross-reactivity studies were conducted using molecules structurally similar to PQS produced by *P. aeruginosa* (HHQ, HQNO, DHQ, 2-AA, and PYO). The ELISA mAb5.4.2.3/PQS-BSA (HD=3) for the detection of PQS in buffer, as described earlier, was performed by adding these molecules as analytes at concentrations ranging from 2 µM to 0.13 nM.

Matrix effect assay: The ELISA mAb5.4.2.3/PQS-BSA (HD=3) for the detection of PQS in buffer was followed, but the analyte dilutions were prepared in sterile MH and MH diluted one half, one fifth, one tenth, and one twentieth.

ELISA mAb5.4.2.3/PQS-BSA (HD=3) for the detection of PQS in MH. Microtiter plates were coated with 0.875 µg·mL^{-1} of PQS-BSA HD=3 in coating buffer and left overnight at 4ºC. The following day, the plates were washed (4 x 300 µL, PBST), and solutions of PQS standards (ranging from 2 µM to 0.13 nM in sterile MH, 50 µL·well-1) and the samples were added. Subsequently, the solution of mAb5.4.2.3 was added (0.80 µg·mL^{-1}, and the microplate was left for 30 minutes at 37 ºC. After another round of washing (4 x 300 µL, PBST), a solution of goat anti-mouse IgG labeled with HRP (1/6000 in PBST) was added and incubated for an additional 30 minutes at room temperature. Following another wash (4 x 300 µL, PBST), the substrate solution (100 µL) was added and left for 30 minutes at room temperature in the dark. The enzymatic reaction was halted by the addition of 4N H_2SO_4 solution (50 µL·well^{-1}), and the absorbance was measured at 450 nm.

3.9.8. Measurement of PQS in supernatants of *P. aeruginosa*

Bacterial isolate frozen stocks of PAO1 and *P. aeruginosa* PqsR mutants were streaked onto Columbia agar plates supplemented with 5% sheep blood (*Biomerieux* Ref. 43041) and then incubated overnight at 37 ºC. The following day, a colony from each isolate was transferred using a sterile swab into 10 mL Falcon tubes containing 3 mL of MH liquid media. These were then incubated with gentle shaking (500 rpm) at 37 ºC. Once the turbidity reached OD_{600} values between 0.2-0.3 (equivalent to a McFarland turbidity containing approximately $1{\cdot}10^8$ CFUs·mL^{-1}), sample aliquots (3 µL) were taken and diluted in MH broth (3 mL). The prepared bacterial suspensions were then incubated at 37 ºC with gentle shaking (500 rpm) for 16 hours. Subsequently, the cultures were centrifuged at 500 g for 5 minutes. The pellet was discarded, and the supernatant was analyzed using the ELISA mAb5.4.2.3/PQS-BSA (HD=3) described in section 3.9.7.

3.10 References

1. Barr, H. L.; Halliday, N.; Cámara, M.; Barrett, D. A.; Williams, P.; Forrester, D. L.; Simms, R.; Smyth, A. R.; Honeybourne, D.; Whitehouse, J. L.; Nash, E. F.; Dewar, J.; Clayton, A.; Knox, A. J.; Fogarty, A. W., Pseudomonas aeruginosa quorum sensing molecules correlate with clinical status in cystic fibrosis. *The European respiratory journal* **2015,** *46* (4), 1046-54.
2. CAMARA, M.; WILLIAMS, P.; BARRETT, D.; HALLIDAY, N.; KNOX, A.; SMYTH, A.; FOGARTY, A.; BARR, H.; FORRESTER, D. ALKYL QUINOLONES AS BIOMARKERS OF PSEUDOMONAS AERUGINOSA INFECTION AND USES THEREOF. 20.11.2014, 2014.
3. Lin, J.; Cheng, J.; Wang, Y.; Shen, X., The Pseudomonas Quinolone Signal (PQS): Not Just for Quorum Sensing Anymore. *Frontiers in cellular and infection microbiology* **2018,** *8*, 230.
4. Heeb, S.; Fletcher, M. P.; Chhabra, S. R.; Diggle, S. P.; Williams, P.; Cámara, M., Quinolones: from antibiotics to autoinducers. *FEMS Microbiol Rev* **2011,** *35* (2), 247-74.
5. Schütz, C.; Empting, M., Targeting the Pseudomonas quinolone signal quorum sensing system for the discovery of novel anti-infective pathoblockers. *Beilstein J Org Chem* **2018,** *14*, 2627-2645.
6. Ortori, C. A.; Dubern, J. F.; Chhabra, S. R.; Cámara, M.; Hardie, K.; Williams, P.; Barrett, D. A., Simultaneous quantitative profiling of N-acyl-L-homoserine lactone and 2-alkyl-4(1H)-quinolone families of quorum-sensing signaling molecules using LC-MS/MS. *Anal Bioanal Chem* **2011,** *399* (2), 839-50.
7. Webb, K.; Fogarty, A.; Barrett, D. A.; Nash, E. F.; Whitehouse, J. L.; Smyth, A. R.; Stewart, I.; Knox, A.; Williams, P.; Halliday, N.; Cámara, M.; Barr, H. L., Clinical significance of Pseudomonas aeruginosa 2-alkyl-4-quinolone quorum-sensing signal molecules for long-term outcomes in adults with cystic fibrosis. *J Med Microbiol* **2019,** *68* (12), 1823-1828.
8. Zain, N. M. M.; Webb, K.; Stewart, I.; Halliday, N.; Barrett, D. A.; Nash, E. F.; Whitehouse, J. L.; Honeybourne, D.; Smyth, A. R.; Forrester, D. L.; Knox, A. J.; Williams, P.; Fogarty, A.; Cámara, M.; Bruce, K. D.; Barr, H. L., 2-Alkyl-4-quinolone quorum sensing molecules are biomarkers for culture-independent Pseudomonas aeruginosa burden in adults with cystic fibrosis. *J Med Microbiol* **2021,** *70* (10).
9. Abdalla, M. Y.; Hoke, T.; Seravalli, J.; Switzer, B. L.; Bavitz, M.; Fliege, J. D.; Murphy, P. J.; Britigan, B. E., Pseudomonas Quinolone Signal Induces Oxidative Stress and Inhibits Heme Oxygenase-1 Expression in Lung Epithelial Cells. *Infection and immunity* **2017,** *85* (9).
10. Zhou, L.; Glennon, J. D.; Luong, J. H.; Reen, F. J.; O'Gara, F.; McSweeney, C.; McGlacken, G. P., Detection of the Pseudomonas Quinolone Signal (PQS) by cyclic voltammetry and amperometry using a boron doped diamond electrode. *Chem Commun (Camb)* **2011,** *47* (37), 10347-9.
11. Oziat, J.; Elsen, S.; Owens, R. M.; Malliaras, G. G.; Mailley, P., Electrochemistry provides a simple way to monitor Pseudomonas aeruginosa metabolites. *Annu Int Conf IEEE Eng Med Biol Soc* **2015,** *2015*, 7522-5.
12. Buzid, A.; Luong, J. H. T.; Reen, F. J.; O'Gara, F.; Glennon, J. D.; McGlacken, G. P., Rapid Electrochemical Detection of Pseudomonas aeruginosa Signaling Molecules by Boron-Doped Diamond Electrode. *Methods Mol Biol* **2018,** *1673*, 107-116.
13. Buzid, A.; Shang, F.; Reen, F. J.; Muimhneacháin, E. Ó.; Clarke, S. L.; Zhou, L.; Luong, J. H. T.; O'Gara, F.; McGlacken, G. P.; Glennon, J. D., Molecular Signature of Pseudomonas aeruginosa with Simultaneous Nanomolar Detection of Quorum Sensing Signaling Molecules at a Boron-Doped Diamond Electrode. *Scientific Reports* **2016,** *6* (1), 30001.
14. MARCO COLÁS, M. P.; MONTAGUT CAÑETE, E. J. IN VITRO METHOD FOR DETECTION OF INFECTIONS CAUSED BY PSEUDOMONAS AERUGINOSA. 07.10.2021.
15. Montagut, E. J.; Vilaplana, L.; Martin-Gomez, M. T.; Marco, M. P., High-Throughput Immunochemical Method to Assess the 2-Heptyl-4-quinolone Quorum Sensing Molecule as a

Potential Biomarker of Pseudomonas aeruginosa Infections. *ACS Infectious Diseases* **2020,** *6* (12), 3237-3246.
16. Montagut, E. J.; Raya, J.; Martin-Gomez, M.-T.; Vilaplana, L.; Rodriguez-Urretavizcaya, B.; Marco, M.-P., An Immunochemical Approach to Detect the Quorum Sensing-Regulated Virulence Factor 2-Heptyl-4-Quinoline N-Oxide (HQNO) Produced by Pseudomonas aeruginosa Clinical Isolates. *Microbiology Spectrum* **2022,** *10* (4), e01073-21.
17. Montagut, E. J.; Martin-Gomez, M. T.; Marco, M. P., An Immunochemical Approach to Quantify and Assess the Potential Value of the Pseudomonas Quinolone Signal as a Biomarker of Infection. *Analytical Chemistry* **2021,** *93* (11), 4859-4866.
18. Michalet, S.; Allard, P. M.; Commun, C.; Ngoc, V. T. N.; Nouwade, K.; Gioia, B.; Dijoux-Franca, M. G.; Wolfender, J. L.; Doléans-Jordheim, A., Alkyl-Quinolones derivatives as potential biomarkers for Pseudomonas aeruginosa infection chronicity in Cystic Fibrosis. *Scientific reports* **2021,** *11* (1), 20722.
19. Capatina, D.; Feier, B.; Hosu, O.; Tertis, M.; Cristea, C., Analytical methods for the characterization and diagnosis of infection with Pseudomonas aeruginosa: A critical review. *Analytica chimica acta* **2022,** *1204*, 339696.
20. Harrison, R. O.; Goodrow, M. H.; Hammock, B. D., Competitive inhibition ELISA for the s-triazine herbicides: assay optimization and antibody characterization. *Journal of Agricultural and Food Chemistry* **1991,** *39* (1), 122-128.
21. Sanvicens, N.; Pichon, V.; Hennion, M.-C.; Marco, M. P., Preparation of Antibodies and Development of an Enzyme-Linked Immunosorbent Assay for Determination of Dealkylated Hydroxytriazines. *Journal of Agricultural and Food Chemistry* **2003,** *51* (1), 156-164.
22. Nichkova, M.; Galve, R.; Marco, M. P., Biological monitoring of 2,4,5-trichlorophenol (I): preparation of antibodies and development of an immunoassay using theoretical models. *Chem Res Toxicol* **2002,** *15* (11), 1360-70.
23. Montagut, E. J.; Acosta, G.; Albericio, F.; Royo, M.; Godoy-Tena, G.; Lacoma, A.; Prat, C.; Salvador, J. P.; Marco, M. P., Direct Quantitative Immunochemical Analysis of Autoinducer Peptide IV for Diagnosing and Stratifying Staphylococcus aureus Infections. *ACS infectious diseases* **2022,** *8* (3), 645-656.
24. Bredenbruch, F.; Geffers, R.; Nimtz, M.; Buer, J.; Häussler, S., The Pseudomonas aeruginosa quinolone signal (PQS) has an iron-chelating activity. *Environmental microbiology* **2006,** *8* (8), 1318-29.
25. Fletcher, M. P.; Diggle, S. P.; Crusz, S. A.; Chhabra, S. R.; Cámara, M.; Williams, P., A dual biosensor for 2-alkyl-4-quinolone quorum-sensing signal molecules. *Environmental microbiology* **2007,** *9* (11), 2683-93.
26. Buzid, A.; Reen, F. J.; Langsi, V. K.; Muimhneacháin, E. Ó.; O'Gara, F.; McGlacken, G. P.; Luong, J. H. T.; Glennon, J. D., Direct and Rapid Electrochemical Detection of Pseudomonas aeruginosa Quorum Signaling Molecules in Bacterial Cultures and Cystic Fibrosis Sputum Samples through Cationic Surfactant-Assisted Membrane Disruption. **2017,** *4* (3), 533-541.
27. Barr, H. L.; Halliday, N.; Barrett, D. A.; Williams, P.; Forrester, D. L.; Peckham, D.; Williams, K.; Smyth, A. R.; Honeybourne, D.; J, L. W.; Nash, E. F.; Dewar, J.; Clayton, A.; Knox, A. J.; Cámara, M.; Fogarty, A. W., Diagnostic and prognostic significance of systemic alkyl quinolones for *P. aeruginosa* in cystic fibrosis: A longitudinal study. *Journal of cystic fibrosis : official journal of the European Cystic Fibrosis Society* **2017,** *16* (2), 230-238.
28. Buzid, A.; Shang, F.; Reen, F. J.; Muimhneacháin, E.; Clarke, S. L.; Zhou, L.; Luong, J. H.; O'Gara, F.; McGlacken, G. P.; Glennon, J. D., Molecular Signature of Pseudomonas aeruginosa with Simultaneous Nanomolar Detection of Quorum Sensing Signaling Molecules at a Boron-Doped Diamond Electrode. *Scientific reports* **2016,** *6*, 30001.
29. Yang, J.; Shen, M. H., Polyethylene glycol-mediated cell fusion. *Methods in molecular biology (Clifton, N.J.)* **2006,** *325*, 59-66.

4. The Las and the RhI systems: DEVELOPMENT OF IMMUNOCHEMICAL ASSAYS FOR THE HOMOSERINE LACTONES 3-oxo-C12- HSL and C4-HSL

4.1 Chapter presentation

In this chapter, the development of polyclonal antibodies for detecting the molecules 3-oxo-C12-HSL and C4-HSL is described. These molecules are the AIs of the two most frequently studied QS systems in *P. aeruginosa*: the Las system and the RhI system, respectively. ELISAs have been developed and optimized to detect these molecules in complex biological samples, with the objective of acquiring the complete QS profile in MH growth medium. The chapter's structure is depicted in Figure 4.1.

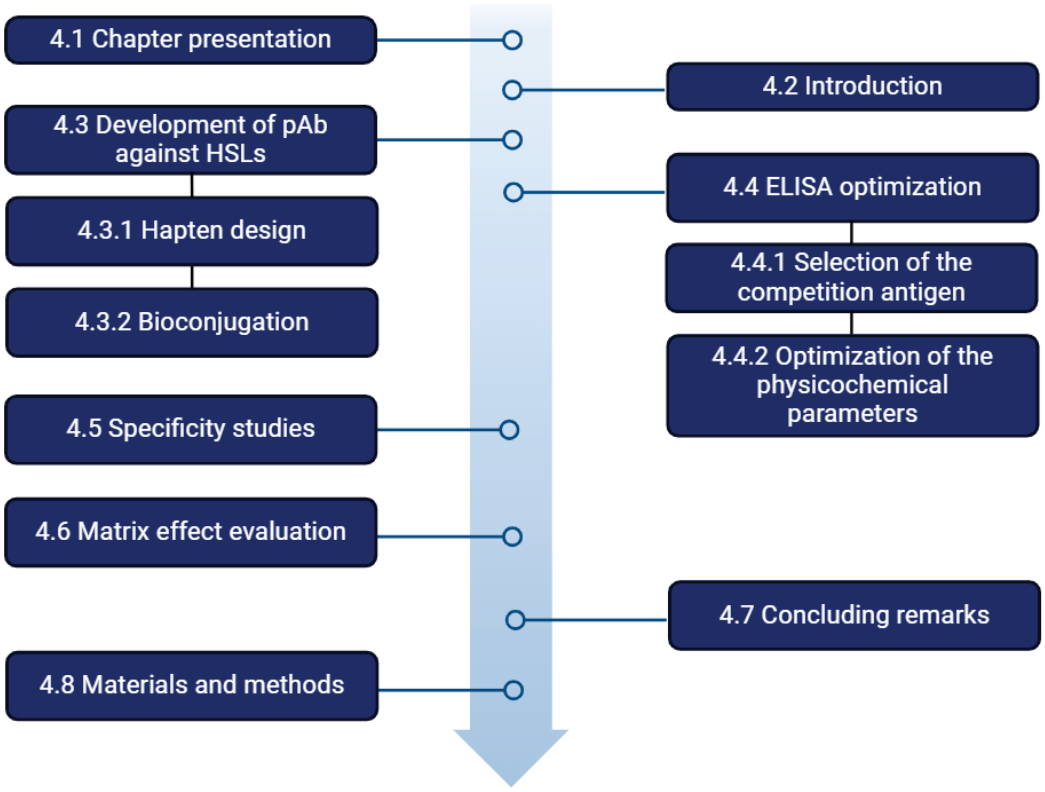

Figure 4.1: Structure of Chaper 4

4.2 Introduction

Gram-negative bacteria utilize HSL-type molecules as AIs for communication in various QS systems. These compounds can diffuse through the bacterial wall and, therefore, accumulate in the extracellular space. All HSLs are characterized by a homoserine lactone moiety and a fatty acyl group that can vary in length, ranging from 4 to 14 carbons. They may also contain 3-oxo, 3-hydroxyl, or completely reduced methylene groups at the C3 position, or have unsaturations at different positions in the chain[1].

P. aeruginosa possesses two QS systems with HSL as AIs. These are the Las system, with 3-oxo-HSL-C12 as the AI molecule, and the Rhl system, with C4-HSL as the AI molecule[2]. Although these molecules are not specific to *P. aeruginosa*, there is significant interest in quantifying them because they regulate the expression of many bacterial genes. This information can provide insights into bacterial behavior. Although specificity is considered fundamental to QS, HSLs may have also a cross talk role between species on polymicrobial communities[3].

Conventional analytical methods such as chromatography, mass spectrometry, and NMR have been satisfactorily used for HSL identification[4-6]. HPLC-MS can be used to simultaneously quantify different HSLs despite the structural similarities. These molecules, having a lactone ring, are easily hydrolyzable, rendering them inactive (See Figure 4.2). Through HPLC-MS methods, it is possible also to distinguish between their open and closed forms[7]. Lepine *et al.* have described various HPLC-MS methods for their detection using an electrospray interface with positive ionization conditions to analyze culture medium and biological samples of infected mouse muscle tissue after an extraction process[8]. Other methods involve sample pretreatment, involving a prior extraction in organic solvent (ethyl acetate) and concentration before analysis by HPLC-MS[9].

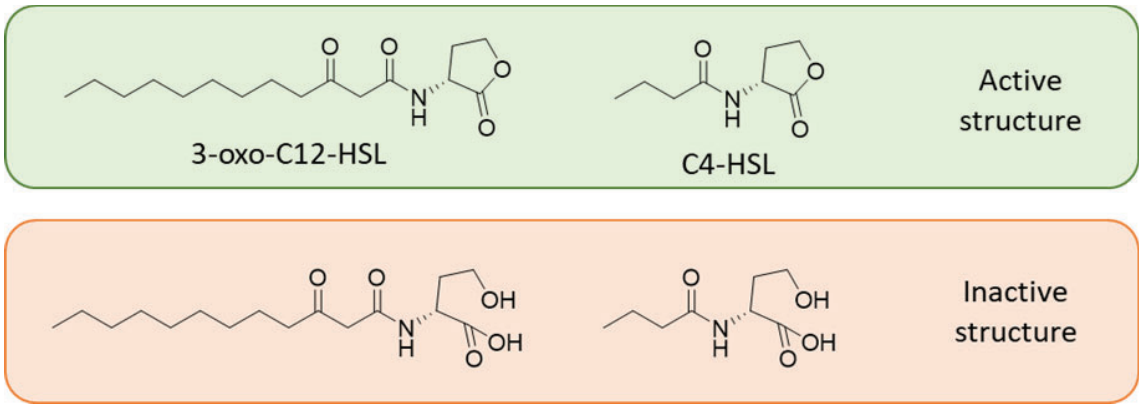

Figure 4.2: Structure of the active form of 3-oxo-C12-HSL and C4-HSL (top), and its hydrolyzed and inactive form (bottom).

Highly sensitive and selective electrochemical and optical sensors have also been developed for the detection of HSLs. Sismaet *et al.* developed an electrochemical sensor using methylene blue as a redox marker, recognition was achieved through high-affinity aptamers for 3-oxo-C12-HSL and C4-HSL, reaching detectabilities between 0.1 and 100 µM for both analytes in buffer[10]. Molecularly imprinted polymers (MIP) have also been used as recognition elements[11, 12]. For their preparation, 2,5-dimethyl-4-hydroxy-3(2H)-furanone, a molecule similar in shape, size, and functionality, was employed as template. The MIPs have been reported to be used on two electrochemical sensor configurations. One of them uses magnetic MIPs and quantify the HSLs through differential pulse voltammetry (DPV)[11], while the other uses quantum dots (QD)[12]. Both

demonstrate good reproducibility, stability, and recovery when used to detect HSLs in bacterial culture supernatants after an extraction and concentration steps reaching LODs of 0.8 and 0.5 nM, respectively.

Bacterial biosensors have also been developed for the detection and quantification of HSL (See Figure 4.3). These sensors are based on genetically modified bacteria that contain a promoter as a recognition agent. When this promoter is activated, it initiates the transcription of a reporter gene, resulting in the production of a reporter protein that can be optically detected (chemiluminescence, colorimetry, bioluminescence, or fluorescence). Several sensors have been developed for HSL detection using *Pseudomonas*. These involve mutations in *lasI* or *rhlI* synthases and use *luxCDABE* or *lacZ* as a reporter[13]. There are also various examples using genetically modified *E. coli* for detection. One of them contains the plasmid pSD908, which detects long-chain HSL and the *lacZ* gene, encoding for a β-galactosidase. This enzyme can be optically quantified using different substrates[14]. O'Connor *et al.* developed paper strips containing these genetically modified bacteria, allowing colorimetric detection of HSL in saliva using 5-bromo-4-chloro-3-indolyl-β-D-galactoside as a substrate[15].

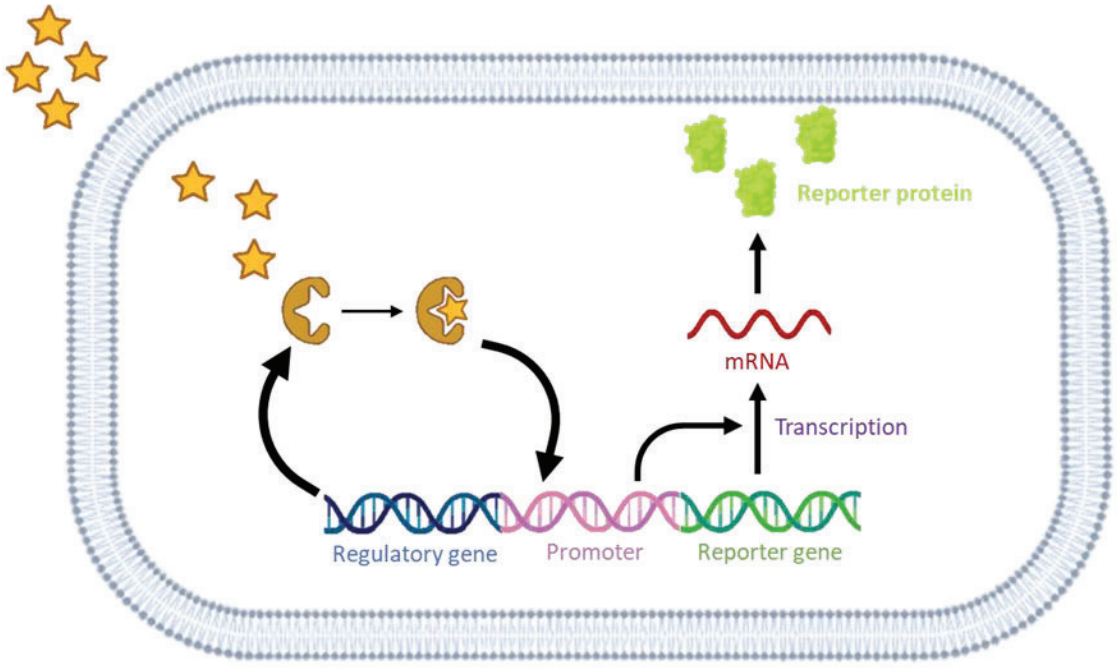

Figure 4.3: Example of a whole cell bacterial biosensor. An analyte is sensed, triggering a transcriptional cascade and production of a reporter protein.

So far, only two research groups have attempted to develop antibodies against this type of molecules. The firsts to report them were Chen *et al.*, who developed rat monoclonal antibodies for diagnostic purposes. The antibodies were characterized by ELISA and used to detect a collection of HSLs with different lengths of the side chain, functional groups at C3 position, and also HSLs with the lactone ring hydrolyzed. Surprisingly, the best IC_{50} values were obtained for the analyte 3-oxo-C10-HSL (450 nM) and C6-HSL (2 µM), and demonstrated that the IC_{50} value could be improved for the corresponding hydrolyzed form of these analytes to 25 nM and 38 nM, respectively. For the analytes of interest in our research, which are 3-oxo-C12-HSL and C4-HSL, they show IC_{50} values of 1.15 µM and 13 µM, respectively. Interestingly, they do not show the corresponding IC_{50} values for the hydrolyzed products[16]. The fact that a much lower IC_{50} is

obtained for the hydrolyzed forms of the analytes demonstrates that the antibodies had truly been developed against the hydrolyzed HSL. Thus, at some point in the conjugation process, immunization, or even within the animal, the hapten could had been hydrolyzed, which explains that the obtained antibodies better recognize this form. The same group later published a comparison between the detection of HSL by ELISA or with an optical immunosensor based on surface plasmon resonance (SPR) using the antibodies they had previously developed. The study shows that the sensitivity achieved by SPR improves compared to that obtained by ELISA[17].

A few years later, Kaufmann *et al.* also developed antibodies against these molecules. Due to the aforementioned hydrolysis issue, they decided to conduct a study to select the most appropriate immunizing haptens to avoid hydrolysis. They opted to replace the lactone ring by a lactam despite it represented a substantial change in the electronic configuration of such small molecules. After evaluating the antibodies obtained through competitive indirect ELISA, the best antibodies showed IC_{50} values of 3.1 µM and 6.2 µM for the detection of 3-oxo-C12-HSL and C4-HSL, respectively. These antibodies were not used for diagnosis but for in vitro studies with therapeutic purposes. They observed that the production of the virulent factor PYO decreased as they added increasing concentrations of the developed antibodies to a culture of *P. aeruginosa*[18], indicating somehow an inhibitory action of the pathways that trigger the biosynthesis of this virulence factor.

Due to the poor detectabilities achieved in the aforementioned studies with antibodies against *P. aeruginosa* HSLs, in comparison to LODs obtained in immunoassays, which on our group are usually in the low nM range, we decided to undertake the development of new antibodies against these molecules. In the development of these antibodies, stability studies of the immunizing hapten, which were not conducted in previous studies, have been carried out, along with an optimization of the physicochemical parameters of the ELISA. Finally, more comprehensive cross-reactivity and accuracy studies have been conducted than those published so far, aiming to achieve a more sensitive and specific assay for the detection of these molecules.

4.3 Development of polyclonal antibodies against HSLs

4.3.1 Hapten design and synthesis

Due to the low molecular weight of these molecules, they are not immunogenic and must be conjugated to a protein of higher molecular weight to be recognized by the animal's immune system and generate antibodies. In Figure 4.4, which shows the structure of the immunizing haptens, it can be observed that a carboxylic group was placed at the end of the hydrocarbon chain, through which conjugation to the corresponding protein will occur. Similar to the antibodies mentioned in the previous section, the carboxylic group was placed in that position so that the most characteristic part of each molecule was more exposed to the immune system recognition, thereby eliciting better antibodies. As can be seen in Figure 4.4, for each of the analytes to be detected, two different haptens were designed and synthesized, one with the lactone ring and the other with a lactam ring, more stable, as reported before by the group of Kaufmann *et. al*. It was decided to immunize with both forms to ensure recognition of the non-hydrolyzed form of the molecule. Despite Kauffmann *et al.* did no accomplish very good detectabilities, previous work by Chen *et al.* demonstrated that using the lactone hapten gave rise to antibodies against the hydrolyzed form. Moreover, previously in our group, Montagut *et al.* demonstrated that using a more labile lactone immunizing peptide allowed to obtain superior antibodies than using the corresponding lactam of the *Staphylococcus aureus* AI peptide IV (AIP-IV), pointing at the important contribution of lactone electronic and conformational properties when raising antibodies[19]. To minimize the risk of the lactone hydrolysis, our intention was to control the stability conditions of the molecule during storage and bioconjugation reaction, although once inside the animal, the conditions cannot be controlled. Despite taken all the necessary precautions, the molecule could be hydrolyzed once immunizing giving rise to antibodies against the hydrolyzed form. For this reason, we decided to immunize also with the corresponding HSL lactam ring haptens.

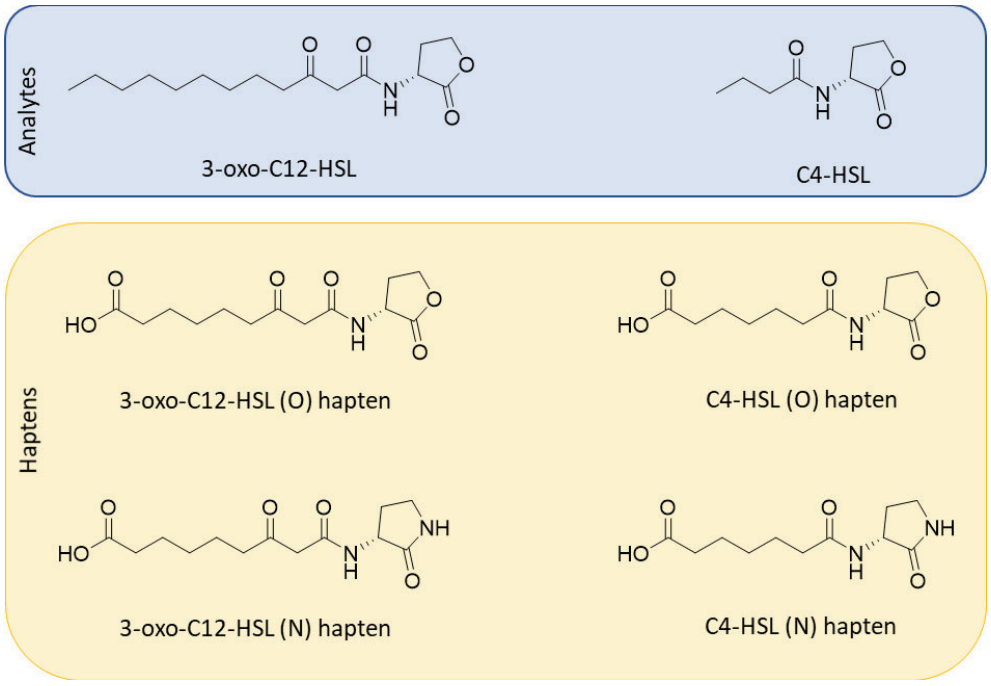

Figure 4.4: Chemical structure of HSL analytes and haptens.

Generally, immunizing haptens should be designed to closely mimic the target molecule, maintaining as much of the analyte's original steric and electronic properties as possible. However, even when most of the functional groups are unchanged, they might still be masked by the protein's tertiary structure. When a small molecule is covalently attached to a carrier protein, significant masking can occur around the linkage site, resulting in antisera with reduced specificity for the masked determinant groups. To avoid this problem, it is crucial to ensure the hapten structure is positioned away from the carrier surface. This can be achieved by using a spacer arm to extend the hapten outward. However, if the spacer arm is too long, it may cause the hapten molecule to fold back towards the protein surface, resulting in the masking of the hapten's determinant groups[20].

In this case, the ideal approach would have been to use spacer arms of 12 and 4 carbons, as these are the lengths of the hydrocarbon chains in the original molecules. However, for the production of antibodies that recognize the 3-oxo-C12-HSL molecule, it was decided to shorten the hydrocarbon chain to 9 carbons during hapten synthesis, due to the reasons explained earlier. Conversely, for the C4-HSL molecule, three extra carbons were added to ensure the molecule remained sufficiently exposed.

According to the literature, the antibodies produced by Chen *et. al.*[16] were raised using different haptens with varying hydrocarbon chain lengths, ranging from 12 to 6 carbons. In Kaufmann's case, the hydrocarbon chain lengths were the same as those used in this research—9 carbons for the 3-oxo-C12-HSL hapten and 7 carbons for the C4-HSL hapten[18]. However, they only immunized with the lactam rings.

For the synthesis of the haptens, a strategy similar to that used by Kaufmann *et. al*. was decided upon[18] with the assistance of the SIMchem service (IQAC-CSIC). For the synthesis of the C4-HSL haptens, the process began with heptanedioic acid, where one of the acids was protected with a tert-butyl group (see compound **1** in Figure 4.5). This was then reacted in the presence of 1-ethyl-3-(3-dimethylaminopropyl)carbodiimide (EDC) with 3-aminodihydrofuran-2(3H)-one (**2** in Figure 4.5) or 3-aminopyrrolidin-2-one (**3** in Figure 4.5) to obtain the lactone or lactam, respectively. Next, the tert-butyl protecting group was removed in an acidic medium to yield the corresponding acids.

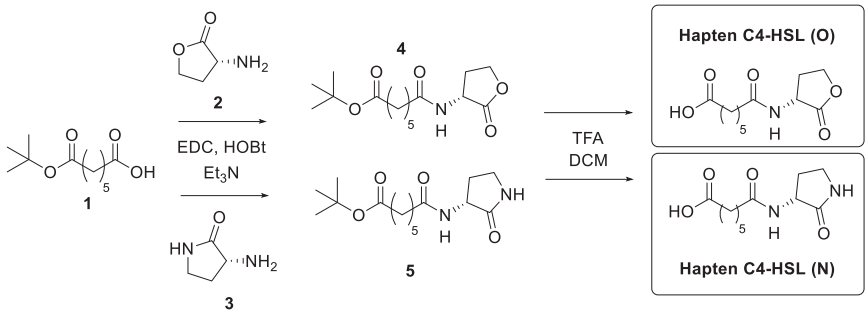

Figure 4.5: Synthetic route for the production of the C4-HSL (O) and C4-HSL (N) haptens.

For the synthesis of the 3-oxo-C12-HSL haptens, the process started with the same initial acid (see compound **1** in Figure 4.6), but it was first reacted with 2,2-dimethyl-1,3-dioxane-4,6-dione (6, Figure 4.6) in the presence of EDC. This allowed for the insertion of the carbonyl group contained in these structures. It was then reacted with 3-aminodihydrofuran-2(3H)-one (**2** in Figure 4.6) or 3-aminopyrrolidin-2-one (**3** in Figure 4.6) to obtain the lactone or lactam, respectively. Finally, the protecting group was removed in an acidic medium as in the previous case to obtain the carboxylic acids.

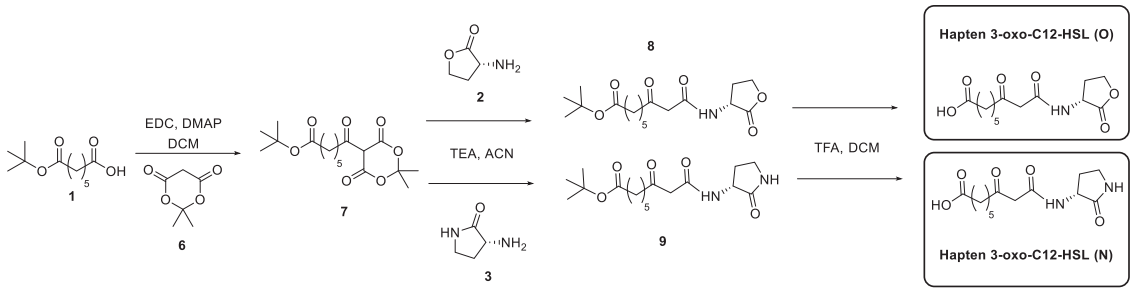

Figure 4.6: Synthetic route for the production of the 3-oxo-C12-HSL (O) and 3-oxo-C12-HSL (N) haptens.

The haptens were characterized by spectroscopic and spectrometric methods ensuring that the lactone moiety was preserved at the end of the whole synthetic process (See materials and methods, section 4.9.6).

4.3.2 Preparation of the Bioconjugates

In this part of the project, was crucial to study the stability of the lactone ring under different conditions, as it was highly possible that could be hydrolyzed during the bioconjugation reaction to the protein. Hence, in many cases, a slightly basic pH is required to promote the reaction, at which the HSL can easily hydrolyze.

To prepare the bioconjugates for immunization, we often prefer using the mixed anhydride (MA) method (explained in section 3.3.1) because it usually renders cleaner bioconjugates without the formation of side products that could create further undesired epitopes on the bioconjugate. Commonly used bioconjugation methods, such as those using carbodiimides, have been reported to often yield undesired stable N-acylurea residues on the protein which are highly immunogenic promoting antibody generation against these residues rather than for the molecule of interest[21, 22]. Unfortunately, the MA method is usually performed at a pH of 8.7 to favor the nucleophilicity of the amino groups of the protein's lysines, which may affect the stability of the lactone. For this reason, stability studies were conducted.

4.3.2.1 Stability Studies of the HSL haptens and target analytes

Studies addressed to get knowledge of the stability of the haptens were performed using HPLC-MS. Solutions of the haptens were prepared at different pHs and maintained at room temperature for 1.5 hours (the usual duration of the bioconjugation reaction). Figure 4.7 depicts the chromatograms resulting from these studies for each hapten.

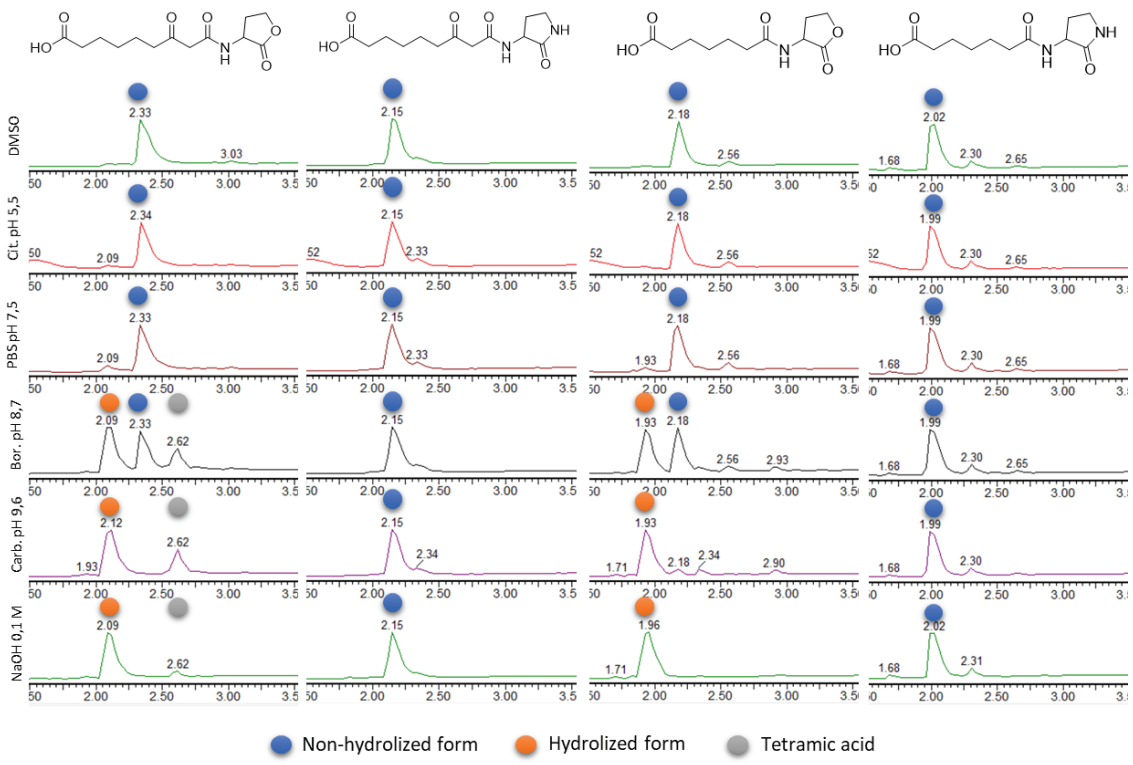

Figure 4.7: Result of the chromatographic analysis of the four haptens after being treated with different pH levels

It can be observed that, already at pH 7.5, a small pick appears corresponding to the hydrolysis product of the 3-oxo-C12-HSL(O) hapten, while at higher pH values, the concentration of this product increases. At pH 8.7, the formation of a third unknown specie was also observed that could correspond to the tetramic acid (3-(1-hydroxydecylidene)-5-(2-hydroxyethyl)pyrrolidine-2,4-dione) reported by Kaufmann *et al.*[23] . The mechanism of formation of this compound is through a Claisen-like intramolecular alkylation of the β-ketoamide moiety. The α-carbon between the ketone and the amide moiety is deprotonated, forming an anion that can cyclize intramolecularly with the lactone, generating the tetramic acid (see Figure 4.8). It has been reported that this tetramic acid is very stable, and its decomposition to the initial HSL has not been detected. Additionally, this compound has also been detected in *P. aeruginosa* culture medium[23].

The same study shows that this substance has an important biological function; it has been reported to be toxic to a large number of gram-positive bacteria but not to gram-negative bacteria, which are the ones that synthesize it. This is an interesting observation since it would indicate that HSLs may be used by these bacteria as a strategy to avoid the intrusion of competing gram-positive bacteria in its environment. Additionally, it has also been reported to have significant siderophore activity, as it can chelate iron, providing another method for *P. aeruginosa* to solubilize Fe^{3+} [23].

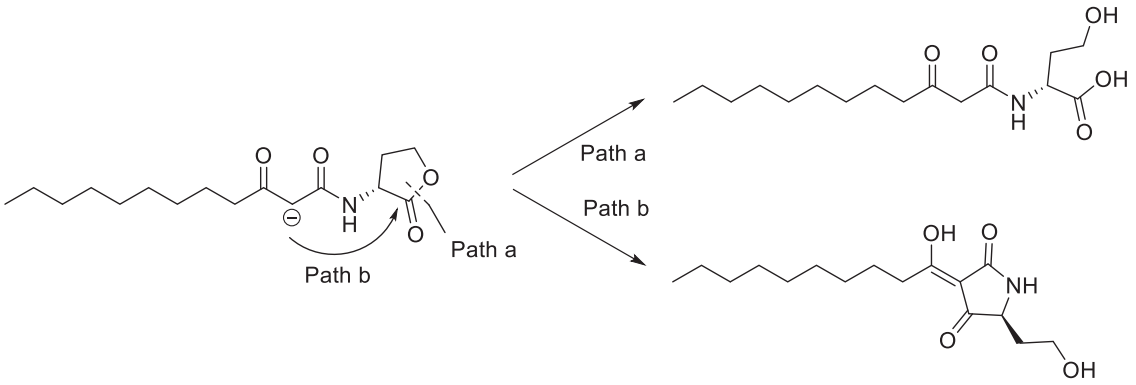

Figure 4.8: Reaction of 3-oxo-C12-HSL to generate lactone hydrolysis product (path a) and 3-(1-hydroxydecylidene)-5-(2-hydroxyethyl)pyrrolidine-2,4-dione (path b).

If we increase the pH of the hapten to a higher pH, such as 12, it is observed that the lactone ring is no longer detected, and the tetramic acid also decreases. This is because the hydrolysis of the lactone occurs so rapidly that there is barely enough time for the Claisen-like intramolecular reaction to take place.

It can be observed that the two haptens with the lactam ring, as expected, do not undergo any degradation and remain stable across the entire pH range. In contrast, for the hapten corresponding to C4-HSL, at pH 8.7, the hydrolyzed form is detected, and in this case, the formation of the corresponding tetramic acid is not observed since the anion cannot be formed at the α-carbon of the amide.

With this information, it was clear that the conjugation reaction should not be performed at a pH higher than 7.5 if the non-hydrolyzed form of the HSL wanted to be preserved. In the case of the antibodies generated by Chen *et al.*, the conjugation reactions were carried out at pH 7.6, so it is very probable that part of the haptens were hydrolyzed during the bioconjugation reaction[16]. In the case of Kaufmann *et al.*, the pH of the conjugation is not specified[18]. For this reason, a reactivity study of the conjugation reaction at pH values below 7.5 was conducted to confirm that the conjugation reaction using the MA method would take place. For this purpose, 5-phenylpentanoic acid and tert-butyl (3-aminopropyl)carbamate were used as model molecules to carry out the reaction under the same conditions used for the bioconjugation with isobutyl chloroformiate (IBC) and tributylamine (TBA) but at pH values 6, 6.5 and 7. The analysis of the reaction crudes by HPLC-MS allowed to observe that the desired product was formed in all cases (see Figure 4.9), demonstrating that it was possible to carry out the bioconjugation reaction using slightly acidic pH conditions.

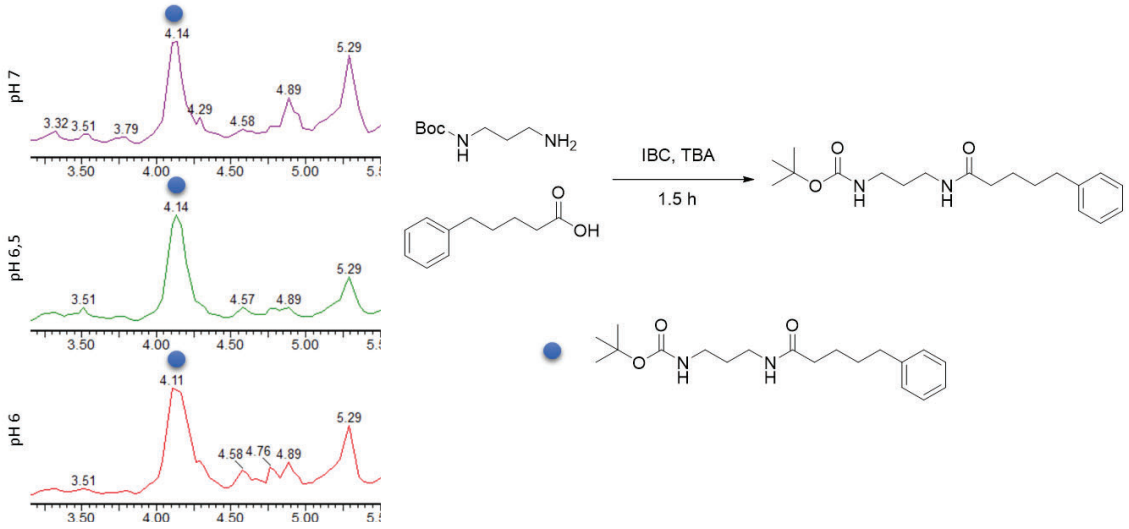

Figure 4.9: Standard reaction to verify the method's reactivity when changing pH conditions. The chromatographic result is shown after conducting the reaction at three different pH levels.

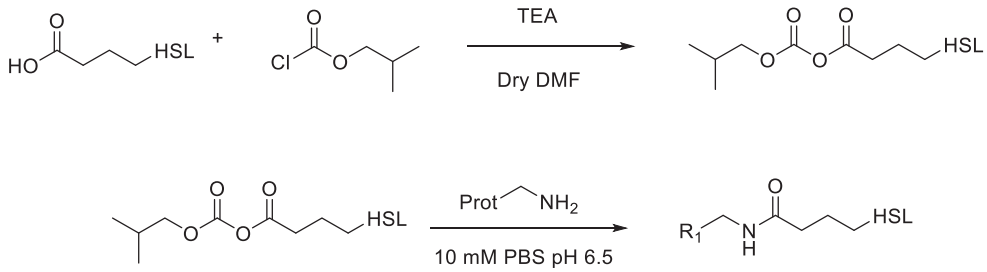

Figure 4.10: Conjugation reaction by the lysines of the proteins using the MA method.

The four haptens were thus conjugated to KLH and BSA simultaneously using the MA method in PBS at pH 6.5 (See Figure 4.10) and further on purified by size exclusion chromatography. Performing the conjugation at this pH aims to obtain antibodies that recognize the non-hydrolyzed form of these HSLs, thereby improving the results obtained by previous research groups. The characterization of the bioconjugates by MALDI-TOF MS showed that suitable hapten densities (HD) were achieved (see Table 4.1).

Table 4.1: HDs obtained for the four haptens

Bioconjugate	HD
3-oxo-C12-HSL (O) – BSA	6
3-oxo-C12-HSL (N) – BSA	6
C4-HSL (O) – BSA	6
C4-HSL (N) – BSA	5

The bioconjugates were obtained using the MA method. HD was calculated using the equation: [MW(conjugate) – MW(native protein)]/[MW(hapten)-MW(lost atoms)].

Subsequently, the haptens were also conjugated to BSA, CONA (conalbumin) and OVA (ovalbumin) to introduce heterology (see section 3.4.1) on the bioconjugates competitors used to develop the ELISAs.

For the preparation of these bioconjugate competitors, the risk of formation of secondary byproducts due to the use of carbodiimides was not an issue since there were not aimed to be used for antibody production. Therefore, we decided to introduce also heterology in respect to the conjugation procedure by using the active ester (AE) method employing EDC / NHS as activators. This method performs well at a slightly acidic pH of 6.5, which was perfect for avoiding the hydrolysis of the haptens.

The bioconjugates were also purified by size exclusion chromatography and analyzed by MALDI-TOF MS. Table 4.2 shows the HD obtained for each of the bioconjugates.

Table 4.2: HD obtained of the bioconjugates produced using the AE method.

	3-oxo-C12-HSL (O) hapten	3-oxo-C12-HSL (N) hapten	C4-HSL (O) hapten	C4-HSL (N) hapten
BSA	2	2	2	2
OVA	2	2	2	2
CONA	8	7	8	8

HD was calculated using the equation: [MW(conjugate) – MW(native protein)]/[MW(hapten)-MW(lost atoms)].

4.3.3 Antibody Development

Two white New Zealand rabbits were immunized with each of the four KLH conjugates prepared using the protocols established in our research group and described in the experimental section. Table 4.3 shows the number of the antiserum (As) obtained for each of the immunized hapten: 3-oxo-C12-HSL(O) (As419 and As420), 3-oxo-C12-HSL(N) (As 421 and As422), C4-HSL(O) (As423 and As424) and C4-HSL(N) (As425 and As 426).

Table 4.3: Number of antisera obtained after immunization with each of the haptens.

Antiserum	*Immunization* hapten
419	3-oxo-C12-HSL (O)
420	
421	3-oxo-C12-HSL (N)
422	
423	C4-HSL (O)
424	
425	C4-HSL (N)
426	

4.4 Antisera evaluation and ELISA development

4.4.1 Analyte stability studies

On a first instance it was evaluated whether if the antibodies produced had higher avidity for the cyclized or the open forms of the two HSLs of interest. For this purpose, the HSLs had to be hydrolyzed.

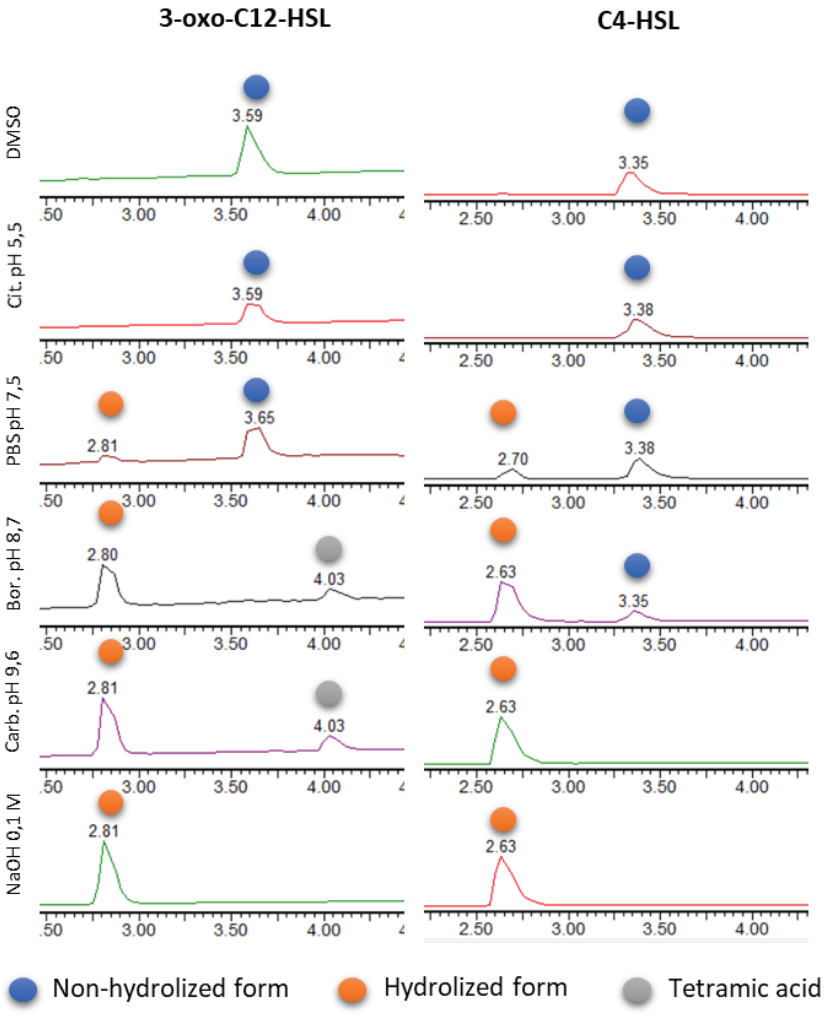

Figure 4.11: Chromatograms obtained as a result of the stability study of 3-oxo-C12-HSL and C4-HSL at different pH conditions. Solutions of the analyte were prepared at different pHs and analyzed by HPLC-MS after 15 minutes.

A stability study similar to the one previously performed for the haptens was conducted, but with the two analytes of interest (See Figure 4.11) by preparing solutions at different pHs. The reaction was monitored by HPLC-MS after 15 minutes. For 3-oxo-C12-HSL it can be observed that at pH 7.5, the hydrolyzed product is started to be detected after this time, but still the most remain stable. However, at pH 8.7, the product is completely hydrolyzed and the tetramic acid presented in section 4.2.2 starts to be detected. Same happens at pH 9.6 while pH 12, only the hydrolyzed form was detected since, as explained before, under these conditions the hydrolysis of the lactone occurs so rapidly that there is barely enough time for the Claisen-like intramolecular reaction to take place. For the case of C4-HSL, at pH 7.5 the hydrolyzed form was

detected, and in this case, the formation of the corresponding tetramic acid was not observed since the anion cannot be formed at the α-carbon of the amide.

4.4.2 Selection of the competition antigen

The eight antisera obtained were evaluated against the twelve bioconjugates produced using "combined 1D" competitive indirect ELISA experiments, in which the microplates were coated with the bioconjugates at 1 μg·mL^{-1} and dilutions (1/500 to 1/32000) of the different antisera were added to three different columns of the microplate, one without analyte and the other two with the open and close forms of the HSLs at 1 μM. For antisera 419-422, both the cyclized and hydrolyzed forms of 3-oxo-C12-HSL were added. Similarly, for antisera 423-426, the analyte C4-HSL was added, also in both its cyclized and hydrolyzed forms.

Out of the total of 96 As/bioconjugate/analyte combinations assayed, Figure 4.12 shows the six that exhibited the highest recognition of the targets, either in the open or on the close form: three for the 3-oxo-C12-HSL and three for the C4-HSL.

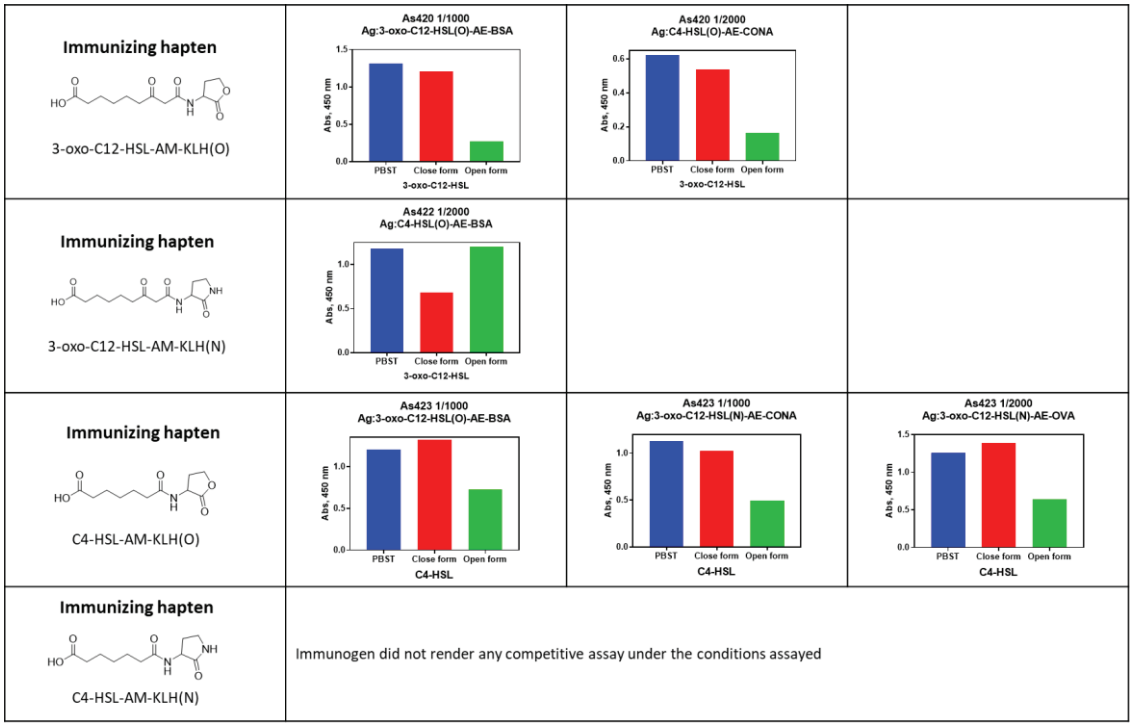

Figure 4.12: Best combinations of antiserum/antigen for the detection of 3-oxo-C12-HSL and C4-HSL, for both non-hydrolyzed and hydrolyzed forms. Blue: No competition. Red: Non-hydrolyzed analyte. Green: Hydrolyzed analyte. The selection of the combinations shown was made after analyzing the behavior of 96 combinations on "combined 1D" experiments. The data shown corresponds to the signals recorded when the microplates were coated with the bioconjugate competitors at 1μg·mL^{-1} and the target analytes (open and close forms) were added to the microplates at a concentration of 1 μM. The dilution of the antisera was chosen to provide 1 unit of absorbance on each case and it is indicated on each graph.

For the case of the antisera generated towards the lactone haptens, it can be observed how, despite efforts to minimize hapten hydrolysis, there is greater avidity towards the open HSL forms than the cyclic ones, indicating that antibodies had been produced against the hydrolyzed lactone. It is very likely that this hydrolysis could have occurred within the animal, where conditions cannot be controlled. It is also possible that the hydrolyzed form is more

immunogenic than the cyclic one, favoring the production of antibodies for its recognition, even if only a small fraction of the hapten was hydrolyzed.

However, it's important to note that this is one of the few examples demonstrating the generation of tight-binding antibodies to structures that are primarily aliphatic, lacking aromaticity, charge, and offering few hydrogen bond donor/acceptor opportunities. These interactions are typically regarded as crucial for producing antibodies with high affinity and specificity. This could explain why the antibodies recognize the hydrolyzed form with greater affinity, as it exposes a carboxylic acid and an alcohol, allowing for many interactions.

As for the antisera produced against lactam haptens, only one combination showed considerable competition with the intact lactone under the conditions used, and it was the case of 3-oxo-C12-HSL using the combination As422/C4-HSL(O)-AE-BSA. It is possible that the substitution of the lactone by the lactam had an impact on the electronic distribution of the molecule, preventing the obtention of antibodies that recognize the non-hydrolyzed HSLs. Nonetheless, the fact that there was a combination that showed competition towards the cyclic form points to perhaps certain geometrical similarities between the cyclized analyte and the lactam, despite differences in the molecules' electronic configuration.

For each of the combinations selected on the above experiments, a two-dimensional (2D) noncompetitive ELISA was performed to select the optimal antigen concentrations and serum dilutions. Subsequently, using the selected conditions, competitive indirect ELISAs were conducted as depicted in Figure 4.13.

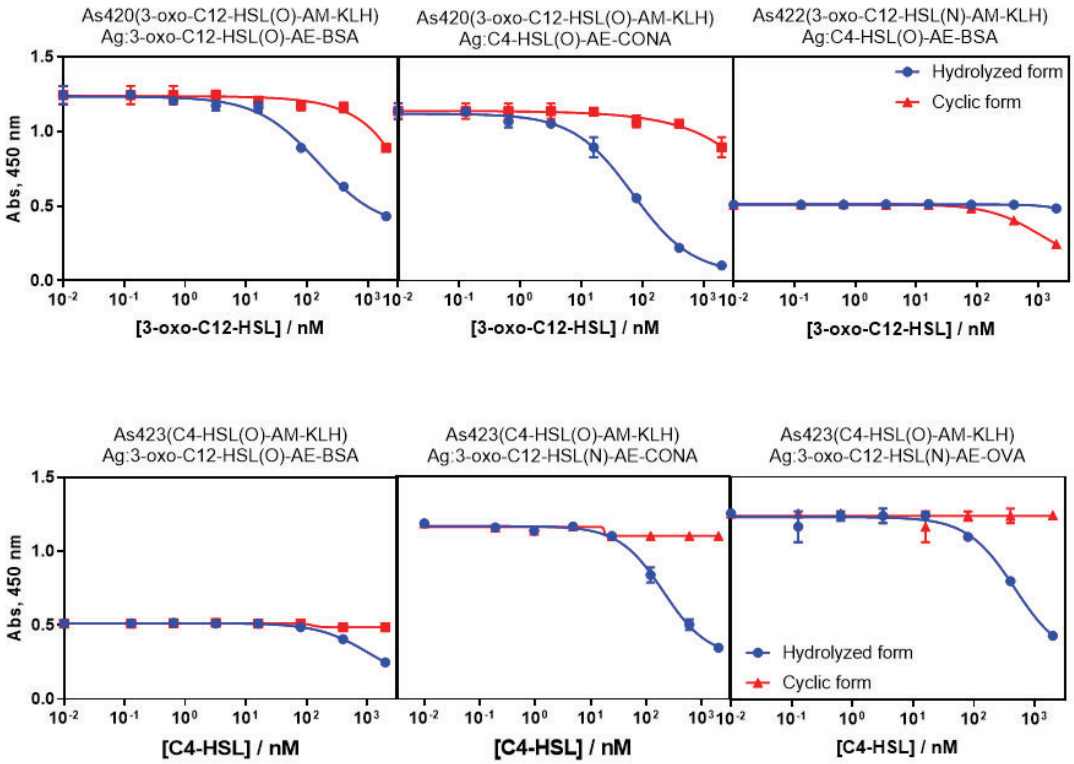

Figure 4.13: Indirect competitive ELISA calibration curves for the detection of 3-oxo-C12-HSL (top) and C4-HSL (bottom) from the previously selected antiserum/antigen combinations. Both non-hydrolyzed (red) and hydrolyzed forms (blue) are studied.

The recognition profile of all combinations is similar to that observed in Figure 4.12. Combinations with higher detectability for each analyte were selected, corresponding to As420/C4-HSL(O)-AE-CONA for the detection of hydrolyzed 3-oxo-C12-HSL and As423/3-oxo-C12-HSL(N)-AE-CONA for the detection of hydrolyzed C4-HSL. It can be observed that the combinations resulting in greater competition are heterologous combinations for both the competing antigen and the conjugation method. This is because heterology allows the antibody affinity constant to shift towards recognizing the analyte, as it reduces recognition of the coating antigen, thereby achieving greater detectability.

At this point, and at the light of the results obtained, the idea of recognizing the intact HSL was discharged and we focused on the detection of the hydrolyzed forms. This fact was not considered a significant problem, as any sample could always be easily hydrolyzed with a simple basic treatment prior to the assay, as demonstrated in section 4.4.1.

4.4.3 Evaluation of the Effect of Physicochemical Parameters of the ELISA for 3-oxo-C12-HSL.

Although there was observe competition by the analyte on the Ab/bioconjugate combination selected, the detectability achieved (IC_{50}= 70 nM, hydrolyzed form) under the standard ELISA conditions used was not enough for our purposes. To improve the ELISA performance, the effect of distinct physicochemical parameters of the assay were evaluated to determine if any could enhance the detectability of the assay. Additionally, this study provided information on how robust the assays were against different changes in the assay conditions. As for the case of the PQS (see Chapter 3), the pre-incubation time, competition time, Tween20 concentration, conductivity, and buffer pH were studied. All these studies were carried out using the hydrolyzed form of the HSL, which was freshly prepared, each time just before starting the experiments (15 min in 0.1 M NaOH, explained in section 4.9.6). Figure 4.14 depicts the results obtained for the As420/C4-HSL(O)-AE-CONA ELISA assay for quantifying 3-oxo-C12-HSL.

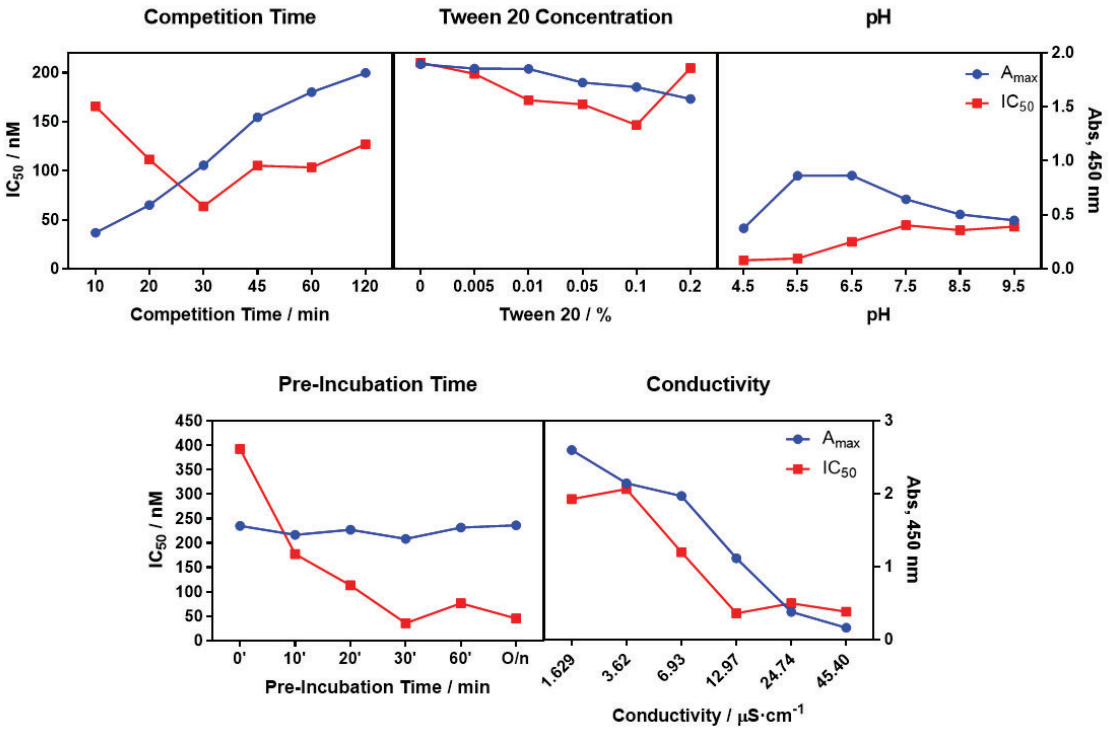

Figure 4.14: The figure shows the maximum absorbance (right axis) and the IC_{50} (left axis) of the calibration curves of the indirect competitive ELISA As420/C4-HSL(O)-CONA under different pre-incubation times, competition times, concentration of Tween 20, conductivity and pH.

As observed in the graphs, a significant improvement in the IC_{50} is noted with a 30-minute pre-incubation, reducing the IC_{50} from 398 nM to 44 nM. Regarding the competition time, the optimal duration is also 30 minutes. Concerning the concentration of Tween 20, no significant difference is observed, so it was decided to continue using the standard concentration of 0.05%. Similarly, no improvement was observed in conductivity compared to the standard which was 15 $\mu S \cdot cm^{-1}$, and the signal decreases dramatically with the raise of conductivity of the media. Finally, regarding pH, a decrease to pH 5.5 was observed to improve both the IC_{50} and the maximum assay absorbance.

Table 4.4 and Table 4.5 summarize the optimized physicochemical conditions and the analytical parameters achieved of the 3-oxo-C12-HSL ELISA .

Table 4.4: Conditions of the ELISA As420/C4-HSL(O)-AE-CONA for the detection of 3-oxo-C12-HSL.

	Optimized values
As 420	1/1500
[C4-HSL(O)-CONA] / µg·mL^{-1} HD=8	0.875
Pre-Incubation Time / min	30
Competition Time / min	30
Tween 20 %	0.05
Conductivity / µS·cm^{-1}	15
pH	5.5

Table 4.5: Main parameters of the calibration curve of the ELISA As420/C4-HSL(O)-AE-CONA for the detection of 3-oxo-C12-HSL.

	Optimized values
A_{min}	0.07 ± 0.01
A_{max}	0.92 ± 0.10
Slope	-1.05 ± 0.07
IC_{50} / nM	50.99 ± 5.77
Dynamic Range / nM	164.22 ± 9.89 to 8.42 ± 0.79
LOD / nM	3.75 ± 0.30
R^2	0.995 ± 0.001

The data shows is the average and standard deviation of three assays run in three different days. On each assay the standard used on the calibration curve were measured using three well-replicates. The analytical parameters were extracted from the four-parameter logistic equation used to fit the standard curve.

4.4.4 Evaluation of the Effect of Physicochemical Parameters of the ELISA for C4-HSL.

The same physicochemical optimization was carried out for the ELISA As423/3-oxo-C12-HSL(N)-AE-CONA for the quantification of the hydrolyzed form of C4-HSL. Figure 4.15 displays the optimization results.

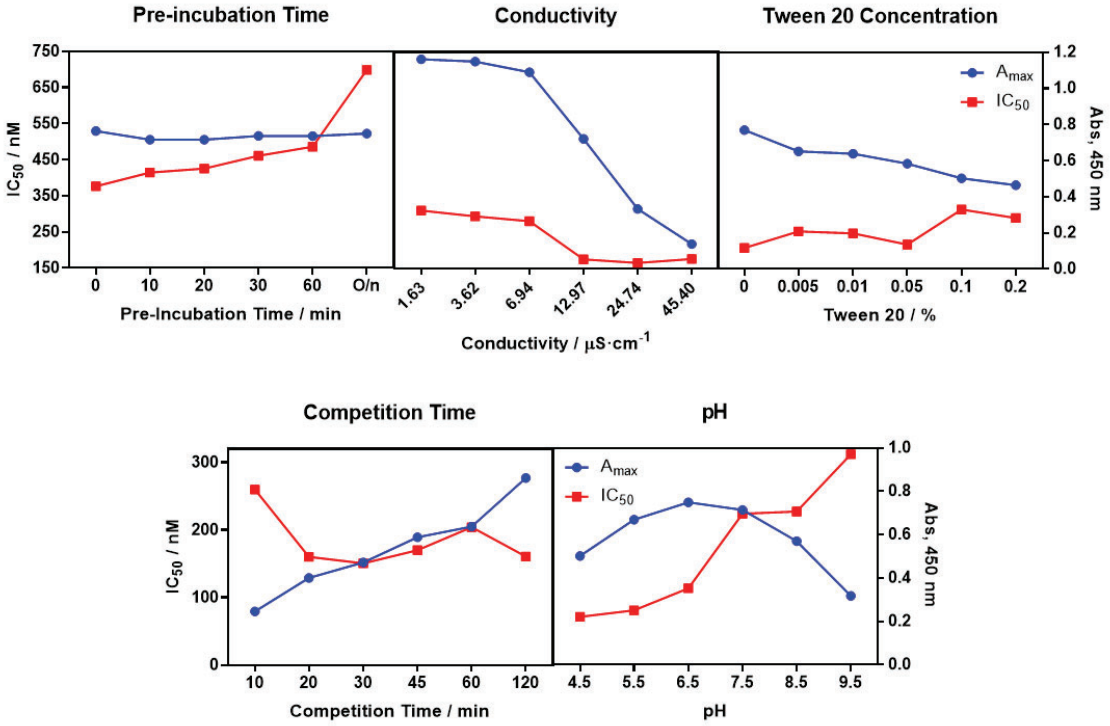

Figure 4.15: The figure shows the maximum absorbance (right axis) and the IC50 (left axis) of the calibration curves of the indirect competitive ELISA As423/3-oxo-C12-HSL(N)-CONA under different pre-incubation times, competition times, concentration of Tween 20, conductivity and pH.

As it can be observed, for this assay, the pre-incubation does not produce an improvement of the detectability. Regarding the competition time, 30 minutes was selected as a compromise in which the detectability remains more or less similar to that recorded after 120 minutes, but the assay time was reasonable, although the maximum absorbance was lower. The concentration of Tween 20, as with the previous assay, was set at 0.05% despite in this case the decrease of the maximum absorbance was more significant. A conductivity of 15 $\mu S \cdot cm^{-1}$ appears to be optimum, since higher levels produce a significant decrease of the maximum signal, while lower levels decrease the detectability. Concerning pH, an improvement in assay sensitivity was observed upon decreasing the value (from an IC_{50} of 205 nM to 89 nM) for which reason pH 5.5 was also selected as the most suitable to carry out this assay.

Table 4.6 and Table 4.7 summarize the optimized physicochemical conditions and the analytical parameters of the C4-HSL ELISA.

Table 4.6: Conditions of the ELISA As423/3-oxo-C12-HSL(N)-CONA to analyze C4-HSL.

	Optimized values
As 423	1/500
[3-oxo-C12-HSL (N)-CONA] / $\mu g \cdot mL^{-1}$ HD=7	5
Pre-Incubation Time / min	0
Competition Time / min	30
Tween 20 %	0.05
Conductivity / $\mu S \cdot cm^{-1}$	15
pH	5.5

Table 4.7: Parameters of the calibration curve of the ELISA As423/3-oxo-C12-HSL(N)-CONA for C4-HSL

	Optimized values
A_{min}	0.28 ± 0.01
A_{max}	0.70 ± 0.04
Slope	-1.13 ± 0.09
IC_{50} / nM	88.11 ± 6.39
Dynamic Range / nM	319.15 ± 10.98 to 30.85 ± 1.29
LOD / nM	16.29 ± 0.96
R^2	0.983 ± 0.006

The data shows is the average and standard deviation of three assays run in three different days. On each assay the standard used on the calibration curve were measured using three well-replicates. The analytical parameters were extracted from the four-parameter logistic equation used to fit the standard curve.

4.5 Specificity studies

Despite only two homoserine lactones involved in the QS of *P. aeruginosa* are reported (3-oxo-C12-HSL and C4-HSL), other molecules with similar structures have been detected in *P. aeruginosa* cultures. Those detected in higher concentrations are as follows: N-hexanoyl-L-homoserine lactone (C6-HSL), N-octanoyl-L-homoserine lactone (C-8-HSL) and N-(3-oxodecanoyl)-L-homoserine lactone (3-oxo-C10-HSL)[24]. To determine which regions of the homoserine lactones were more recognized by the developed antibodies, a cross-reactivity (CR) study was performed using compounds with sharing similar structure moieties but with variations such as the length of the hydrocarbon chain, changes in its functional groups, or substitution of the hydrocarbon chain with an aromatic system, as shown in Figure 4.16, as well as their corresponding hydrolyzed forms.

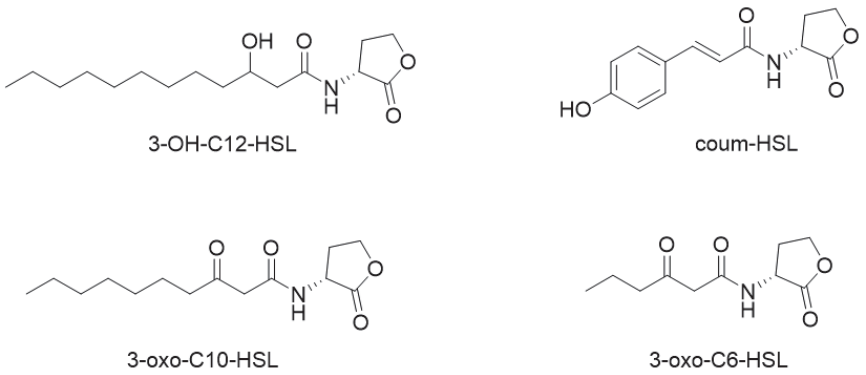

Figure 4.16: Structure of the cross-reactants used in the cross-reactivity studies.

For this purpose, calibration curves for each of these analytes were built and measure with the C4-HSL and 3-oxo-C12-HSL ELISAs to determine their IC_{50} values. The CR was calculated as the percentage of each IC_{50} in respect to that of the hydrolized forms of the target HSLs. Table 4.8 shows the cross-reactivity data of each HSL, both hydrolyzed and non-hydrolyzed, in the 3-oxo-C12-HSL and C4-HSL ELISAs developed.

Table 4.8: The percentage of CR is presented for each of the developed assays for the non-hydrolyzed and hydrolyzed forms of the previously presented structures.

Compound	CR % with ELISA 3-oxo-C12-HSL	CR % with ELISA C4-HSL
3-oxo-C12-HSL	7	1
3-oxo-C12-HSL hydrolized	**100**	2
C4-HSL	4	20
C4-HSL hydrolized	12	**100**
3-OH-C12-HSL	0	0
3-OH-C12-HSL hydrolized	40	0
3-oxo-C10-HSL	0	0
3-oxo-C10-HSL hydrolized	31	45
Coum-HSL	1	0
Coum-HSL hydrolized	31	21
3-oxo-C6-HSL	3	0
3-oxo-C6-HSL hydrolized	43	12

CR is determined using the formula: CR (%) = (IC_{50} of Cross Reactant / IC_{50} of Analyte) x 100.

It can be observed that for both ELISAs, there was consistently greater recognition of the hydrolyzed molecules compared to the non-hydrolyzed ones. For instance, in the 3-oxo-C12-HSL ELISA, a CR of 40% and 31% was obtained for the hydrolyzed 3-OH-C12-HSL and 3-oxo-C10-HSL molecules, respectively, while the same non-hydrolyzed molecules were not recognized at the concentrations assayed. This phenomenon supports the fact that a significant portion of the recognition of these molecules occurs through the hydrolyzed part of the molecule, as has already been discussed.

It is important to note that the CR between the two signaling molecules (3-oxo-C12-HSL and C4-HSL) was low, with only 12% recognition of hydrolyzed C4-HSL by the ELISA for detecting 3-oxo-

C12-HSL, and 2% recognition of hydrolyzed 3-oxo-C12-HSL by the ELISA for C4-HSL. This allows for distinguishing the levels of these two molecules without interference between them.

Regarding the ELISA for 3-oxo-C12-HSL, it can be observed that as the length of the hydrocarbon chain increases, the CR also increases when compared to the recognition of C4-HSL. However, the CR does not exceed 43%, even with molecules where only a carbonyl group has been replaced with an alcohol or the number of carbons in the aliphatic chain has been reduced.

For the ELISA of C4-HSL, it surprisingly shows the highest CR with 3-oxo-C10-HSL, a 45 %, a molecule with an extra carbonyl group and a significantly longer aliphatic chain. The remaining molecules do not represent considerable CR, clearly indicating that the hydrolyzed molecules were more recognized compared to the cyclic ones.

4.6 Matrix effect evaluation

In order to quantify the concentration of HSLs produced by clinical isolates of *P. aeruginosa* in MH culture medium, the matrix effect of the medium on the developed ELISAs was evaluated. For this purpose, calibration curves were generated in MH broth at various concentrations and measured with the 3-oxo-C12-HSL ELISA.

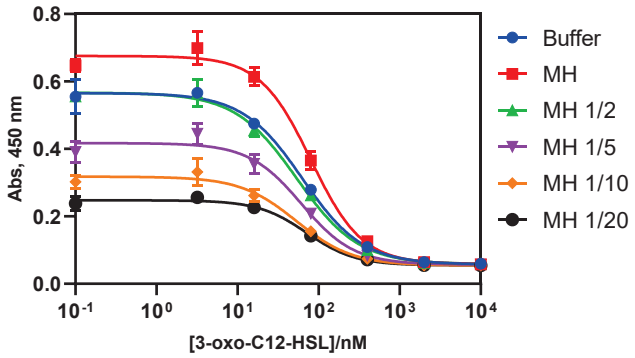

Figure 4.17: Calibration curves obtained in the MH matrix effect evaluation. Each calibration point was measured in triplicates on the same ELISA plate and the data shown is the average and standard deviation.

The calibration curves obtained are shown in Figure 4.17 where it can be observed that the curve in MH medium half diluted with buffer is the one most closely resembling the buffer, and that further dilution of the MH media delivered curves with lower signal and same or lower detectability. This is quite uncommon phenomena since, in general, dilution of a sample matrix with the buffer usually delivers calibration curves that resembled more to the buffer. Up to now, we have not found a satisfactory explanation to that behavior. Despite this, since a good IC_{50} was achieved calibrating with undiluted MH, we proceeded to perform two-dimensional assays using MH to set the optimal concentrations of immunoreagents for this medium. Subsequently, calibration curves were built and measured in the ELISA. Table 4.9 outlines the concentrations of immunoreagents and the parameters of the calibration curves in both buffer and MH culture broth.

Table 4.9: Concentrations of the immunoreagents used and parameters of the 3-oxo-C12-HSL ELISA in buffer and in MH.

	Buffer	MH
As 420 dilution	1/1500	1/750
[C4-HSL(O)-CONA(HD=8)] / µg·mL^{-1}	0.875	0.875
A_{min}	0.07 ± 0.01	0.06 ± 0.01
A_{max}	0.92 ± 0.10	0.70 ± 0.07
Slope	-1.05 ± 0.07	-1.22 ± 0.17
IC_{50} / nM	50.99 ± 5.77	65.59 ± 13.28
Dynamic Range / nM	164.22 ± 9.89 to 8.42 ± 0.79	212.45 ± 36.45 to 19.95 ± 3.05
LOD / nM	3.75 ± 0.30	9.95 ± 3.05
R^2	0.995 ± 0.001	0,994 ± 0,005

The 3-oxo-C12-HSL ELISA uses As420/C4-HSL(O)-AE-CONA as immunoreagent combination. The data shows is the average and standard deviation of three assays run in three different days. On each assay the standard used on the calibration curve were measured using three well-replicates. The analytical parameters were extracted from the four-parameter logistic equation used to fit the standard curve.

Even though the IC_{50} and LOD values of the curve in MH were higher compared to those in the curve run in buffer, not having to dilute the medium would simplify the use of the assay. Moreover, it eliminates the need to dilute the sample, which could compromise the assay's detectability. The LOD achieved was below the values reported to be found in the culture medium, which are in the micromolar range[25-28]. It is also lower than values detected in sputum from CF patients, where concentrations of up to 22 nM have been reported[29]. Furthermore, compared to other quantification techniques, the presented ELISA allows direct quantification of 3-oxo-C12-HSL in the culture medium without requiring any complex sample extraction or treatment. Additionally, the ELISA provides results in less than two hours, is easy to perform, and enables high-throughput screening due to its microplate configuration.

To confirm the accuracy of the developed assay in the MH medium, which is where quantification will take place, a test was conducted where the MH medium was blind spiked with 3-oxo-C12-HSL at various concentrations. Subsequently, quantification was performed using the optimized ELISA As420/C4-HSL(O)-CONA.

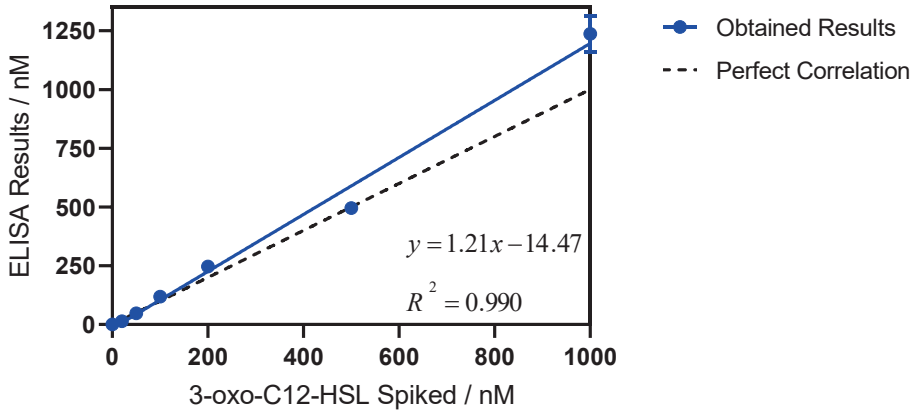

Figure 4.18: Results from the accuracy study. The graph shows the linear regression analysis of 3-oxo-C12-HSL spiked concentration and the concentration measured with the ELISA As420/C4-HSL(O)-AE-CONA. Assays were run in MH culture media. Each calibration point was measured in triplicates on the same ELISA plate.

As observed in Figure 4.18, the correlation coefficient between the spiked samples and the ELISA result was excellent (R^2=0.990). This demonstrates that the optimized assay in the complex MH growth medium exhibits good accuracy and can be used for quantifying 3-oxo-C12-HSL in *P. aeruginosa* isolates.

For the C4-HSL ELISA (As423/3-oxo-C12-HSL(N)-AE-CONA), a similar study was conducted to assess any unspecific matrix effect of the MH growth medium. The results obtained are depicted in Figure 4.19.

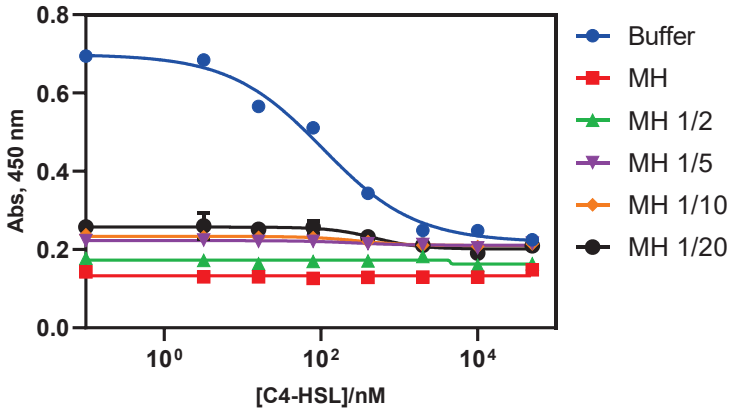

Figure 4.19: Calibration curves obtained in the MH matrix effect evaluation.

As observed, in this assay the MH growth medium exerts a significant matrix effect, completely inhibiting the assay even when diluted by twenty times. Further dilutions of the growth medium were attempted, but dilutions greater than 100 times were needed to obtain a quantifiable curve. This behavior significantly compromises the assay's detectability, addressing the investigation of sample treatment procedures prior immunochemical analysis as an alternative to sample dilution is nowadays under investigation by other members of the Nb4D group. Options such as organic solvent extractions, protein precipitation from the medium to reduce medium interferences, or adjustments in the medium's salinity will be explored.

4.7 Performance evaluation of the 3-oxo-C12-HSL ELISA with *P. aeruginosa* mutant strains

As proof of concept of the performance of the 3-oxo-C12-HSL ELISA, a reference strain of *P. aeruginosa*, PAO1, and different strains provided by Son Espases Hospital (Palma de Mallorca, Balearic Islands), which were genetically characterized and confirmed to have the Las system mutated, were cultured. These last strains should be unable to biosynthesize the 3-oxo-C12-HSL compared to the reference strain PAO1 that should be able to do it.

All the above-mentioned strains were grown in MH medium simultaneously under the same temperature and agitation conditions. After 16 h, samples of the media were collected, centrifuged, and used directly for ELISA measurements. The results found are shown in Table 4.10

Table 4.10: Concentrations of 3-oxo-C12-HSL obtained from P. aeruginosa PAO1 and LasR mutants.

Strain	Mutation in LasR	[3-oxo-C12-HSL] / nM
PAO1	-	2402
Mutant 1	Pro117Arg	LLOD
Mutant 2	Ile197Arg	LLOD
Mutant 3	Arg216Gln	LLOD
Mutant 4	Ser223Phe	LLOD

Concentrations of 3-oxo-C12-HSL in the supernatants of PAO1 and LasR mutants after 16 h of growth in MH. The supernatants were analyzed with the 3-oxo-C12-HSL ELISA with the conditions described in section 4.6.

As can be observed, 3-oxo-C12-HSL was not detected in any of the supernatants in which strains with mutations in LasR were grown. In contrast, as expected, a concentration level of 2402 nM was detected in the supernatant of the reference strain of *P. aeruginosa* PAO1. These results indicates that the ELISA is reliable, that there is no interference derived from bacterial growth that influences the detection of 3-oxo-C12-HSL, and that could be used to monitor 3-oxo-C12-HSL levels and occurrence of mutations in the *las* genes of bacteria strains. Hence, *P. aeruginosa* exhibits a great capacity to adapt to the environment and mutations are frequently reported on chronic or long-term ICU patients. The accumulation of spontaneous mutations has also been identified as the main driver of increasing resistance, which has been demonstrated by large genomic longitudinal studies of isolates from patients with CF [30, 31]and COPD [30]. Particularly, it is known that *P. aeruginosa* regulates virulence via two synthase/transcription factor receptor pairs: LasI/R and RhlI/R. LasR is considered the master transcriptional regulator of QS, as it upregulates *rhlI/R*. *lasR* QS mutations have been shown to frequently arise in CF lung infections, but also in wounds and other environments. Therefore, lower levels of 3-oxo-C12-HSL could be indicators of chronification of the infection and/or disease progression[32].

4.8 Concluding remarks

- For the first time, a comprehensive study has been conducted on the stability conditions of immunizing haptens for the production of polyclonal antibodies against 3-oxo-C12-HSL and C4-HSL. However, antibodies obtained exhibited significant avidity toward the hydrolyzed form of HSL molecules, suggesting hydrolysis likely occurs within the animal after immunization. Alternatively, both species might have been present, with the hydrolyzed form being significantly more immunogenic than the non-hydrolyzed form.

- Immunizing haptens preserving the lactone group provided better assay results, even when recognizing the hydrolyzed form of HSLs, compared to those with a lactam group. Although the latter were designed to recognize the intact HSLs, detectability for 3-oxo-C12-HSL was very low, and no competitive assay was obtained for C4-HSL. This result, supported by similar previous observations in our group, highlights relevant conformational and electronic differences between lactone and lactam functionalities that impact immunochemical recognition.

- A thorough screening involving up to 48 combinations was performed for each ELISA developed, aiming to identify the optimal pAb/bioconjugate combination for analyte recognition. Additionally, the physicochemical parameters of the assays were optimized, improving detectability, with detection limits of 3.75 nM for 3-oxo-C12-HSL and 16.29 nM for C4-HSL.

- A cross-reactivity study with other HSL molecules revealed some cross-reactivity with structurally similar molecules. Notably, there was consistently greater recognition of the hydrolyzed form, suggesting that this molecular epitope plays a significant role in recognition.

- The matrix effect of MH medium on each developed assay was evaluated. For the 3-oxo-C12-HSL ELISA, excellent accuracy was achieved with direct analysis of undiluted MH growth medium without prior sample treatment. However, this same medium completely inhibited the C4-HSL assay. Treatment alternatives, such as protein precipitation, analyte extraction with organic solvents, or increasing the medium's salinity, are under investigation.

- The ELISAs reported here could be used to monitor the progression of pathogenesis by assessing 3-oxo-C12-HSL levels as indicators of Las mutants associated with chronic infections. Furthermore, considering the role of the Las and Rhl QS systems, quantifying HSLs holds potential for early-stage infection detection. However, further studies involving well-characterized patient cohorts are necessary to validate this hypothesis.

4.9 Materials and methods

4.9.1 Chemicals and biochemicals.

All chemical substances and proteins used have been purchased from Sigma-Aldrich.

4.9.2 Equipment.

The description of all the equipment used in this chapter can be found in section 3.8.2.

4.9.3 Buffers

All buffers are the same as those explained in section 3.8.1. The buffer used for both assays developed in this chapter consists of PBST at pH 5.5.

4.9.4 Purification procedures

The purification procedures are the same as those explained in section 3.8.2.

4.9.5 MALDI-TOF MS analysis and HD calculation

The procedures for performing MALDI-TOF MS spectra and calculating the HD are the same as those explained in section 3.8.3.

4.9.6 Haptens and analytes

The haptens were synthesized by the "Servicio de síntesis de de moléculas de alto valor añadido" (SIMChem) of the Medicinal Chemistry and Synthesis group at IQAC-CSIC. All analytes used in this chapter were purchased from Sigma-Aldrich. The spectroscopic and spectrometric characterization of the haptens is as follows:

Hapten for 3-oxo-C12-HSL (O). ^{1}H NMR (400 MHz, $CDCl_3$) δ 7.70 (d, 1H), 4.46 (m, 1H), 4.51 (t, 1H), 4.32 (m, 1H), 3.54 (s, 2H), 2.81 (m, 1H), 2.58 (t, 2H), 2.38 (t, 2H), 2.25 (m, 1H), 1.67 (m, 4H), 1.39 (m, 2H). ^{13}C NMR (101 MHz, $CDCl_3$) δ 206.41, 178.42, 175.26, 166.59, 65.71, 51.06, 48.36, 41.68, 34.08, 30.33, 28.58, 24.43, 22.58. HRMS: *m/z* (ES+) for $C_{13}H_{19}NO_6$ [$(M+H)^+$] calculated 285.12 found 286.00 (0.88 ppm).

Hapten for 3-oxo-C12-HSL (N). ^{1}H NMR (400 MHz, DMSO-d_6) δ 11.99 (s, 1H), 8.34 (d, 1H), 7.86 (s, 1H), 4.28 (1, 1H), 3.32 (s, 2H), 3.19 (m, 2H), 2.68 (t, 1H), 2.33 (m, 2H), 2.19 (t, 2H), 1.77 (m, 1H), 1.46 (m, 4H), 1.23 (m, 2H). ^{13}C NMR (101 MHz, DMSO-d_6) δ 206.38, 179.14, 178.43, 166.53, 59.02, 47.98, 41.69, 38.81, 34.12, 28.48, 24.45, 22.53, 21.25. HRMS: *m/z* (ES-) for $C_{13}H_{20}N_2O_5$ [$(M-H)^-$] calculated 284.14 found 282.99 (-1.15 ppm).

Hapten for C4-HSL (O). ^{1}H NMR (400 MHz, DMSO-d_6) δ 11.94 (s, 1H), 8.31 (d, 1H), 4.36 (dq, 2H), 4.34 (t, 1H), 2.39 (m, 2H), 2.15 (m, 4H), 1.54 (m, 4H), 1.29 (m, 2H). ^{13}C NMR (101 MHz, DMSO-d_6) δ 178.41, 175.06, 173.93, 65.71, 51.34, 36.55, 34.02, 30.37, 28.03, 25.34, 24.04. HRMS: *m/z* (ES-) for $C_{11}H_{17}NO_5$ [$(M-H)^-$] calculated 243.11 found 242.04 (-1.07 ppm).

Hapten for C4-HSL (N). ^{1}H NMR (400 MHz, DMSO-d_6) δ 11.97 (s, 1H), 8.02 (d, 1H), 0.78 (s, 1H), 4.27 (1, 1H), 3.17 (m, 2H), 2.31 (m, 1H), 2.19 (t, 2H), 2.09 (t, 2H), 1.76 (m, 1H), 1.49 (quint., 4H), 1.26 (m, 2H). ^{13}C NMR (101 MHz, DMSO-d_6) δ 179.10, 178.41, 173.93, 59.34, 36.82, 36.14, 34.01, 28.14, 25.33, 24.06, 21.09. HRMS: *m/z* (ES-) for $C_{11}H_{18}N_2O_4$ [$(M-H)^-$] calculated 242.13 found 241.95 (-0.18 ppm).

For the hydrolysis of the analytes, 2 µL of a 1 mM stock in DMSO was added to 48 µL of a 0.1 M NaOH solution. The solution was vortexed several times over 15 minutes. The resulting solution

was analyzed by UPLC-MS as described in section 4.4.1, and the hydrolyzed HSLs were characterized by H-NMR, as shown in Figure 4.20.

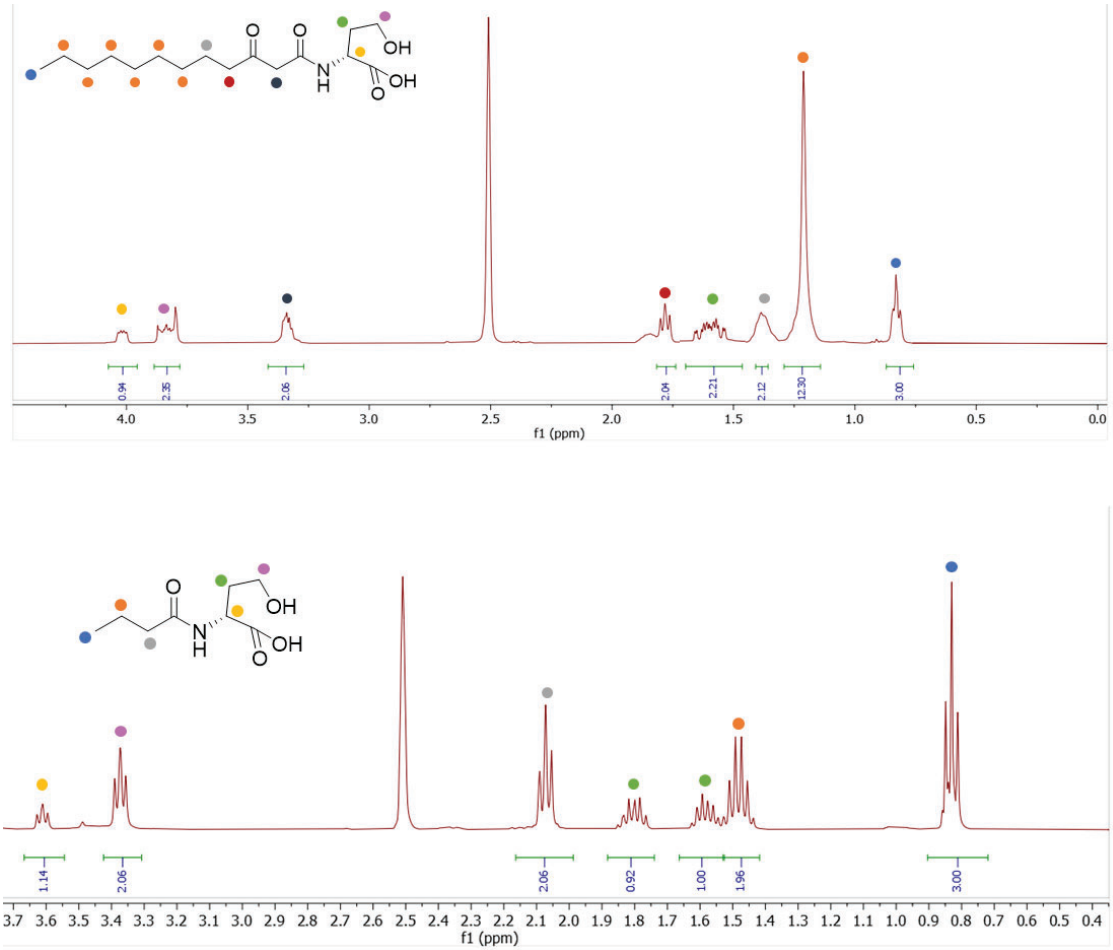

Figure 4.20: NMR spectrum of the hydrolyzed 3-oxo-C12-HSL molecule (top) and hydrolyzed C4-HSL (bottom).

4.9.7 UPLC-MS analysis

UPLC-MS analysis were performed on a Waters Alliance 2795 with an automated injector and a photodiode array detector Waters 2996 coupled to an electrospray ion source (ESI-MS) Micromass ZQ mass detector, and the MassLynx 4.1 software. The instrument was operated in the positive ESI (+) ion mode. All the HPLC-MS analyses were carried out using elution conditions 1: XSelectTM C18 column (2.1 mm×100 mm, 1.7 µm). Elution solvent system: A: 20 mM formic acid in H_2O and B: 20 mM formic acid in acetonitrile. Gradient: 10 %B to 100 % B over 8 min at a flow rate of 2.0 mL/min. λ= 220 nm and 254 nm. Volume of injection 10 µL.

4.9.8 Synthesis of bioconjugates

Synthesis of bioconjugates HSL-KLH and HSL-BSA through MA method: The HSL haptens (10 µmol) were dissolved in 400 µL of anhydrous DMF. While stirring in an ice bath, 2.80 µL (12 µmol, 1.2 eq.) of tributylamine and 1.52 µL (12 µmol, 1.2 eq.) of isobutyl chloroformate were added. The reactions were stirred on ice for 15 minutes. Then, 200 µL of the reaction were added dropwise to a protein solution (BSA or KLH, 2.5 mg mL^{-1}, 2 mL in 10 mM PBS, pH 6.5). The reaction was left stirring for 1.5 hours. The bioconjugates were purified with ÄKTA Prime Plus equipment

with two HiTrap desalting columns. Subsequently, they were frozen at -80°C and lyophilized. A total of 4.38 mg of the BSA-3-oxo-C12-HSL(O), 4.59 mg of BSA-3-oxo-C12-HSL(N), 4.33 mg of BSA-C4-HSL(O), 4.42 mg of BSA-C4-HSL(N), 4.12 mg of KLH-3-oxo-C12-HSL(O), 4.25 mg of KLH-3-oxo-C12-HSL(N), 4.10 mg of KLH-C4-HSL(O) and 4.29 mg of KLH-C4-HSL(N).

Synthesis of bioconjugates HSL-BSA, HSL-CONA and HSL-OVA through AE method: A solution of protein (2.5 mg·mL^{-1}; 2 mL) in PBS at pH 6.5 was prepared in 3 mL vials. The hapten (2.5 µmol in 200 µL), previously dissolved in dry DMF, was added dropwise to the protein solution under stirring. Then, 0.72 mg (3.75 µmol, 1.5 eq.) of 1-ethyl-3-(3-dimethylaminopropyl) carbodiimide (EDC) and 0.43 mg (3.75 µmol, 1.5 eq.) of NHS were added. The reaction was stirred at room temperature (RT) with agitation at 110 rpm for 2 hours and then left overnight at 5°C without agitation. The bioconjugates were purified with ÄKTA Prime Plus equipment with two HiTrap desalting columns. Subsequently, they were frozen at -80°C and lyophilized. A total of 4.43 mg of the BSA-3-oxo-C12-HSL(O), 4.67 mg of CONA-3-oxo-C12-HSL(O), 4.24 mg of OVA-3-oxo-C12-HSL(O), 4.20 mg of BSA-3-oxo-C12-HSL(N), 4.33 mg of CONA-3-oxo-C12-HSL(N), 4.28 mg of OVA-3-oxo-C12-HSL(N), 4.12 mg of BSA-C4-HSL(O), 4.69 mg of CONA-C4-HSL(O), 4.39 mg of OVA-C4-HSL(O), 4.24 mg of BSA-C4-HSL(N), 4.25 mg of CONA-C4-HSL(N) and 4.70 mg of OVA-C4-HSL(N).

4.9.9 Immunochemistry

4.9.9.1 Polyclonal antibody production

Antibodies were generated with the support of the ICTS “NANBIOSIS”, specifically through the Custom Antibody Service (CAbS, CIBER-BBN, IQAC-CSIC). Eight female New Zealand white rabbits weighing 1–2 kg each were immunized with four different antigens: KLH-3-oxo-C12-HSL(O), KLH-3-oxo-C12-HSL(N), KLH-C4-HSL(O), and KLH-C4-HSL(N), with two rabbits per antigen. The immunizations followed approved procedures at the Research and Development Center (CID) of the Spanish Research Council (CSIC) under Registration Number: B9900083, ensuring minimal discomfort for the animals. The protocol was in accordance with institutional guidelines, licensed by the local government (DAAM 7463), and approved by the Institutional Animal Care and Use Committee at the CID-CSIC. Following six immunizations, the animals were exsanguinated, and blood was collected in vacutainer tubes with serum separation gel. Antisera were obtained by centrifugation and stored at −80 °C with 0.02% sodium azide as a preservative. Antibody titers were evaluated using non-competitive indirect ELISA throughout the immunization process. Microtiter plates were coated with a fixed concentration of corresponding BSA bioconjugates (1 mg mL^{-1}), and antibody avidity was determined by preparing serial dilutions of the antisera.

4.9.9.2 ELISA

Competitive indirect ELISA for the antigen and antiserum selection (1D ELISAs). The ELISA plates with 96 wells each were coated with the twelve antigen combinations at a concentration of 1 mg·mL^{-1} in coating buffer. They were left overnight at 4°C. Subsequently, the plates were washed four times with 300 µL of PBST each. For each As/Ag combination, 50 µL of PBST, 50 µL of the corresponding non-hydrolyzed analyte at a concentration of 1 µM, and 50 µL of the analyte at 1 µM previously treated for 15 minutes with a 0.1M NaOH solution and neutralized with 1M HCl were added to two columns of the plate. Then, 50 µL of anti-serum dilutions were added per well (seven dilutions starting from 1/500 dilution of the corresponding antiserum in

PBST, with the final dilution being PBST). After washing the plates, a solution of goat anti-rabbit IgG-HRP (1/6000 in PBST) was added (100 µL per well) and incubated for an additional 30 minutes at room temperature. The plates were washed again, and then 100 µL of substrate solution was added to each well and left for 30 minutes at room temperature in the dark. The enzymatic reaction was stopped by adding 50 µL of 4N H_2SO_4 solution to each well, and the absorbance was read at 450 nm.

Non-competitive indirect two-dimensional titration. A microtiter plate was coated with varying concentrations of the corresponding coating antigen, ensuring that each row contained a different concentration (ranging from 10 µg·mL^{-1} to 10 ng·mL^{-1}, and zero in coating buffer, 100 µL·well^{-1}). The plate was left overnight at 4ºC. Subsequently, the plate was washed (4 x 300 µL, PBST), and different concentrations of antiserum were added (ranging from 1/100 to 1/6400, and zero in the assay buffer, 100 µL·well^{-1}). The plate was incubated for 30 minutes at room temperature, followed by a washing step (4 x 300 µL, PBST). Next, 100 µL/well of goat anti-rabbit IgG-HRP (1/6000 in PBST) was added, and the plate was incubated for an additional 30 minutes at RT. Subsequently, the plate was washed (4 x 300 µL, PBST), and the substrate solution (100 µL/well) was added, incubating another 30 minutes at room temperature, shielded from light. The enzymatic reaction was stopped by adding 4M H_2SO_4 (50 µL·well-1), and the absorbance was finally read at 450 nm.

ELISA As420/C4-HSL(O)-CONA for the detection of 3-oxo-C12-HSL in buffer. Microtiter plates were coated with 0.875 µg·mL^{-1} of C4-HSL(O)-CONA in coating buffer and left overnight at 4ºC. The following day, 75 µL of solutions of hydrolyzed 3-oxo-C12-HSL (treated for 15 minutes with NaOH 0.1 M and neutralized with HCl 1M) ranging from 10 µM to 0.64 nM in PBST at pH 5.5 were added to a 96-well plate. Then, 75 µL of a 1/1500 solution in PBST at pH 5.5 of As420 were added over the analyte. The mixture was left for 30 minutes at room temperature. Later, the microtiter plate was washed four times with 300 µL of PBST. Subsequently, 100 µL per well of the analyte/As mixture was added and left for 30 minutes at room temperature. After another round of washing (4 x 300 µL, PBST), a solution of goat anti-rabbit IgG-HRP (1/6000 in PBST) was added and incubated for an additional 30 minutes at room temperature. Following this, another wash step (4 x 300 µL, PBST) was performed, and then 100 µL of substrate solution was added to each well and left for 30 minutes at room temperature in the dark. The enzymatic reaction was halted by the addition of 50 µL of 4N H_2SO_4 solution to each well, and the absorbance was measured at 450 nm.

ELISA As423/3-oxo-C12-HSL(N)-CONA for the detection of C4-HSL in buffer. Microtiter plates were coated with 5 µg·mL^{-1} of 3-oxo-C12-HSL(N)-CONA in coating buffer and left overnight at 4ºC. The following day, 75 µL of solutions of hydrolyzed C4-HSL (treated for 15 minutes with NaOH 0.1 M and neutralized with HCl 1M) ranging from 10 µM to 0.64 nM in PBST at pH 5.5 were added to a 96-well plate. Then, 75 µL of a 1/1500 solution in PBST at pH 5.5 of As420 were added over the analyte. The mixture was left for 30 minutes at room temperature. Later, the microtiter plate was washed four times with 300 µL of PBST. Subsequently, 100 µL per well of the analyte/As mixture was added and left for 30 minutes at room temperature. After another round of washing (4 x 300 µL, PBST), a solution of goat anti-rabbit IgG-HRP (1/6000 in PBST) was added and incubated for an additional 30 minutes at room temperature. Following this, another wash step (4 x 300 µL, PBST) was performed, and then 100 µL of substrate solution was added

to each well and left for 30 minutes at room temperature in the dark. The enzymatic reaction was halted by the addition of 50 µL of 4N H_2SO_4 solution to each well, and the absorbance was measured at 450 nm.

Cross-reactivity studies were conducted for each of the optimized assays. Both the non-hydrolyzed and hydrolyzed forms of the following cross-reactants were utilized: 3-oxo-C12-HSL, C4-HSL, 3-OH-C12-HSL, 3-oxo-C12-HSL, Coum-HSL, and 3-oxo-C6-HSL. A non-competitive indirect ELISA, as previously described, was performed by adding these molecules as analytes at concentrations ranging from 10 µM to 0.64 nM. The cross-reactivity (CR) was calculated using the formula: CR (%) = IC_{50}(Cross reactant)/IC_{50}(Analyte) x 100.

Matrix effect assay: The same procedure as in the non-direct competitive ELISA was followed, but the analyte dilutions were prepared in sterile MH and MH diluted one half, one fifth, one tenth, and one twentieth.

ELISA As420/C4-HSL(O)-CONA for the detection of 3-oxo-C12-HSL in MH. Microtiter plates were coated with 0.875 µg·mL^{-1} of C4-HSL(O)-CONA in coating buffer and left overnight at 4ºC. The following day, 75 µL of solutions of hydrolyzed 3-oxo-C12-HSL (treated for 15 minutes with NaOH 0.1 M and neutralized with HCl 1M) ranging from 10 µM to 0.64 nM in PBST at pH 5.5 were added to a 96-well plate. Then, 75 µL of a 1/750 solution in PBST at pH 5.5 of As420 were added over the analyte. The mixture was left for 30 minutes at room temperature. Later, the microtiter plate was washed four times with 300 µL of PBST. Subsequently, 100 µL per well of the analyte/As mixture was added and left for 30 minutes at room temperature. After another round of washing (4 x 300 µL, PBST), a solution of goat anti-rabbit IgG-HRP (1/6000 in PBST) was added and incubated for an additional 30 minutes at room temperature. Following this, another wash step (4 x 300 µL, PBST) was performed, and then 100 µL of substrate solution was added to each well and left for 30 minutes at room temperature in the dark. The enzymatic reaction was halted by the addition of 50 µL of 4N H_2SO_4 solution to each well, and the absorbance was measured at 450 nm.

Accuracy studies. Blind spiked samples in MH culture broth were prepared and measured using the ELISA As420/C4-HSL(O)-CONA in MH. The samples were measured in triplicate.

4.9.10 Measurement of 3-oxo-C12-HSL in supernatants of *P. aeruginosa*

The same procedure described in section 3.9.8 was followed, but performing the ELISA As420/C4-HSL(O)-CONA for the detection of 3-oxo-C12-HSL in MH.

4.10 References

1. Cataldi, T. R. I.; Bianco, G.; Palazzo, L.; Quaranta, V., Occurrence of N-acyl-l-homoserine lactones in extracts of some Gram-negative bacteria evaluated by gas chromatography–mass spectrometry. *Analytical Biochemistry* **2007,** *361* (2), 226-235.
2. Kumari, A.; Pasini, P.; Daunert, S., Detection of bacterial quorum sensing N-acyl homoserine lactones in clinical samples. *Analytical and Bioanalytical Chemistry* **2008,** *391* (5), 1619-1627.
3. Wellington, S.; Greenberg, E. P., Quorum Sensing Signal Selectivity and the Potential for Interspecies Cross Talk. *mBio* **2019,** *10* (2).
4. Shaw, P. D.; Ping, G.; Daly, S. L.; Cha, C.; Cronan, J. E., Jr.; Rinehart, K. L.; Farrand, S. K., Detecting and characterizing N-acyl-homoserine lactone signal molecules by thin-layer chromatography. *Proceedings of the National Academy of Sciences of the United States of America* **1997,** *94* (12), 6036-41.
5. Götz-Rösch, C.; Sieper, T.; Fekete, A.; Schmitt-Kopplin, P.; Hartmann, A.; Schröder, P., Influence of bacterial N-acyl-homoserine lactones on growth parameters, pigments, antioxidative capacities and the xenobiotic phase II detoxification enzymes in barley and yam bean. *Frontiers in plant science* **2015,** *6*, 205.
6. Fekete, A.; Frommberger, M.; Rothballer, M.; Li, X.; Englmann, M.; Fekete, J.; Hartmann, A.; Eberl, L.; Schmitt-Kopplin, P., Identification of bacterial N-acylhomoserine lactones (AHLs) with a combination of ultra-performance liquid chromatography (UPLC), ultra-high-resolution mass spectrometry, and in-situ biosensors. *Analytical and bioanalytical chemistry* **2007,** *387* (2), 455-67.
7. Patel, N. M.; Moore, J. D.; Blackwell, H. E.; Amador-Noguez, D., Identification of Unanticipated and Novel N-Acyl L-Homoserine Lactones (AHLs) Using a Sensitive Non-Targeted LC-MS/MS Method. *PLoS One* **2016,** *11* (10), e0163469.
8. Lépine, F.; Milot, S.; Groleau, M.-C.; Déziel, E., Liquid Chromatography/Mass Spectrometry (LC/MS) for the Detection and Quantification of N-Acyl-L-Homoserine Lactones (AHLs) and 4-Hydroxy-2-Alkylquinolines (HAQs). In *Quorum Sensing: Methods and Protocols*, Leoni, L.; Rampioni, G., Eds. Springer New York: New York, NY, 2018; pp 49-59.
9. Yang, Y.; Zhou, M.; Hardwidge, P. R.; Cui, H.; Zhu, G., Isolation and Characterization of N-acyl Homoserine Lactone-Producing Bacteria From Cattle Rumen and Swine Intestines. *Frontiers in cellular and infection microbiology* **2018,** *8*, 155.
10. Sismaet, H. J. Development and optimization of electrochemical sensors to detect bacterial pathogens for point-of-care applications. Boston, Massachusetts : Northeastern University, 2017.
11. Jiang, H.; Jiang, D.; Shao, J.; Sun, X., Magnetic molecularly imprinted polymer nanoparticles based electrochemical sensor for the measurement of Gram-negative bacterial quorum signaling molecules (N-acyl-homoserine-lactones). *Biosens Bioelectron* **2016,** *75*, 411-9.
12. Habimana, J. d. D.; Ji, J.; Pi, F.; Karangwa, E.; Sun, J.; Guo, W.; Cui, F.; Shao, J.; Ntakirutimana, C.; Sun, X., A class-specific artificial receptor-based on molecularly imprinted polymer-coated quantum dot centers for the detection of signaling molecules, N-acyl-homoserine lactones present in gram-negative bacteria. *Analytica Chimica Acta* **2018,** *1031*, 134-144.
13. Miller, C.; Gilmore, J., Detection of Quorum-Sensing Molecules for Pathogenic Molecules Using Cell-Based and Cell-Free Biosensors. *Antibiotics (Basel)* **2020,** *9* (5).
14. McCready, A. R.; Paczkowski, J. E.; Henke, B. R.; Bassler, B. L., Structural determinants driving homoserine lactone ligand selection in the Pseudomonas aeruginosa LasR quorum-sensing receptor. *Proceedings of the National Academy of Sciences of the United States of America* **2019,** *116* (1), 245-254.

15. O'Connor, G.; Knecht, L. D.; Salgado, N.; Strobel, S.; Pasini, P.; Daunert, S., Whole-Cell Biosensors as Tools for the Detection of Quorum-Sensing Molecules: Uses in Diagnostics and the Investigation of the Quorum-Sensing Mechanism. *Adv Biochem Eng Biotechnol* **2015**.
16. Chen, X.; Kremmer, E.; Gouzy, M.-F.; Clausen, E.; Starke, M.; Wöllner, K.; Pfister, G.; Hartmann, A.; Krämer, P. M., Development and characterization of rat monoclonal antibodies for N-acylated homoserine lactones. *Analytical and bioanalytical chemistry* **2010,** *398* (6), 2655-2667.
17. Wöllner, K.; Chen, X.; Kremmer, E.; Krämer, P. M., Comparative surface plasmon resonance and enzyme-linked immunosorbent assay characterisation of a monoclonal antibody with N-acyl homoserine lactones. *Analytica chimica acta* **2010,** *683* (1), 113-8.
18. Kaufmann, G. F.; Sartorio, R.; Lee, S. H.; Mee, J. M.; Altobell, L. J., 3rd; Kujawa, D. P.; Jeffries, E.; Clapham, B.; Meijler, M. M.; Janda, K. D., Antibody interference with N-acyl homoserine lactone-mediated bacterial quorum sensing. *Journal of the American Chemical Society* **2006,** *128* (9), 2802-3.
19. Montagut, E. J.; Acosta, G.; Albericio, F.; Royo, M.; Godoy-Tena, G.; Lacoma, A.; Prat, C.; Salvador, J. P.; Marco, M. P., Direct Quantitative Immunochemical Analysis of Autoinducer Peptide IV for Diagnosing and Stratifying Staphylococcus aureus Infections. *ACS infectious diseases* **2022,** *8* (3), 645-656.
20. Kim, Y. J.; Cho, Y. A.; Lee, H.-S.; Lee, Y. T.; Gee, S. J.; Hammock, B. D., Synthesis of haptens for immunoassay of organophosphorus pesticides and effect of heterology in hapten spacer arm length on immunoassay sensitivity. *Analytica chimica acta* **2003,** *475* (1), 85-96.
21. Nakajima, N.; Ikada, Y., Mechanism of amide formation by carbodiimide for bioconjugation in aqueous media. *Bioconjug Chem* **1995,** *6* (1), 123-30.
22. Davis, L. E.; Roth, S. A.; Anderson, B., Antisera specificities to 1-ethyl-3-(3-dimethylaminopropyl) carbodiimide adducts of proteins. *Immunology* **1984,** *53* (3), 435-41.
23. Kaufmann, G. F.; Sartorio, R.; Lee, S.-H.; Rogers, C. J.; Meijler, M. M.; Moss, J. A.; Clapham, B.; Brogan, A. P.; Dickerson, T. J.; Janda, K. D., Revisiting quorum sensing: Discovery of additional chemical and biological functions for 3-oxo-N-acylhomoserine lactones. **2005,** *102* (2), 309-314.
24. Cataldi, T. R. I.; Bianco, G.; Abate, S., Accurate mass analysis of N-acyl-homoserine-lactones and cognate lactone-opened compounds in bacterial isolates of Pseudomonas aeruginosa PAO1 by LC-ESI-LTQ-FTICR-MS. **2009,** *44* (2), 182-192.
25. Pearson, J. P.; Passador, L.; Iglewski, B. H.; Greenberg, E. P., A second N-acylhomoserine lactone signal produced by Pseudomonas aeruginosa. *Proceedings of the National Academy of Sciences of the United States of America* **1995,** *92* (5), 1490-4.
26. Charlton, T. S.; de Nys, R.; Netting, A.; Kumar, N.; Hentzer, M.; Givskov, M.; Kjelleberg, S., A novel and sensitive method for the quantification of N-3-oxoacyl homoserine lactones using gas chromatography-mass spectrometry: application to a model bacterial biofilm. *Environmental microbiology* **2000,** *2* (5), 530-41.
27. Ortori, C. A.; Dubern, J. F.; Chhabra, S. R.; Cámara, M.; Hardie, K.; Williams, P.; Barrett, D. A., Simultaneous quantitative profiling of N-acyl-L-homoserine lactone and 2-alkyl-4(1H)-quinolone families of quorum-sensing signaling molecules using LC-MS/MS. *Analytical and bioanalytical chemistry* **2011,** *399* (2), 839-50.
28. Le Berre, R.; Nguyen, S.; Nowak, E.; Kipnis, E.; Pierre, M.; Ader, F.; Courcol, R.; Guery, B. P.; Faure, K., Quorum-sensing activity and related virulence factor expression in clinically pathogenic isolates of Pseudomonas aeruginosa. *Clinical Microbiology and Infection* **2008,** *14* (4), 337-343.
29. Erickson, D. L.; Endersby, R.; Kirkham, A.; Stuber, K.; Vollman, D. D.; Rabin, H. R.; Mitchell, I.; Storey, D. G., Pseudomonas aeruginosa quorum-sensing systems may control virulence factor expression in the lungs of patients with cystic fibrosis. *Infection and immunity* **2002,** *70* (4), 1783-90.

30. Rossi, E.; La Rosa, R.; Bartell, J. A.; Marvig, R. L.; Haagensen, J. A. J.; Sommer, L. M.; Molin, S.; Johansen, H. K., Pseudomonas aeruginosa adaptation and evolution in patients with cystic fibrosis. *Nat Rev Microbiol* **2021,** *19* (5), 331-342.
31. Klockgether, J.; Cramer, N.; Fischer, S.; Wiehlmann, L.; Tümmler, B., Long-Term Microevolution of Pseudomonas aeruginosa Differs between Mildly and Severely Affected Cystic Fibrosis Lungs. *Am J Respir Cell Mol Biol* **2018,** *59* (2), 246-256.
32. Simanek, K. A.; Schumacher, M. L.; Mallery, C. P.; Shen, S.; Li, L.; Paczkowski, J. E., Quorum-sensing synthase mutations re-calibrate autoinducer concentrations in clinical isolates of Pseudomonas aeruginosa to enhance pathogenesis. *Nat Commun* **2023,** *14* (1), 7986.

5. IMMUNOCHEMICAL DETECTION OF QUORUM SENSING Pqs SIGNALING MOLECULES IN SPUTUM CLINICAL SAMPLES

5.1 Chapter presentation

This chapter explains the implementation of ELISAs mAb5.4.2.3/PQS-BSA(HD=3) and As382/PQS-BSA for the detection of PQS and HHQ, respectively, in complex clinical samples such as sputum. To achieve this goal, an initial analysis of the sputum composition was conducted to then study, in a rational manner, a series of sample treatments, aimed at eliminating the undesired matrix effect that this complex sample introduces to ELISAs. Finally, the quantification of both PQS and HHQ in sputum samples from patients infected with *P. aeruginosa* bacteria is presented.

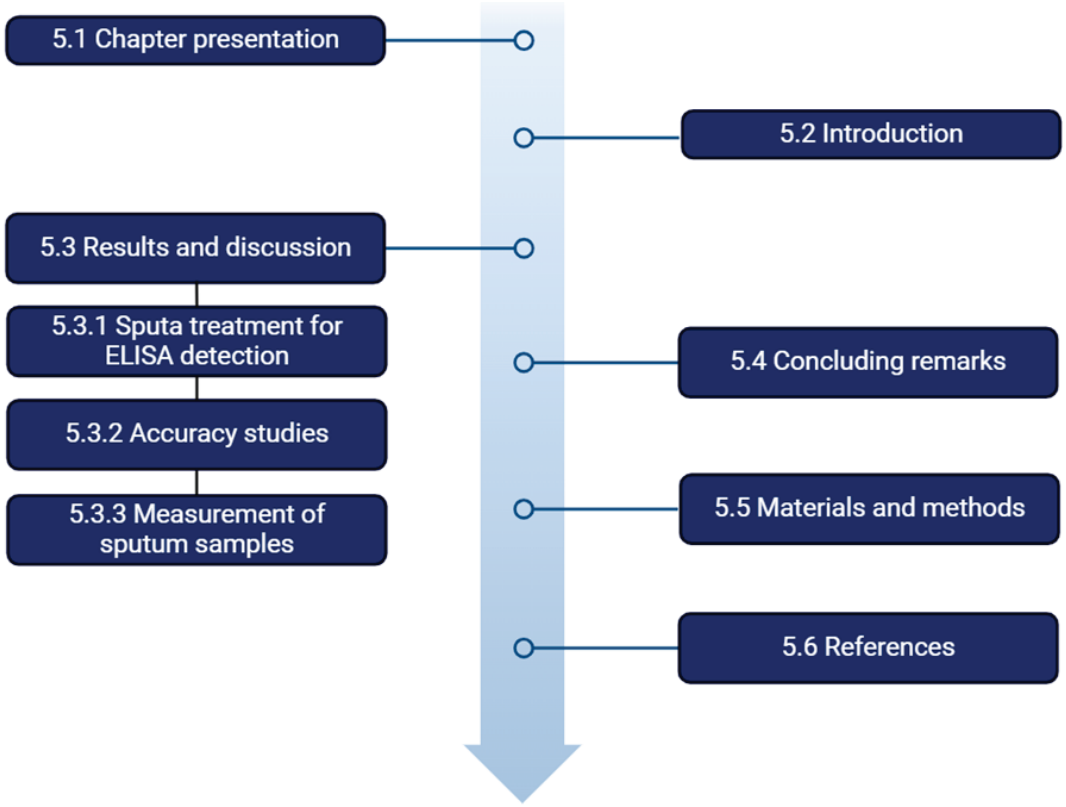

Figure 5.1: Structure of Chapter 5.

5.2 Introduction

In normal lung function, mucus and mucociliary clearance are vital aspects of the innate immune system. Airway mucus serves to keep the airways moist and traps particles, bacteria, and viruses. Additionally, mucus possesses antioxidant, antiprotease, and antimicrobial properties[2].

Although often the terms "sputum" and "mucus" are used interchangeably, they refer to different substances. Typically, normal mucus primarily consists of gel-forming mucins, but in chronic airway diseases, this composition can change. Chronic inflammation may damage the ciliated epithelium responsible for clearing mucin, leading to an increased volume of secretions that often require expulsion through coughing. These expelled secretions are known as sputum[3].

Mucins encompass a family of molecules comprising both polymerizing and non-polymerizing forms. In the airways, secreted mucins with polymeric structures consist of a protein core divided into two main regions: a central linear region rich in proline, serine, and threonine amino acids, and a cysteine-rich region containing hydrophobic amino acids and intramolecular disulfide bonds. In the central region, there are glycosides linked to the amino acids and constitutes up to 80% of mucin's molecular weight, creating negatively charged hydrophilic zones that shield the protein core from protease degradation. Each glycan attached to the mucin contains 2–20 neutral and/or negatively charged sugars, initiated by the addition of N-acetylgalactosamine to serine or threonine residues. The glycan structures consist in a core composed of N-acetylgalactosamine, galactose, and N-acetylglucosamine. These core structures undergo further elongation and modification through the addition of fucose and sialic acid, as well as small amounts of mannose and sulfate. The complexity and diversity of mucin glycans confer significant resistance to microbial proteases, glycosidases, and sialidases due to the multitude of specific enzymes required to degrade the various glycan linkages. The cysteine-rich regions also form disulfide bridges with cysteine-rich regions of other mucin chains, creating a complex interconnected network that contributes to the high viscosity of the mucin (see Figure 5.2)[1].

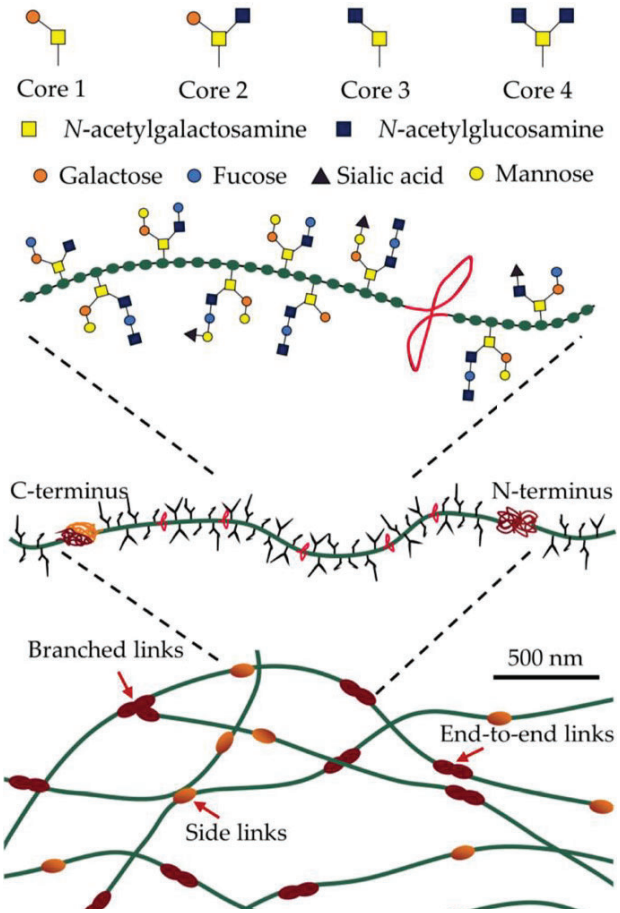

Figure 5.1: Sputum structure. Image extracted from Meldrum et. al.[1].

To maintain normal function, mucus clearance relies on ciliary motion, which necessitates a delicate balance between the volume and composition of the mucus, sufficient periciliary liquid

volume, and normal ciliary beat frequency. This equilibrium can be disrupted by inflammatory conditions, leading to excessive mucin production and hypersecretion[4].

In diseases such as CF and other chronic inflammatory airway conditions, the composition of airway secretions shifts, with other large polymers becoming predominant. These polymers include DNA, filamentous actin, proteoglycans, and biofilms, along with bacteria and inflammatory cells, collectively forming sputum. The accumulation of excessive sputum overwhelms ciliary clearance mechanisms, obstructing the airways and contributing to the morbidity and mortality associated with chronic inflammatory lung diseases such as asthma, CF, and COPD[5].

The majority of adults living with CF are continuously infected with *P. aeruginosa*, a condition associated with a rapid decline in lung function[6], increased occurrences of pulmonary exacerbations, and elevated mortality rates[7]. The effectiveness of *P. aeruginosa* as an opportunistic pathogen is partially attributed to its ability for collective action among bacterial populations, achieved through cell-to-cell communication mediated by quorum sensing AI[8].

QS controls more than 10% of the *P. aeruginosa* genome, influencing various crucial functions such as swarming motility and biofilm maturation. Additionally, QS governs the production of virulence factors like elastases, PYO, cyanide, and exotoxins[8]. In patients with CF, bronchial secretions exhibit elevated levels of QS-dependent virulence factors during pulmonary exacerbations, implying a potential link between QS AIs and changes in clinical status[9].

There have been few studies reporting the detection of AIs in sputum, plasma, and urine collected from CF patients. Some even correlate their levels between different types of samples[10-14]. These studies suggest that AIs could function as biomarkers for *P. aeruginosa* infection in different biological samples, assisting in diagnosing and assessing the response to treatments in both pulmonary and non-pulmonary situations. Additionally, it has been demonstrated that systemic concentrations of several AIs are related to changes in the patient clinical status[13], supporting even more their potential as novel biomarkers airway infections caused by *P. aeruginosa*.

Detecting pathogens causing pneumonia typically relies on bacterial culture of respiratory samples, considered the gold standard (see chapter 1). However, this method is time-consuming, taking several days for results. Meantime, mismanagement of *P. aeruginosa* infection through empirical therapy can lead to a rapid progression towards deadly sepsis[15, 16]. Therefore, there's a pressing need to develop bedside technologies for the rapid detection of *P. aeruginosa* in respiratory samples. This would enable fine-tuning antibiotic therapies based on the presence of this multidrug-resistant pathogen.

To accomplish this aim, this chapter presents the investigations conducted in the context of this PhD thesis for the implementation of the ELISA technologies developed in our group [17-20] to detect QS molecules from the Pqs system of *P. aeruginosa* in sputum. The PQS and HHQ AIs have been targeted due to their specificity for the *P. aeruginosa* QS. Other *Pseudomonas spp.* do not produce such alkylquinolones [21]. Although some studies have identified HHQ biosynthetic systems in non-*Pseudomonas* species such as *Burkholderia pseudomallei*, *B. cepacia*, *B. thailandensis*, and *B. ambifaria*, the function of these HHQ analogues remains to be elucidated[22, 23]. These species are known to produce and release various 4-hydroxy-3-methyl-2-

alkylquinolines (HMAQs). However, while these exoproducts play several roles in *P. aeruginosa* virulence and survival, the available literature is very limited on their distribution and function in *Burkholderia*. Hence, *Burkholderia cenocepacia* (a member of the *B. cepacia* complex) and *P. aeruginosa* usually coexist and cause life-threatening infections in CF patients. However, *B. cenocepacia* mainly employs two types of QS systems, the cis-2-dodecenoic acid (BDSF) system and the HSL system, to regulate biological functions and virulence[24].

5.3 Results and discussion

5.3.1 Sputa treatment for ELISA detection

The use of QS molecules as biomarkers of infection at the PoC requires detecting them directly in clinical samples. Sputum was the target sample since it is directly in contact with the infective bacteria and can be obtained without the need for invasive procedures. Hence, sputum is already the sample of choice used to diagnose lower respiratory tract infections and monitor chronic patients. Obtaining adequate sputum samples can be challenging (should be collected following precise instructions and ensuring that there will not be mouth bacteria in the sputum collected), not all the patients are able to expectorate, particularly, children or young patients, in which case upper respiratory tract specimens (oropharyngeal (OP) swabs, nasopharyngeal (NP) swabs, NP aspirates, OP suction) are recommended. However, there is a strong concern on whether the results reflect the cause of lower respiratory tract infection [25]. Several studies addressing the suitability of easy to obtain upper respiratory specimens usually report a superior sensitivity of the sputum followed by the aspirates (or suction) and the swabs being the last recommended ones[26-30].

Sputum is a highly heterogeneous and viscous sample that requires homogenization and complete solubilization before analysis. Due to its complexity, there are a variety of protocols reported in the literature to treat the sample, mostly based on the use of mucolytics to disrupt the sputum[31]. These mucolytics are based on reducing agents such as dithiothreitol (DTT)[31-34] and N-acetyl-L-cysteine (NAC)[35, 36] (See Figure 5.3). These agents contain thiol groups that cleave the disulfide bridges forming the different mucin chains, significantly reducing the viscosity of the sputum. Additionally, after treatment with reducing agents, other procedures such as filtration or centrifugation are often used to remove particles that may interfere with subsequent analyses. Moreover, in some cases, samples are heated or treated with other agents such as enzymes or strong oxidizing agents. For instance, Peter *et al.* developed an ELISA protocol for diagnosing tuberculosis using sputum samples that included adding a DTT solution to break the sulfide bonds and homogenize the sample, followed by filtration, heating at 95°C for 30 minutes, and centrifugation at 12,500 rpm[37]. On the other hand, Arias-Bouda *et al.* also developed an ELISA protocol for the same purpose in which they initially treated the sputum with NAC as a solubilizing agent, then added proteinase K to break down the amino acid chains forming the mucin, and finally thermally deactivated the enzyme and performed a final filtration[35]. Additionally, Clemente *et al.* developed a paper-based sensor for the direct detection of P. aeruginosa in sputum with a limit of detection (LOD) of 10^5 cells/mL. The detection process involves simply adding hydrogen

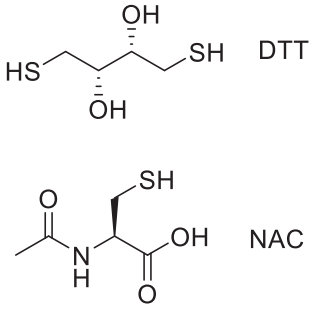

Figure 5.2: Chemical structure of DTT and NAC.

peroxide, which is decomposed by the sample's own catalases, generating oxygen that disrupts the sputum[38].

Another challenge of analyzing sputa sample is the high variability (composition, aspect, density) within individuals, or even within the same patient. Many guidelines recommend collecting the sample 3 expectorated morning sputa to minimize in-patient variability. Hence, sputum varies significantly among different patients, displaying noticeable differences in color, texture, and viscosity. These variations can often be observed with the naked eye, highlighting the diverse nature of sputum samples. For instance, some sputum samples might be thick and sticky, while others could be thin and watery. The color can range from clear or white to yellow, green, or even brown, each indicating different underlying conditions. In fact, sputum appearance has been correlated with certain pathologies according to the Oxford Medical Education (see Table 5.1).

Table 5.1: The classification of sputum based on its appearance

Type	Characteristics	Associated pathology
Purulent	Thick, yellow/Green sputum	Infectious – pneumonia, bronchiectasis and abscess
Mucoid	Clear, grey/White	Chronic obstructive pulmonary disease and asthma
Serous	Clear, frothy, can be pink	Pulmonary oedema
Blood	Blood	Malignancy, pulmonary embolus, clotting disorders, infection

Data extracted from Oxford Medical Education[39].

In this work, we have attempted to implement ELISA technologies to the analysis of sputa sample for which reason several sample treatments have been evaluated. On a first instance, pooled sputum samples were used to obtain information on the behavior of the ELISAs, believing that pooling distinct samples would provide more representative results. First studies were carried out treating the sputa with usually reported reducing agents targeting the disulfide bridges to liquefy and homogenize the samples. However, these treatments were found not completely solve the undesired nonspecific interferences or the variability between sputa. For this reason several other treatments have also been evaluated as it is described in the next sections.

5.3.1.1. Treatment with the reducing agent DTT

To ensure accurate quantification, the effect of the sputum matrix on the PQS and HHQ ELISAs was assessed. The mAb5.4.2.3/PQS-BSA(HD=3) ELISA for the PQS detection and the As382/PQS-BSA ELISA for the HHQ detection developed by Montagut *et. al.*[19] were used for the initial assays. These studies were performed creating a pool of a total of 14 sputum samples testing negative for *P. aeruginosa* (from now on "blank sputum"). This pool was treated with a solution of 0.2 % DTT, then centrifuged and filtered to remove solid impurities that could interfere with the assay (protocol described in section 5.5.2.1). A concentration of 125 mg of sputum·mL^{-1} was obtained after the treatment.

To assess the potential nonspecific interferences caused by the sputum, calibration curves of PQS and HHQ were prepared in the assay buffer and in treated sputum at different dilutions, and subsequently run in the PQS and HHQ ELISAs. The resulting curves are shown in Figure 5.4

demonstrate that the matrix effect generated by the sputum pool was different on each of the assays. In both cases, all calibration curves obtained were parallel (with a slope around -0.7) to the one obtained in the buffer but show, in general, lower maximum absorbance. Unexpectedly, dilution of the sample matrix did not seem to overcome this undesired nonspecific effect on the PQS ELISA. In contrast, on the HHQ ELISA, the curve built on sputum diluted 5 times in the assay buffer showed a close behavior to that of the buffer, however further dilution of the sample provided calibration curves with higher maximum absorbance. At present, we have not been able to find an explanation for this behavior in which the assay buffer with just a 5% of sputum shows an absorbance which is near twice that of the buffer.

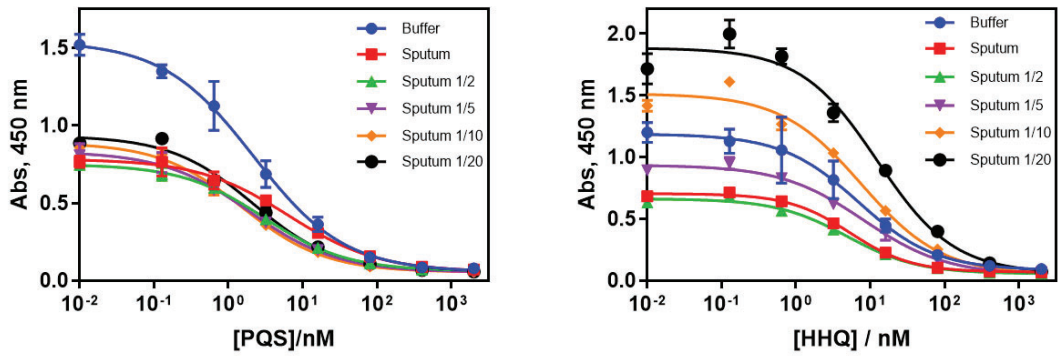

Figure 5.4: Matrix effect of the DTT treated sputum undiluted (125 mg·mL^{-1}; red) and diluted 2 (green), 5 (purple), 10 (orange) and 20 (black) times in PBST on the performance of mAb5.4.2.3/PQS-BSA(HD=3) ELISA for the PQS detection and the As382/PQS-BSA ELISA for the HHQ detection. The standard calibration curve in buffer is shown in blue. Each calibration point was measured in duplicates on the same ELISA plate and the results were all obtained on the same day.

When reference sample matrices can be found commercially available a possible solution is to calibrate the assay with the sample matrix instead of on the assay buffer; however, this is not possible for the case of sputa. On an attempt to overcome this problem we addressed varying the conditions of the buffer assay to prepare the calibration curve in buffer in order to mimic the behavior of the sputum. As observed in Figure 5.5, adjusting the antibody concentration in the buffer allowed to obtain calibration curves in buffer that behave similar to that of sputum at 1/2 and 1/5 dilutions for the quantification of PQS and HHQ, respectively. Hence, for the PQS ELISA, an A_{max} of 1.23 and 1.04 with IC_{50s} of 3.37 and 6.05 nM were obtained in buffer and in 1/2 diluted sputum, respectively. For the HHQ ELISA, an A_{max} of 1.37 and 1.14 with IC_{50s} of 4.96 and 3.74 nM were obtained in buffer and in 1/5 diluted sputum, respectively. Although at this point, we thought that these results pointed to the realistic possibility to quantify PQS and HHQ in sputa with a simple treatment consisting in just treating the samples with DTT, filtering through a 0.45 µm filter, and subsequently diluting them with the assay buffer, there was still the problem to be solved that quantification could only have been performed at these particular dilutions of the matrix, which is not realistic considering that there may exists a wide variation on the concentration range of these molecules when released from the bacteria

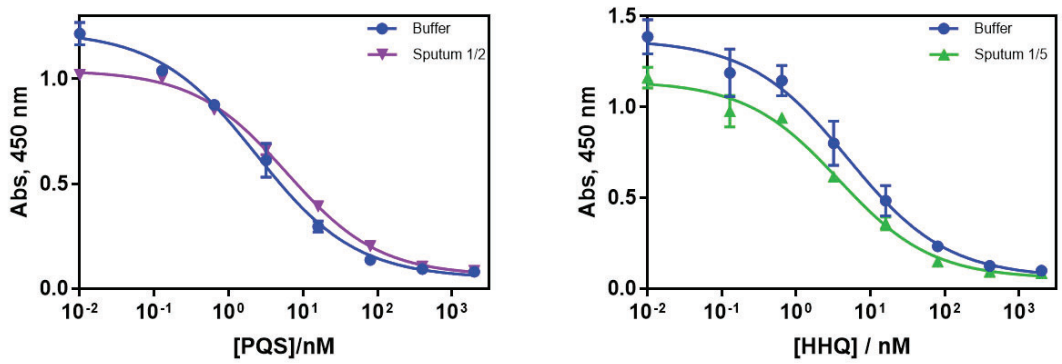

Figure 5.5: On the left, the calibration curve of PQS in buffer (Blue) and the calibration curve in the pool of sputum treated with DTT diluted 1/2 (Purple) are represented. On the right, the calibration curve of HHQ in buffer (Blue) and the calibration curve in the pool of sputum treated with DTT and diluted 1/5(Green) are represented. The curves were obtained using the ELISAs mAb5.4.2.3 (0.37 µg·mL^{-1})/PQS-BSA HD=3 (0.20 µg·mL^{-1}) ELISA for PQS detection and the As382 (1/20,000)/PQS-BSA (0.25 µg·mL^{-1}) ELISA for HHQ detection. Each calibration point was measured in duplicates on the same ELISA plate and the results shown were all obtained on the same day.

Nevertheless, to confirm whether the developed protocol could be a first approximation to use the developed ELISAs to measure sputum samples, five blank sputum samples from distinct individuals, different from those used to prepare the sputum pool, were divided into two groups. One group was spiked with 5 nM prior to the addition of DTT, and the other was processed unspiked. The same treatment was applied to all samples, both spiked and unspiked, before measuring them with the PQS (mAb5.4.2.3/PQS-BSA(HD=3)) and HHQ (As382/PQS-BSA) ELISAs under previously readjusted conditions. The objective was to find out if the sample treatment was going to have an effect on the recovery of the target analytes.

Table 5.2: Values obtained of PQS and HHQ in blank samples before and after spiking.

	PQS ELISA (mAb5.4.2.3/PQS-BSA(HD=3)		HHQ ELISA (As382/PQS-BSA)	
	Non-Spiked, [PQS]/nM	Spiked 5 nM, [PQS]/nM	Non-spiked, [HHQ]/nM	Spiked 5 nM, [HHQ]/nM
Sputa 1	0.03	2.58	<LLOD	<LLOD
Sputa 2	5.88	61.54	0.82	3.52
Sputa 3	<LLOD	0.02	<LLOD	<LLOD
Sputa 4	1.42	12.27	0.17	0.66
Sputa 5	4.20	50.93	1.97	6.29

Sputum samples were treated following the procedure explained in section 5.5.2.1 and were directly measured by ELISA. The calibration curves and samples were measured under the following conditions: mAb5.4.2.3 (0.37 µg·mL^{-1})/PQS-BSA HD=3 (0.20 µg·mL^{-1}) ELISA for PQS detection and As382 (1/20,000)/PQS-BSA (0.25 µg·mL^{-1}) ELISA for HHQ detection. Each calibration point and sample were measured in triplicate on the same ELISA plate, and the results shown were all obtained on the same day.

PQS and HHQ immunoreactivity was recorded in 4 out of 5 and 3 out of 5 non-spiked samples analyzed, respectively, indicating that the undesired nonspecific matrix interferences had not been completely resolved. Moreover, the concentrations measured on the spiked fractions were far from what it was expected. While two of the samples showed values of PQS significantly higher, with factors of 1200% and 1000% of the spiked value, other showed just a 0.4% recovery. For the case of HHQ, levels could not be quantified in two samples and for the rest, the values were close to the expected value in two of the samples.

These results indicated that on one side the matrix effect produced by the sputum had not been fully resolved, but also that each sputum sample behaves differently and also in a distinct manner to the sputum pool used to set up the assay conditions. In such a scenario, if the sputum pool was not representative of the wide-ranging behavior of the sputum samples, the established protocol could not be generally applied, leading to errors in the quantification of the AIs. At the light of these results, we decided to address the issue of heterogeneity among sputum samples, which was leading to disparate results when distinct samples had been spiked at the same concentration. Hence, alternative homogenization strategies were investigated.

5.3.1.2 Studies on treatments to equalize the behavior of different sputum in the PQS ELISA

For these studies, different sputa samples showing distinct aspects (see Table 5.1 above) were used. The experiments were addressed to find out a sample treatment method that would equalize the behavior of the samples in respect to their immunochemical reactivity recorded with the PQS ELISA.

5.3.1.2.1 Reducing agents

In addition to **DTT**, other reducing agents such as **NAC** or **(S)-2-aminobutane-1,4-dithiol hydrochloride** (**DTBA**) were tested. Although DTBA is not commonly used as a reducing agent for clinical samples, there are some examples in the literature in which this reagent has been used, such as for the reduction of disulfide bridges in sperm samples[40]. So far, its use to treat sputum samples has not been reported. All reducing agents succeed on effectively liquefying the sample and facilitating handling of the sputa. Calibration curves were generated using the sputum treated with the respective reducing agent and compared them with calibration curves obtained in assay buffer containing the same concentration of reducing agent. Prior experiments already confirmed that these concentrations of reducing agents did not affect the assays.

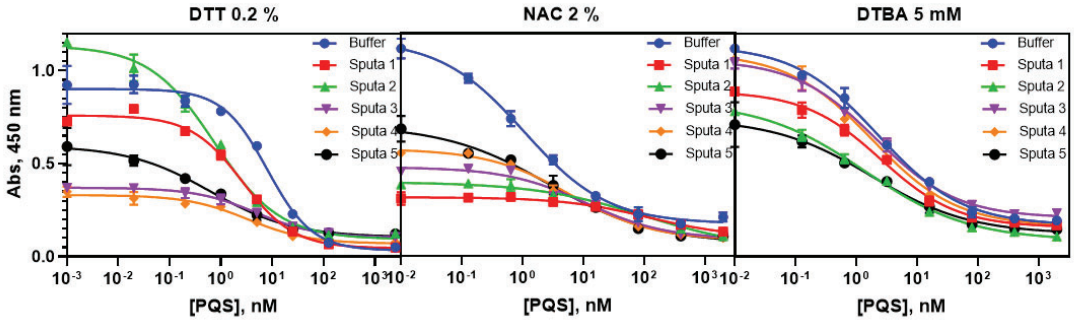

Figure 5.6: Calibration curves for the PQS ELISA after treating 5 different sputum samples with the reducing agents DTT, NAC and DTBA. The curves were obtained using the ELISAs mAb5.4.2.3 (0.37 µg·mL^{-1})/PQS-BSA HD=3 (0.20 µg·mL^{-1}) ELISA for PQS detection with a ½ dilution factor. Each calibration point was measured in duplicates on the same ELISA plate and the results shown were all obtained on the same day.

Figure 5.6 displays the curves obtained for each of the reducing agents tested using 5 different sputum samples from various patients. As expected, based on the results described in section 5.3.1.1, DTT failed to homogenize the behavior of the different sputum samples. The samples treated with NAC delivered calibration curves with a significant lower signal and similar behavior of the different sputa was either not achieved. DTBA, on the other hand, seemed to standardize the behavior of the various sputum samples to a greater extent. However, despite the advantages of that reducing agent in terms of sample liquefaction, which aids in handling, it still failed to produce uniform calibration curves for all the sputum samples. This would prevent the

accurate quantification of QS signals. Therefore, we decided to proceed with exploring other sample treatment alternatives

5.3.1.2.2 Breaking of the extracellular DNA

Due to the reported presence of high levels of extracellular DNA in sputum from chronic patients such as those with CF, it was decided to test the addition of a DNase that could degrade these strands, potentially homogenizing the behavior of sputum from different patients[41]. To investigate this, **DNase I** was applied to five different sputum samples. DNase I is an enzyme crucial in molecular biology for its ability to catalyze DNA hydrolysis, breaking down DNA molecules by cleaving phosphodiester bonds, thus fragmenting DNA into smaller pieces. The sputum samples were treated under conditions previously used in sputum studies[42-44]: incubation for 15 minutes with gentle agitation at 37°C and an enzyme concentration of 2 $U \cdot mL^{-1}$. Subsequently, calibration curves were generated using each of the treated sputum samples, run in the ELISA and compared with a curve in buffer containing the same reagents used for treatment (see Figure 5.7). As it can be observed, the behavior of the sputum samples varies significantly among them, with a notable signal inhibition observed for three of the tested samples, thus rendering this option ineffective as sample treatment for our purposes.

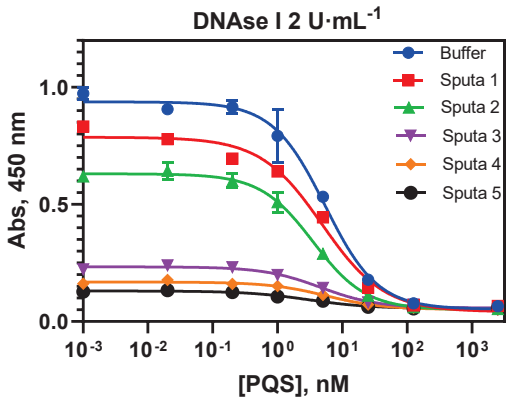

Figure 5.7: Calibration curves for the PQS ELISA after treating 5 different sputum samples with the DNAse I. The curves were obtained using the ELISAs mAb5.4.2.3 (0.37 µg·mL^{-1})/PQS-BSA HD=3 (0.20 µg·mL^{-1}) ELISA for PQS detection with a ½ dilution factor. Each calibration point was measured in duplicates on the same ELISA plate and the results shown were all obtained on the same day.

5.3.1.2.3 Hydrogen peroxide treatment

As previously mentioned, some studies have reported the use **hydrogen peroxide** as a way to disaggregate sputum[38, 45-47]. This treatment involves the addition of hydrogen peroxide, which is decomposed by the catalases of the sample to generate oxygen, thereby liquefying the sputum. This protocol involved adding 0.3 M hydrogen peroxide to the sputum samples for 15 minutes, shaking them every 5 minutes. Bubble formation and partial, but not complete, homogenization of the sputum were observed. After this, the sample was used to prepare calibration curves and measured using ELISA.

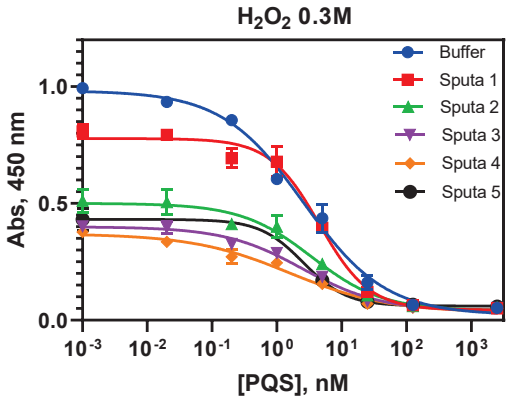

Figure 5.8: Calibration curves for the PQS ELISA after treating 5 different sputum samples with H_2O_2. The curves were obtained using the ELISAs mAb5.4.2.3 (0.37 µg·mL^{-1})/PQS-BSA HD=3 (0.20 µg·mL^{-1}) ELISA for PQS detection with a ½ dilution factor. Each calibration point was measured in duplicates on the same ELISA plate and the results shown were all obtained on the same day.

The results shown in Figure 5.8 show how this treatment also failed to match the behavior of the sputum samples. Moreover, in 4 out of the 5 samples, the maximum signal of the calibration curves decreased by half.

5.3.1.2.4 Proteases

Another strategy was to directly break the amino acid chains of the mucin networks to disperse the mucus. For this purpose, proteinase K was tested. Proteinase K is a proteolytic enzyme commonly employed in molecular biology for protein digestion. It is a serine protease that exhibits high specificity in cleaving peptide bonds of proteins, making it useful for degrading proteins and removing them from biological samples. It is used in various applications such as nucleic acid purification, protein extraction, and degradation of proteins in biological samples prior to further analysis. We used this enzyme to treat sputum samples following various examples where proteinase K was also used for sputum treatment[48-50]. The conditions were quite drastic and involved undergoing a 60-minute treatment at 55°C with constant agitation.

Since the indirect competitive ELISA is a protein-based assay, it was necessary to deactivate proteinase K prior to the assay, as its presence completely inhibited the ELISA. Various methods for inhibiting proteinase K are described in the literature, most of which are based on thermal denaturation. However, in this case, thermal denaturation caused uncertainty about the stability of the molecules being analyzed. Instead, penylmethanesulfonyl fluoride (PMSF),a low molecular weight compound that forms a covalent bond with a specific serine residue located within the active site of proteinase K (See Figure 5.9), was selected as more suitable option for

our purposes. This interaction effectively inhibits the enzymatic activity of proteinase K, rendering it inactive [51].

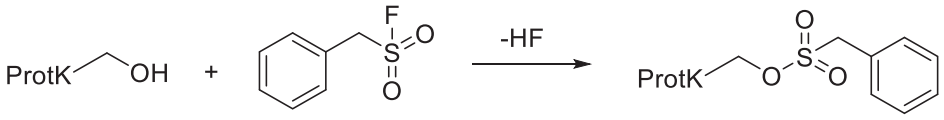

Figure 5.9: PMSF inhibition reaction on Proteinase K.

Hence, as with the previous treatments, five sputum samples were incubated with proteinase K using the conditions mentioned above. Subsequently calibration curves were generated and measured with the PQS ELISA to analyze their behavior in comparison to that of the assay buffer.

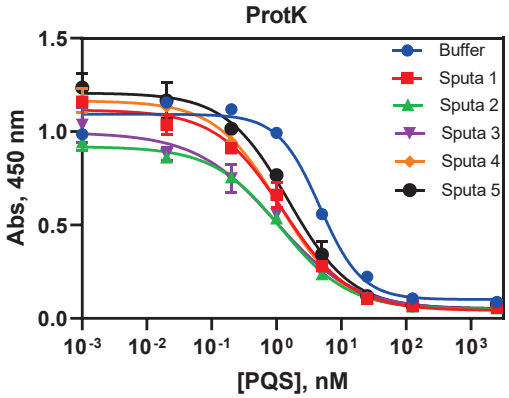

Figure 5.10: Calibration curves for the PQS ELISA after treating 5 different sputum samples with proteinase K. The curves were obtained using the ELISAs mAb5.4.2.3 (0.37 µg·mL^{-1})/PQS-BSA HD=3 (0.20 µg·mL^{-1}) ELISA for PQS detection. Each calibration point was measured in duplicates on the same ELISA plate and the results shown were all obtained on the same day.

The results shown in Figure 5.10 demonstrate in terms of A_{max}, proteinase K is the treatment that most equalizes the sputum samples, as all values are between 0.94 and 1.20. Regarding IC_{50}, the behavior is also quite consistent varying only between 0.95 and 1.52 nM, although slightly different from that of the assay buffer with an IC_{50}, of 4.66 nM.

5.3.1.2.5 Freeze-drying

Due to the large difference in water content among the different samples, it was thought that this could also be a factor influencing the differences in behavior regarding the ELISA response. On the other hand, we had doubts on how should we report the levels of the QS signaling molecules in the sputa. If expressed in respect to the volume, this raised concerns of the reliability of the interpretation considering the high diversity of water content of the sputa.

Lyophilizing and subsequently reconstituting the dried sputum (See Figure 5.11) would allow for standardizing the amount of sample used for immunochemical analyses. This approach would improve accuracy and enable the measurement of biomarker concentrations relative to the amount of dry sputum, thereby ensuring greater homogeneity on the expression of the results found different sputum samples.

Figure 5.11: Sputum after lyophilization

To assess the effect of freeze-drying of the sputa in the ELISA, matrix effect studies were conducted using lyophilized sputum samples that had been resuspended in 10 mM PBS at a concentration of 10 mg of dried sputum residue per mL. Calibration curves of PQS and HHQ were prepared in the reconstituted freeze-dried sputa and used to build standard curves and measure them in the corresponding ELISAs in order to assess the effect of this treatment. Figure 5.12 shows the PQS and HHQ ELISA calibration curves obtained for 5 different sputum samples at 10 $mg \cdot mL^{-1}$.

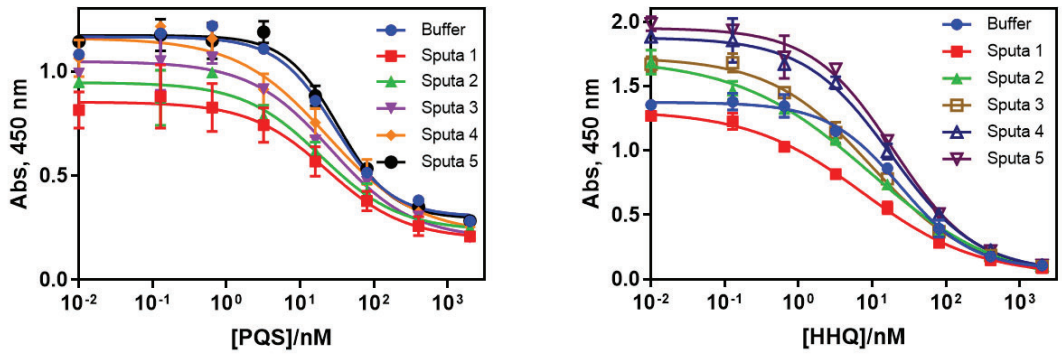

Figure 5.12: The graphs show the matrix effect of different lyophilized sputum samples resuspended at 10 $mg \cdot mL^{-1}$ and compared with a buffer calibration curve. On the left, results for PQS obtained with the ELISA mAb5.4.2.3/PQS-BSA(HD=3) are displayed. On the right, results for HHQ obtained with the ELISA As382 (1/20,000)/PQS-BSA are shown. Each calibration point was measured in duplicates on the same ELISA plate and the results shown were all obtained on the same day.

According to the results obtained, it appeared like if this treatment minimized the differences between the sputum samples, based on adjusting all of them to the same concentration. However, matrix effect was still evident as the calibration curves were close but also not identical across all samples. Moreover, differences are still observed between the behavior of the sputum samples and the buffer, which poses challenges for accurate quantification. In the case of the HHQ ELISA, it was observed that some sputum samples produced calibration curves with higher maximum absorbance than the buffer.

5.3.1.2.6 Comparison of sputum treatments

In the quest to homogenize the response of sputum samples in the ELISA assays, several treatments were evaluated to overcome the variability inherent in untreated samples. This variability, known as the matrix effect, can obscure accurate quantification of the analytes of interest. The treatments tested included various reducing agents, DNase I, hydrogen peroxide, proteinase K, and freeze-drying, each aiming to standardize the sample preparation process and improve assay reliability. Table 5.3 shows the A_{max}, IC_{50}, and slope values for each of the sputum samples tested with each treatment. Additionally, the CV for each treatment is included, indicating how similar the curves of different sputum samples are with the same treatment.

Initially, reducing agents such as DTT, NAC, and DTBA were used to break disulfide bonds in mucin cysteines, which are abundant in sputum. These agents successfully liquefied the samples, facilitating easier handling and processing. However, DTT and NAC did not achieve consistent calibration curves across different sputum samples. While DTBA showed some promise by equalizing the behavior of the samples to a greater extent, it still fell short of

producing uniform calibration curves, essential for accurate quantification. In Table 5.3, it can be seen that the CV values for DTT and NAC are significantly higher than for DTBA. For example, for IC_{50}, CV values of 82% and 136% were obtained respectively compared to 20% for DTBA.

To address the high levels of extracellular DNA present in sputum from chronic patients, DNase I was tested. This enzyme degrades DNA strands, potentially homogenizing the sample behavior. Despite its theoretical benefits, DNase I treatment resulted in significant signal inhibition in some samples, leading to inconsistent results and rendering it ineffective for our purposes.

Hydrogen peroxide treatment was explored due to its reported use in disaggregating sputum through the generation of oxygen bubbles. This method showed partial success in homogenizing the samples but did not fully standardize the response. Furthermore, it significantly decreased the maximum signal of the calibration curves in most samples, indicating that it might disrupt the assay.

Proteinase K, a proteolytic enzyme, was tested to break down mucin networks by cleaving peptide bonds. This approach aimed to disperse the mucus and standardize the sample matrix. Proteinase K treatment produced more consistent calibration curves, suggesting improved sample homogenization. In Table 5.3, it can be seen that proteinase K shows a low CV for A_{max} between the buffer and the five sputum samples tested, only 10%.

Given the large differences in water content among sputum samples, freeze-drying was considered. This method aimed to standardize the sample by removing water and reconstituting the dried sputum in a controlled volume. Lyophilization allowed for a consistent sample concentration, improving accuracy and homogeneity in results. However, matrix effects persisted, as the calibration curves were not entirely consistent across all samples. Some variability remained, suggesting that freeze-drying alone was insufficient to fully eliminate the matrix effect.

While each treatment provided specific advantages, none achieved complete and homogeneous response of the sputum samples on their own. Reducing agents facilitated sample handling but failed to produce uniform calibration curves. DNase I and hydrogen peroxide treatments resulted in significant variability and signal inhibition. Proteinase K showed promise in breaking down mucin networks and producing consistent results, but there is still not complete homogenization of the different curves. Freeze-drying offered standardization of sample concentration but did not entirely eliminate matrix effects.

The combination of freeze-drying with proteinase K treatment appears to be the most effective approach, as it leverages the benefits of both methods. Freeze-drying standardizes the sample content, while proteinase K breaks down mucin networks to further homogenize the sample matrix. This combined strategy will be the next step to eliminate matrix effects and achieve accurate quantification of QS signals in sputum samples.

Table 5.3: Summary of the effect of the different sample treatment agents studied aiming at removing nonspecific interferences and equalize the behavior of the distinct sputa samples in the PQS ELISA.

ST[a] ➢	Reducing Agents[d]									DNase			H_2O_2			Protease			Freeze-drying		
	DTT			NAC			DBTA														
AP[b] ➢	A_{max}	IC_{50}	Slope	A_{max}	IC_{50}	Slope	A_{max}	IC_{50}	Slope	A_{max}	IC_{50}	Slope	A_{max}	IC_{50}	Slope	A_{max}	IC_{50}	Slope	A_{max}	IC_{50}	Slope
Buffer[c]	0,90	5,02	-0,99	0,97	3,06	-0,63	0,95	3,31	-0,63	0,94	5,39	-1,07	0,98	2,59	-0,69	1,09	4,66	-1,35	1,17	5,01	-1,12
SP #1	0,76	2,64	-0,87	0,26	118,90	-0,62	0,74	2,54	-0,69	0,79	4,87	-0,91	0,78	4,52	-1,13	1,12	1,25	-0,84	0,85	23,33	-0,82
SP #2	1,14	0,76	-0,68	0,33	102,40	-0,47	0,69	1,40	-0,51	0,63	3,53	-1,07	0,50	3,45	-0,80	0,92	1,16	-0,83	0,95	19,33	-0,82
SP #3	0,37	4,85	-0,73	0,40	11,23	-0,66	0,88	2,11	-0,65	0,23	4,60	-0,99	0,40	2,50	-0,72	1,00	0,95	-0,71	1,05	26,35	-0,79
SP #4	0,33	3,36	-0,73	0,48	6,10	-0,64	0,91	1,84	-0,62	0,17	5,60	-0,98	0,37	1,59	-0,57	1,17	1,10	-0,88	1,16	23,46	-0,71
SP #5	0,60	0,63	-0,54	0,59	2,78	-0,50	0,62	1,82	-0,54	0,13	3,02	-0,90	0,43	2,56	-1,29	1,21	1,53	-0,90	1,17	33,22	-1,20
% CV	46	82	21	50	136	13	17	20	11	72	23	7	43	35	32	10	18	24	13	19	22

[a] ST, sample treatment method; [b] AP, analytical parameters extracted from the four-parameter logistic equation used to fit the standard curves; [c] the buffer used as reference was treated as the samples and contained the same agent as the samples; [d] the sputa samples were treated with the reducing agents and used undiluted to prepare the standard curves.